Studies of Exocytosis at Single Cells

Keith T. Thornley

A dissertation submitted to the faculty of the University of North Carolina at Chapel Hill in partial fulfillment of the requirements for the degree of Doctor of Philosophy in the Department of Chemistry

Chapel Hill
2009

Approved by:

Dr. R. Mark Wightman

Dr. Linda Spremulli

Dr. Nancy Thompson

Dr. Gary Glish

Dr. Mark Schoenfisch

Abstract

Keith T. Thornley: Studies of Exocytosis at Single Cells
(Under the direction of Dr. R. Mark Wightman)

Intercellular communication via chemical signaling is vital to the healthy functioning of multicellular organisms. In exocytosis, intracellular vesicles undergo Ca^{2+}-triggered fusion with the cell plasma membrane, releasing their chemical messengers into the extracellular space. As exocytosis serves as the primary mechanism of communication at neuronal synapses, great emphasis has been placed on understanding the complex cellular regulation of this process. This dissertation focused on the use of amperometry and fast scan cyclic voltammetry at carbon-fiber microelectrodes to monitor exocytosis in real-time at both isolated neurons and chromaffin cells, well-characterized model cells for neuronal exocytosis. These techniques provide the necessary temporal resolution and sensitivity required to detect the chemical signals resulting from individual vesicular release events. Amperometric recordings at midbrain dopamine neurons showed that somatodendritic dopamine release is exocytotic, with a bimodal distribution of vesicular events. A combinatorial approach was used to demonstrate alterations in biogenic amine exocytosis in mice lacking the mitochondrial uncoupling protein UCP2 or the hormone leptin. Conversely, a mouse model of fragile X syndrome revealed no deficiencies in vesicular release mechanisms. Electrochemical methodologies were developed to distinguish catecholamine transmitters from the L-tyrosine-derived trace amines. Application of these methods revealed poor vesicular accumulation of trace amines precludes their function as false transmitters. Finally, vesicular quantal size in chromaffin cells was shown to be resistant to exogenous application of catecholamine precursors.

To Amy

It took five years and over 150 pages for me to finish this chapter of my life.
It would take ten times as long on both counts for me to adequately express how instrumental you were in seeing me through to this moment.
You are my strength, my spirit, and my soul.

I'm coming home…

Acknowledgements

I would like to acknowledge the vast network of individuals who have generously given of their time and energy during my completion of this dissertation. First and foremost, to my advisor Dr. Mark Wightman: thank you for the opportunity to further my knowledge of science in your lab and for the necessary guidance to make the most of that opportunity. To my undergraduate advisor Dr. Bruce Bursten: thanks for nurturing a young, inquisitive mind and providing the motivation for me to pursue this degree. Thanks to my collaborators from other research institutions: Dr. Lorraine Iacovitti at Thomas Jefferson University; Dr. Brad Lowell, Dr. Helen Freeman, and Dr. Dong Kong at Harvard University; and Dr. Jonathan Sweedler at the University of Illinois at Urbana-Champaign.

A hearty thank you to all the members of the Wightman lab for countless helpful discussions on life, sports, and sometimes even science. In particular, thanks to Dr. Brian Kile, who collected the brain slice data presented in these chapters, fixed the HPLC every time I broke it, and, in general, served as my analytical chemistry textbook. Special thanks to Dr. Charles Miller and Jelena Petrovic for assistance with both research and mouse colony maintenance. Also, a thank you to Paul Walsh, perhaps the best undergraduate researcher ever.

Last, but most certainly not least, I would like to acknowledge my family for their tireless support over the years. To my mom, my dad, Tim, Patti, and even you Ryan: thanks for always being there. It's humbling to think I could make such great people proud.

Table of Contents

List of Tables

List of Figures

List of Abbreviations and Symbols

$[Ca^{2+}]_i$	Intracellular Ca^{2+} concentration
5-HT	5-hydroxytryptamine (serotonin)
ATP	Adenosine triphosphate
CV	Background-subtracted cyclic voltammogram
DAT	Dopamine transporter
E	Epinephrine
ER	Endoplasmic reticulum
FMRP	Fragile X mental retardation protein
FSCV	Fast scan cyclic voltammetry
FXS	Fragile X syndrome
GFP	Green fluorescent protein
GTP	Guanosine triphosphate
HPLC	High performance liquid chromatography
I_{max}	Amplitude
K_d	Dissociation constant
KO	Knock out
L-DOPA	L-3,4-dihydroxy-phenylalanine
LDCV	Large dense core vesicle
MAO	Monoamine oxidase
NAc	Nucleus accumbens
NE	Norepinephrine
PC12	Rat phaeochromocytoma
Q	Quantal size
RP	Reserve pool

RRP	Readily releasable pool
SNc	Substantia nigra pars compacta
SNr	Substantia nigra pars reticulata
SNARE	Soluble NSF attachment protein receptor
SSV	Small synaptic vesicle
$t_{1/2}$	Halfwidth
t_d	Decay time
t_r	Rise time
TH	Tyrosine hydroxylase
UCP2	Uncoupling protein 2
V_{max}	Maximal uptake velocity
*v*BNST	Ventral bed nucleus of the stria terminalis
VGCC	Voltage-gated calcium channel
VMAT	Vesicular monoamine transporter
VTA	Ventral tegmental area
WT	Wild type

Chapter 1

Techniques for the Study of Exocytosis

Introduction

Chemical signaling forms the basis of intercellular communication in multicellular organisms. Following triggered secretion, chemical messengers diffuse to their site of action where they are specifically detected by target cells. Exocytosis is a secretory process in which intracellular vesicles containing chemical messengers fuse with the cell's plasma membrane extruding the vesicular content into the extracellular space. Exocytosis is the primary cellular mechanism for the triggered release of chemical messengers, and has been the object of intense study as it represents the principle method of communication at the neuronal synapse.

In the mammalian nervous system, information is transmitted in pathways via specialized cells called neurons (Figure 1.1). Neurons are excitable cells that communicate with each other through a combination of electrical and chemical signals. Through strict regulation of intracellular and extracellular ion concentrations (mainly Na^+, K^+, and Cl^-), neurons maintain a negative resting potential across the plasma membrane of approximately 70 mV (with the intracellular compartment being more negative) (Squire, 2008). Neurons receive inputs at their dendrites, where the action of chemical messengers on ionotropic receptors produces changes in ion concentration gradients that manifest as fluctuations in membrane potential. These fluctuations can be excitatory or inhibitory, with excitatory responses corresponding to positive deflections in the membrane potential and inhibitory responses to negative deflections. Responses from the entire dendritic field are

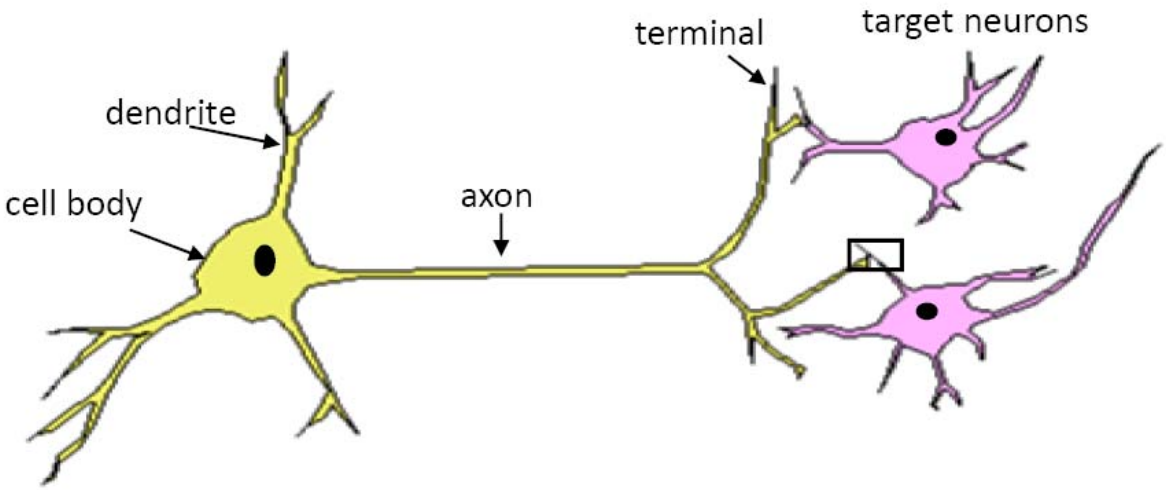

Figure 1.1. Schematic drawing of a neuron. Neurons receive inputs at the dendrites. Inputs are summed at the cell body, or soma. If the inputs are significant , the neuron will fire an action potential that propagates down the axon to the axon terminals, which form specialized specialized connections called synapses (black box) on the dendrites of target neurons.

summed at the cell body, or soma. If the membrane potential is deflected above the threshold, the neuron will fire an action potential. During an action potential, the positive deflections in membrane potential trigger the opening of voltage-gated Na^+ channels and the influx of Na^+ ions into the cell along their concentration gradient, further depolarizing the membrane. As voltage-gated K^+ channels open, prompting efflux of K^+ ions out of the cell along their concentration gradient, and the Na^+ channels begin to inactive, the cell returns to its resting membrane potential. The action potential propagates down the axon as local depolarization stimulates the opening of neighboring Na^+ and K^+ channels, ultimately reaching the synapse, a specialized connection between axon terminals and the dendrites of their target neurons. At the synapse, the invading action potential causes voltage-gated calcium channels (VGCCs) to open, and the resulting Ca^{2+} influx triggers the exocytosis of chemical neurotransmitters (Llinas et al., 1992; Borst and Sakmann, 1996). The transmitters diffuse across the synaptic cleft, a 20-50 nm gap ensuring the electrical depolarization isn't transferred to the next cell, and their actions on postsynaptic receptors begin the signal transduction process anew.

Exocytosis

Figure 1.2 shows a drawing that outlines some of the major steps in the exocytotic process. Vesicles are packaged with neurotransmitters via active transport and then are localized in clusters/pools near the presynaptic active zone. Prior to release, vesicles must be physically relocated to the plasma membrane. In a series of ATP-dependent steps, vesicles are recruited, tethered, and docked to the plasma membrane (Burgoyne and Morgan, 2003). A final priming step renders vesicles competent for Ca^{2+}-triggered formation of the fusion pore and secretion of their contents into the extracellular space. Following release, vesicles are recycled for further rounds of exocytosis through three primary routes depending on whether full fusion and incorporation of the vesicular membrane into the plasma membrane occurred. Vesicles that do not undergo full fusion may be recycled

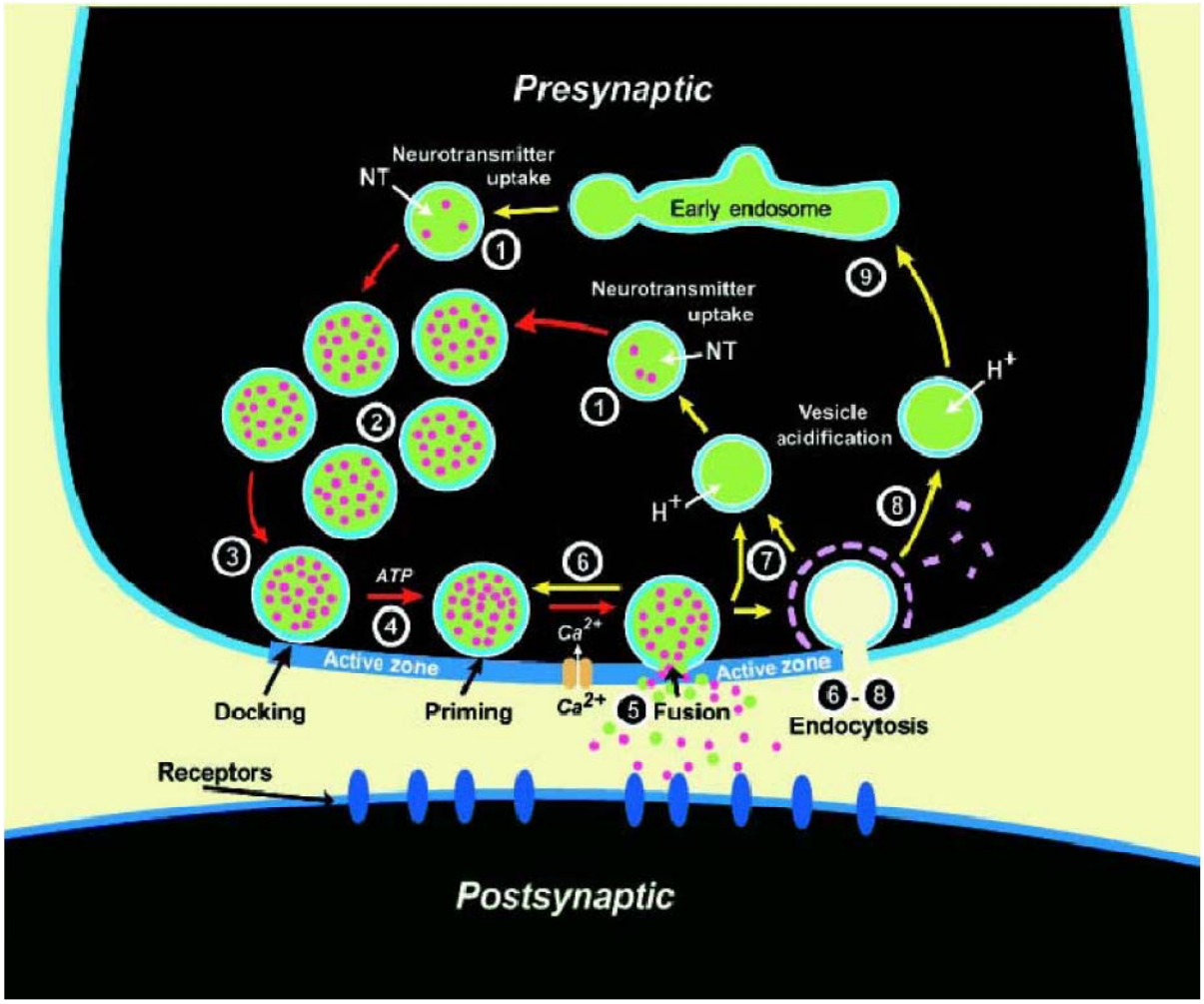

Figure 1.2. The synaptic vesicle cycle. Red arrows indicate steps in exocytosis and yellow arrows indicate steps in endocytosis. Synaptic vesicles are filled with neurotransmitters via active transport (1). Prior to release, vesicles are mobilized from clusters/pools (2) to dock at the plasma membrane (3). Following a priming step (4), vesicles are capable of undergoing Ca^{2+}-triggered fusion (5). Vesicles are recycled via several pathways including local reuse (6), fast recycling without an endosomal intermediate (7), and clathrin-mediated endocytosis with or without an endosomal intermediate (8-9). (Sudhof, 2004)

without undocking, leaving them available for immediate release (sometimes termed "kiss and stay" exocytosis), or can undock and undergo local repackaging ("kiss and run" exocytosis) (Harata et al., 2006). After full fusion, vesicles undergo a slower endocytosis pathway via clathrin-coated pits that may or may not involve an endosomal intermediate (Smith et al., 2008).

Points of Regulation

Neurotransmitters are packaged at high concentrations into vesicles via active transport. Biochemical studies have revealed seven transporter proteins for the classical neurotransmitters: three differentially-expressed transporters for glutamate (Bellocchio et al., 2000; Fremeau et al., 2001; Fremeau et al., 2002), two differentially expressed transporters for all the monoamines (Erickson et al., 1992; Liu et al., 1992), a single transporter for gamma-aminobutyric acid (GABA) and glycine (McIntire et al., 1997; Sagne et al., 1997), and a single transporter for acetylcholine (Roghani et al., 1994). Active transport is driven by a vacuolar-type proton pump that couples hydrolysis of ATP to the movement of H^+ from the cytosol to the vesicle interior, generating an electrochemical gradient (Maycox et al., 1988). The vesicular transporters then couple translocation of transmitter against its concentration gradient with the exchange of H^+ running down its electrochemical gradient (Chaudhry et al., 2008). Transporters play two important roles in chemical communication. First, expression of a particular vesicular transporter is a major determinant in the type of neurotransmitter used at a synapse. As an example, GABAergic neurons transfected with a vesicular glutamate transmitter became capable of releasing glutamate in addition to GABA (Takamori et al., 2000). Second, vesicular transporters help regulate the amount of neurotransmitter released during exocytosis. For instance, overexpression of the vesicular monoamine transporter (VMAT2) has been shown to increase vesicular dopamine content (Pothos et al., 2000), while hemizygous deletion of the

VMAT2 gene lead to significantly reduced dopamine levels in the striatum (Wang et al., 1997).

A second concept crucial to understanding the regulated process of exocytosis is that of vesicle pools. Within a presynaptic terminal, the population of vesicles can be divided into two separate vesicle pools based on morphological and physiological criteria: the readily releasable pool (RRP), consisting of those vesicles docked at the active zone and immediately available for exocytosis, and the reserve pool (RP), consisting of those vesicles clustered at a distance from the plasma membrane and not immediately available for release (Rizzoli and Betz, 2005). Directly following stimulation of the nerve terminal, vesicles in the RRP are released, leading to a depletion of the pool. In response to prolonged or intense stimuli, continued release is dependent on the recycling of vesicles back into the RRP and/or the mobilization of vesicles from the RP to the RRP for subsequent release. The cellular mechanisms responsible for sequestering the RP and controlling vesicle mobilization are still under investigation, but most work to date has focused on synapsins, peripheral membrane proteins associated with synaptic vesicles (Schiebler et al., 1986; Benfenati et al., 1989a; Benfenati et al., 1989b). Mammals express three synapsin genes, with most neuronal synapses expressing synapsins 1 and 2 (De Camilli et al., 1990; Hosaka and Sudhof, 1998a). Conserved among all synapsins are a N-terminal domain containing phosphorylation sites for cAMP-dependent protein kinase and Ca^{2+}/calmodulin-dependent kinases and a large, central domain with a high affinity ATP-binding site (Hosaka and Sudhof, 1998b). Research showing that synapsins bind to cytoskeletal components, particularly actin, as well as synaptic vesicles, and that phosphorylation of synapsins eliminates vesicle binding suggests that synapsin could be involved in regulating the availability of the RP vesicles via a reversible cross-linking between vesicles and/or vesicles and the cytoskeleton (Bahler and Greengard, 1987; Benfenati et al., 1992).

The final point of regulation prior to release of neurotransmitters is the actual fusion of the vesicular membrane with the cell plasma membrane. Four classes of proteins have been identified as the core machinery controlling this process: SNARE proteins, SNARE regulators, Rab proteins, and Rab effectors (Jahn et al., 2003). Rab proteins belong to a family of small guanosine triphosphate (GTP)-binding proteins, and interact with effectors and vesicles in a GTP-dependent manner (Araki et al., 1990; Johnston et al., 1991). Rab proteins are presumed to act as switches, with the active, GTP-bound state rendering vesicles competent for docking to the plasma membrane (Rybin et al., 1996). The phospholipid bilayers comprising the vesicular and plasma membrane are both negatively charged, resulting in an energy barrier to fusion. Soluble NSF attachment protein receptor (SNARE) proteins are membrane-associated proteins that contain a characteristic residue sequence called the SNARE motif. There are three SNARE proteins linked to exocytosis: synaptobrevin located on the vesicular membrane and syntaxin and SNAP-25 on the plasma membrane (Sollner et al., 1993). Synaptobrevin and syntaxin each contain a single SNARE motif, while SNAP-25 contains two SNARE motifs. Association of the four SNARE motifs into a "trans complex," a parallel four helical bundle, overcomes the repulsion energy barrier and forces the vesicular and plasma membrane together (Hanson et al., 1997; Weber et al., 1998). This results in an unstable intermediate from which the fusion pore can form by mixing of the destabilized phospholipid bilayers. SNARE proteins are additionally regulated by the Sec1/Munc18-like proteins. While necessary for fusion, the exact roles of these proteins remain unclear. To date, evidence suggests that these proteins play a role in controlling the availability of syntaxin for SNARE complex formation and the vesicle priming step following establishment of the SNARE complex (Hata et al., 1993; Deak et al., 2009).

Ca^{2+}-Dependence

As mentioned earlier, exocytosis of neurotransmitters is a Ca^{2+}-mediated process. As the action potential reaches the synapse, depolarization of the cell membrane opens

VGCCs, and the resulting influx of Ca^{2+} ions serves as the ultimate trigger for release. The extent to which Ca^{2+} elicits vesicular release is then dependent on two factors: the efficiency of the cellular mechanisms for translating increases in intracellular Ca^{2+} concentration ($[Ca^{2+}]_i$) to vesicle fusion and the time course of the Ca^{2+} signal in the synapse. The putative cellular Ca^{2+} sensor is synaptotagmin, a synaptic vesicle-associated protein with two Ca^{2+}-binding C_2 domains (Perin et al., 1990). Multiple synaptotagmin isoforms have been identified in the brain, with synaptotagmin-1,-2, and -9 implicated as the Ca^{2+} sensors in exocytosis (Xu et al., 2007). The current model suggests that through Ca^{2+}-dependent interactions with phospholipids and the SNARE proteins, synaptotagmins promote fusion pore formation by pulling the SNARE complexes apart (Sudhof, 2004). Supporting the role of synaptotagmins in exocytosis, the micromolar Ca^{2+} affinity of synaptotagmins is consistent with the Ca^{2+} affinity of release measured at the Calyx of Held synapse (Meinrenken et al., 2003), and genetic alterations of synaptotagmin Ca^{2+} affinity produce proportional changes in the Ca^{2+} affinity of release (Fernandez-Chacon et al., 2001). In addition to triggering vesicle fusion via synaptotagmin, Ca^{2+} influx also facilitates vesicle mobilization. Increases in $[Ca^{2+}]_i$ have been shown to relocate docked vesicles closer to Ca^{2+} entry sites (Becherer et al., 2003) and to activate the protein scinderin, which severs F-actin filaments (Rodriguez Del Castillo et al., 1990). Disruption of the cortical actin cytoskeleton serves as a first step in the recruitment of vesicles to the plasma membrane for exocytosis (Burgoyne and Cheek, 1987). Similarly, the mobilization of RP vesicles is thought to depend on Ca^{2+}-mediated phosphorylation of synapsin (Chi et al., 2003).

The Ca^{2+} dynamics in a synapse can be simply represented as a series of fluxes between the extracellular medium, the cytosol, and intracellular organelles (chiefly mitochondria and the endoplasmic reticulum (ER)) (Figure 1.3). At rest these fluxes are minimal, with the $[Ca^{2+}]$ in the cytosol and mitochondrial matrix in the 100 nM range and the $[Ca^{2+}]$ in the extracellular medium and inside the ER above 1 mM. As the action potential

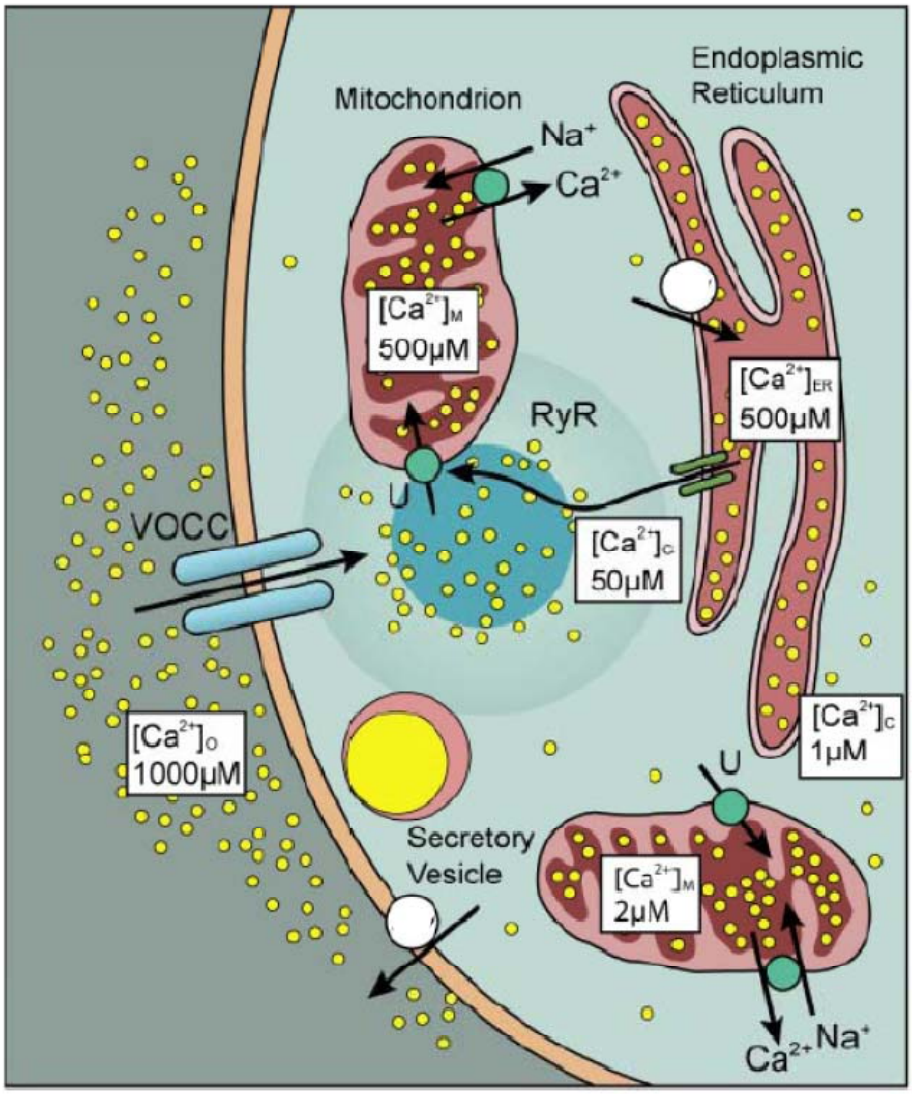

Figure 1.3. Intracellular Ca^{2+} regulation in an adrenal chromaffin cell. Ca^{2+} entry through voltage-gated calcium channels (VOCC) and/or release from the ER generates a local microdomain of high $[Ca^{2+}]$. Cytosolic Ca^{2+} is cleared by ATP-driven pumps (white circles) on the plasma and ER membranes or mitochondrial uptake via the uniporter (U). Spatial organization of the intracellular organelles helps define the boundaries of the microdomain and limit global cytosolic Ca^{2+} increases. (Garcia et al., 2006)

invades the synapse, VGCCs open and Ca^{2+} rushes from the extracellular medium down its concentration gradient into the cytosol. The spatial distribution of the VGCCs coupled with the limited diffusion of Ca^{2+} due to endogenous cytosolic Ca^{2+} buffers produces localized concentration microdomains in the tens of micromolar (Neher, 1998). Ca^{2+} release from the ER, triggered via either the Ca^{2+}-gated ryanodine receptors or second messenger inositol 1,4,5-trisphosphate-gated channels, may also contribute to cytosolic [Ca^{2+}] (Verkhratsky, 2004). Clearance of cytosolic Ca^{2+} occurs at the plasma membrane through the combination of a Na^{+}/Ca^{2+} exchanger and an ATP-driven Ca^{2+} pump. Cytosolic Ca^{2+} may also be cleared by uptake into intracellular organelles. An ATP-driven Ca^{2+} pump resides on the ER membrane, and mitochondria uptake Ca^{2+} through a low affinity uniporter driven by the mitochondrial membrane potential (Gunter and Pfeiffer, 1990). At basal levels of stimulation, the cytosolic Ca^{2+} transient is shaped primarily by diffusion and the endogenous buffers (Neher, 1998). Global cytosolic [Ca^{2+}] reaches levels around 1 μM, and clearance is dominated by the ATP-driven Ca^{2+} pumps on the plasma and ER membranes (Meinrenken et al., 2003; Garcia et al., 2006). During intense stimulation, cytosolic [Ca^{2+}] may reach levels high enough to facilitate uptake through the mitochondrial uniporter. Mitochondrial Ca^{2+} uptake stimulates cellular respiration (Rizzuto et al., 2000), and Ca^{2+} clearance via this mechanism may provide the necessary energy to restore Ca^{2+} to resting levels.

Systems of Interest

Regulated secretory vesicle exocytosis has been documented in a vast array of cell types including neurons, neuroendocrine cells, exocrine cells, hemopoietic cells, endothelial cells, and even sperm. The primary focus of this work is to better understand the cellular mechanisms responsible for neuronal communication, and hence studies have been conducted at individual neurons and chromaffin cells, a well-characterized model system for neuronal exocytosis.

Midbrain Dopamine Neurons

Dopamine, along with serotonin and norepinephrine (NE), belongs to the biogenic amine class of neurotransmitters. Dopamine modulates a wide variety of physiological functions in the brain from control of locomotion to reward seeking behavior. The particular involvement of dopamine in the brain chemistry of addiction and of motor movement disorders such as Parkinson's and Huntington's disease makes the regulated exocytosis of dopamine an especially attractive system for study. The term midbrain refers specifically to those dopamine neurons whose cell bodies are located in the substantia nigra (SN) and the ventral tegmental area (VTA). Dopamine neurons in the SN project to the striatum to form the nigrostriatal pathway, while dopamine neurons in the VTA project to the nucleus accumbens to form the mesolimbic pathway.

Chromaffin Cells

Adrenal medullary chromaffin cells, members of the neuroendocrine system, have been widely used in biochemical studies of vesicular exocytosis owing to their common origin with sympathetic neurons in the neural crest and their relative ease of isolation as homogenous populations in primary culture (Fujita, 1977; Livett, 1984). Chromaffin cells help modulate the body's "fight or flight" response by releasing the catecholamine hormones epinephrine (E) and NE into the bloodstream. A wealth of experimental evidence has revealed that the Ca^{2+} dependence of release and the protein machinery of vesicular docking and fusion are conserved in the chromaffin cell and the synapse (Morgan and Burgoyne, 1997; Burgoyne and Morgan, 2003). Chromaffin cells are an especially useful model of dopaminergic neurons as they both contain the same catecholamine synthesis enzymes and package transmitter into vesicles with VMAT, although via different isoforms (Erickson et al., 1996). The primary distinction between exocytosis at chromaffin cells and neurons is the size of the vesicles. In contrast to the small synaptic vesicles (diameter ≤ 50 nm) found predominantly at presynaptic active zones, chromaffin cells store catecholamine

in large dense core vesicles (LDCVs) with diameters near 300 nm. The greater capacity of LDCVs facilitates measurements of individual vesicular release events.

Techniques for Study of Exocytosis

Real time monitoring of exocytosis is subject to several challenging experimental constraints. First, measurement at spatially resolved regions of isolated cells requires a sensor with physical dimensions in the micron range. Second, observation of individual vesicular events requires a technique with extreme sensitivity. For even though vesicles can contain high concentrations of transmitter (up to 0.5 M), their small size necessitates limits of detection in the zeptomole to attomole range. Third, the rapid time course of vesicular fusion and release requires a technique with microsecond to millisecond resolution. And finally, a cell that releases multiple transmitters or a transmitter of unknown identity requires a technique with chemical selectivity. When used with carbon-fiber microelectrodes, the electrochemical techniques of constant potential amperometry (referred to hereafter as amperometry) and fast scan cyclic voltammetry (FSCV) provide the necessary spatial, temporal, sensitivity, and selectivity characteristics for accurate recordings of the exocytotic process. These techniques take advantage of the fact that several important secreted chemical messengers, including the catecholamines dopamine, NE, and E, are easily oxidized.

Carbon-fiber microelectrodes provide distinct advantages over conventional-sized electrodes for measurements of exocytosis at single cells. The small size of microelectrodes decreases double layer capacitance at the electrode tip, reducing the time constant of the electrode and allowing measurements down to the sub-microsecond time scale (Amatore and Maisonhaute, 2005). As the spatial dimensions of the carbon-fiber microelectrode approximate that of a single cell, the signal to noise ratio is enhanced over sensors with extraneous electroactive surface area (Schroeder et al., 1994). The use of disk geometries is particularly advantageous for single cell recordings. Disk microelectrodes

(Figure 1.4) are fabricated by insulating a carbon fiber (6-10 μm in diameter) in a pulled glass capillary and beveling the tip at 45 degrees to create a flat, elliptical sensor surface (Kawagoe et al., 1993). Disk microelectrodes can be positioned flush with the membrane of a cell, creating an "artificial synapse" configuration where the restricted extracellular volume into which transmitters are released minimizes signal loss due to diffusion and allows the release of a small number of molecules in the local vicinity of the sensor/receptor to be detected with a high signal to noise ratio (Amatore et al., 2008). This same approach is used by nature at the biological synapse.

Constant Potential Amperometry

In amperometry, the electrode is held at a constant potential sufficient to oxidize or reduce an analyte of interest. Analytes are immediately electrolyzed upon contact with the electrode surface, resulting in a measurable current. Unlike FSCV, in which the electrode response is slowed by adsorption and desorption of the analyte to the electrode surface (Bath et al., 2000), the temporal response of amperometry is limited only by mass transport and electron transfer kinetics. Thus, amperometry offers superior temporal resolution compared to FSCV. However, amperometry does not allow for positive analyte identification. If multiple electroactive species are present that can undergo oxidation or reduction at the electrode holding potential, it is impossible to distinguish their corresponding components of the recorded signal. For this reason, precaution must be taken with amperometric measurements in mixed samples to ensure the identity of the released species through knowledge of cell type and neurotransmitter content from complementary techniques such as FSCV and liquid chromatography. Amperometry at carbon-fiber microelectrodes was first used at bovine chromaffin cells, providing the first direct chemical evidence of exocytosis (Leszczyszyn et al., 1990, 1991). The technique has since been applied to directly observe exocytosis at many cell types ranging from pancreatic β-cells to

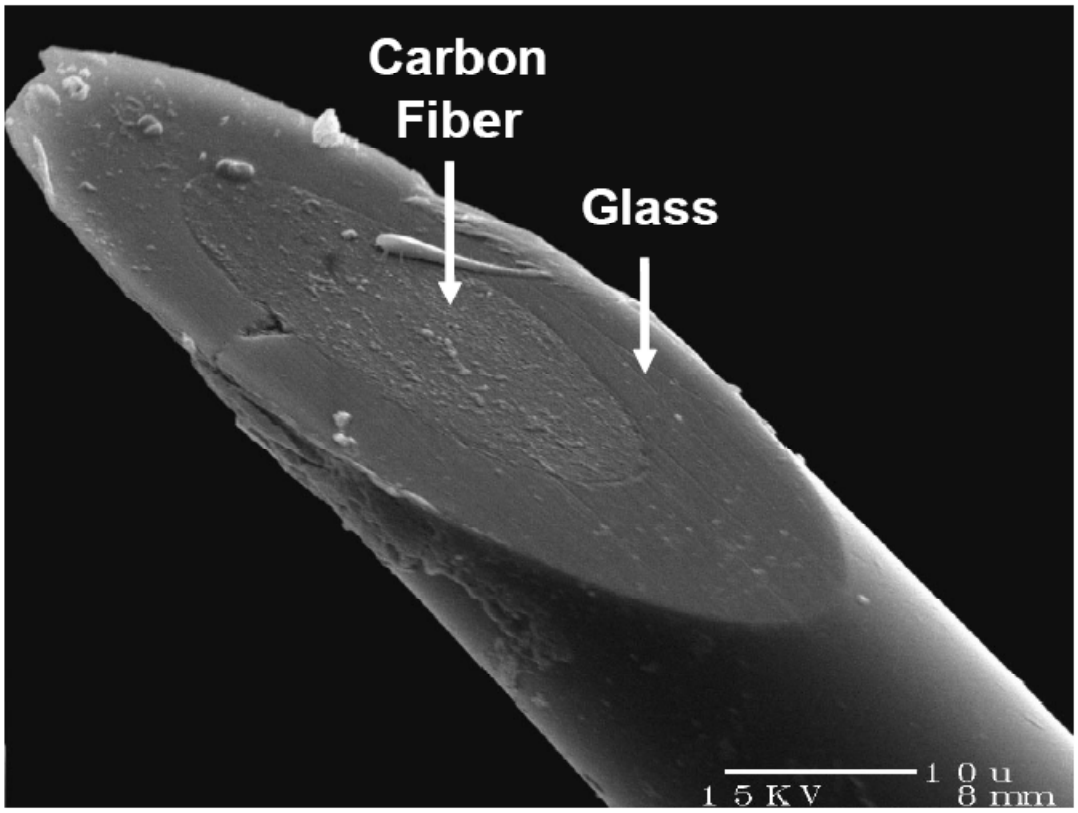

Figure 1.4. Electron micrograph of a disk carbon-fiber microelectrode. The carbon fiber is sealed in a glass capillary, and the electrode is beveled at 45 degrees to create a flat electroactive surface that can be positioned flush with the cell membrane.

neurons (Chen et al., 1994; Bruns and Jahn, 1995; Huang et al., 1995; Zhou and Misler, 1995).

Figure 1.5 (top panel) shows a typical experimental setup for amperometry at a single cell. The disk electrode is positioned flush with cell membrane, and exocytosis is induced via pressure ejection of chemical secretagogues from a nearby stimulating pipette. If the electrode is held at a potential sufficient to oxidize the released transmitter, a series of discrete current spikes are recorded (Figure 1.5, bottom panel). The individual spikes have been shown to correspond to the oxidation of molecules released from single vesicles (Wightman et al., 1991). By examining the number and frequency of current spikes along with the individual spike characteristics, much information can be revealed about the vesicular release mechanisms at target cells. For example, the total number and frequency of events in response to a stimulus can be used to probe the size of the RRP, efficiency of vesicle docking and fusion, the recycling of vesicles back into the RRP, and the mobilization of vesicles from the RP to the RRP.

Figure 1.6 shows an expanded view of an individual amperometric current spike. Spikes are generally characterized by a sharp rise in current, corresponding to a rapid flux of transmitter intro the extracellular space following vesicular fusion, and a more gradual decay to baseline (Schroeder et al., 1996). Additionally, pre-spike features known as feet may sometimes be observed (Chow et al., 1992). These features have been attributed to the leak of transmitter through the fusion pore intermediate that precedes full vesicular fusion. Individual spike characteristics that are commonly measured include the amplitude (I_{max}), halfwidth ($t_{1/2}$), rise time (t_r), decay time (t_d), and area (or quantal size, Q). Spike I_{max} values can be related to the maximal flux of transmitter during a fusion event. The kinetic parameters $t_{1/2}$, t_r, and t_d provide information on the time course of the extrusion of vesicular content following fusion. Spike area is directly related to the number of molecules electrolyzed at the electrode surface. For each spike, the integral of current with respect to

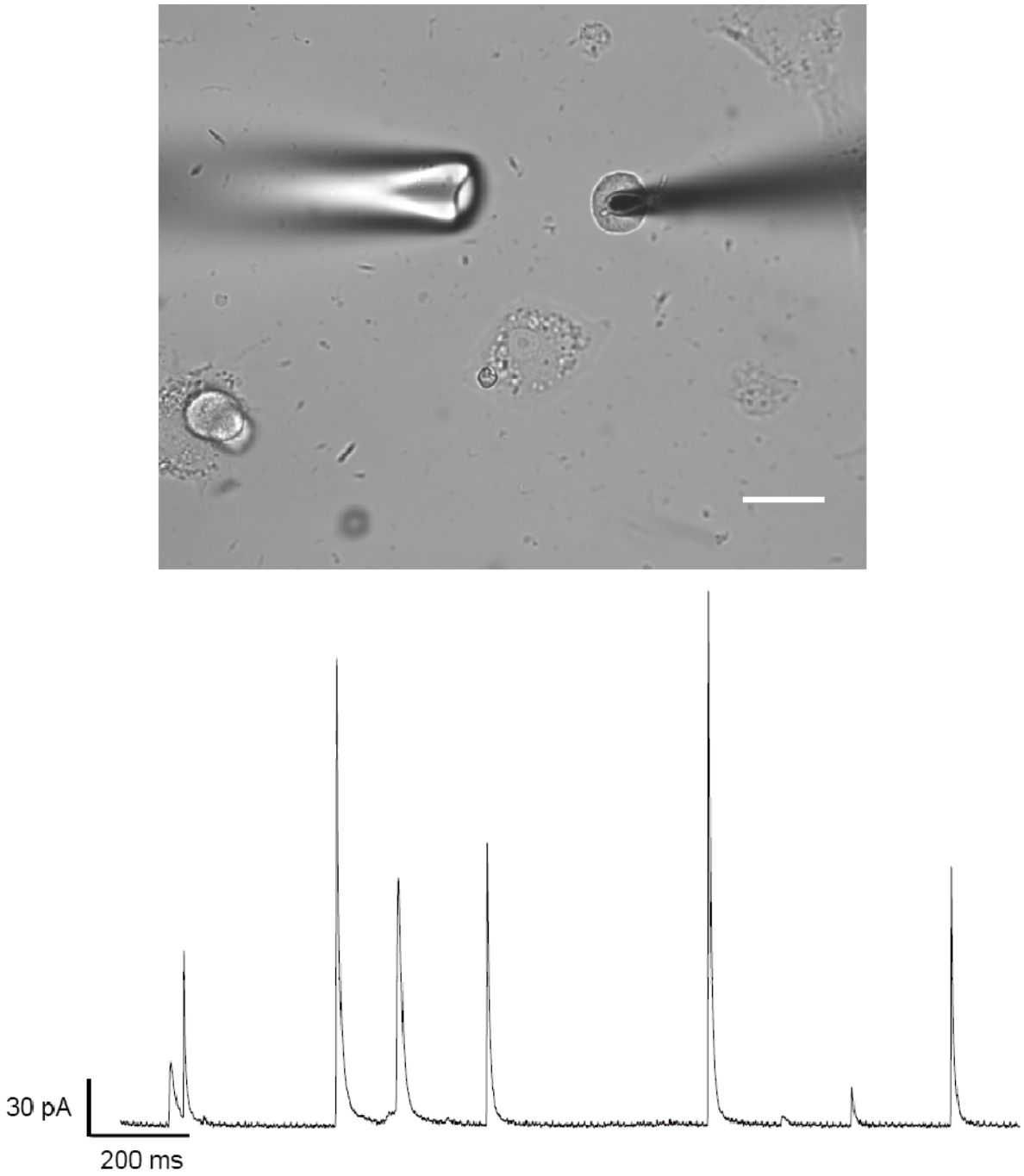

Figure 1.5. Amperometric measurements of exocytosis. Top panel: transmitted light micrograph showing typical experimental setup. The microelectrode (right) is lowered until it contacts the cell membrane. Exocytosis is triggered by pressure ejection of chemical secretagogues from a stim pipette (left) located 20 to 60 μm from the cell. Scale bar = 20 μm. Bottom panel: following stimulation, a series of discrete current spikes are observed at the electrode. Each spike represents the fusion of a single secretory vesicle. Trace is taken from a mouse chromaffin cell stimmed with 60 mM K^+.

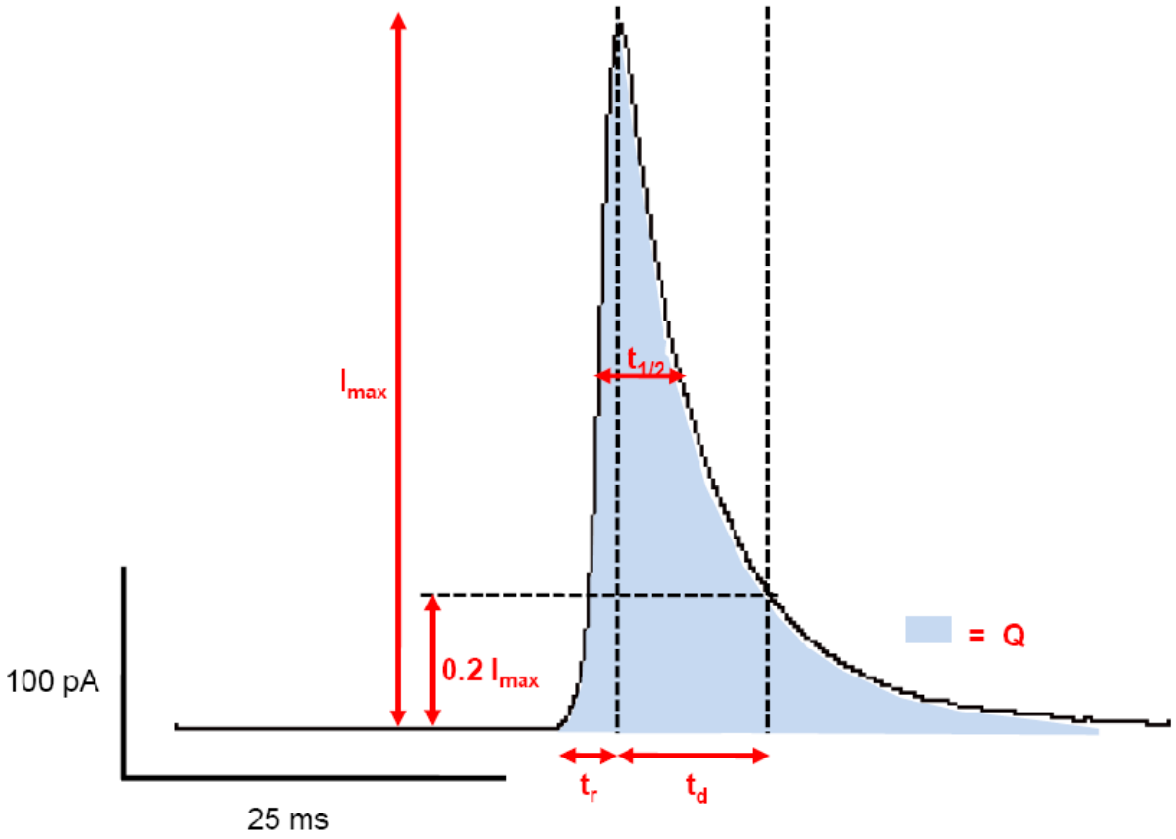

Figure 1.6. Individual amperometric spike characteristics. I_{max} is the peak current or amplitude of the spike. $t_{1/2}$ is the width at half height. t_r and t_d are the rise time and decay time, respectively. The area of the spike corresponds to the amount of transmitter released, also known as the quantal size (Q).

time yields the measured charge (Q, in coulombs), which is proportional to moles of analyte (m) by Faraday's law, Q = nFm, where n is the number of electrons involved in the electrochemical reaction and F is Faraday's constant.

Contrary to the expectations from the quantal hypothesis of neurotransmission, direct measurement of exocytosis with amperometry reveals that individual vesicular events are surprisingly nonuniform. Histograms of raw amperometric spike Q and $t_{1/2}$ data reveal non-Gaussian distributions heavily skewed towards smaller values with the means being larger than the modes (Finnegan et al., 1996; Pothos et al., 1998; Villanueva et al., 2006). If one assumes a uniform concentration of transmitter in the spherical vesicles, then the amperometric spike characteristics should depend on vesicular volume (Bekkers et al., 1990). Vesicle radii ($volume^{1/3}$) show a normal Gaussian distribution in most cells, suggesting that histograms of the cube roots of Q and $t_{1/2}$ should also show a Gaussian distribution. These cube root distributions are indeed Gaussian, with relative standard deviations approximating those for the vesicle radii (Finnegan et al., 1996).

Fast Scan Cyclic Voltammetry

In FSCV, the electrode potential is periodically scanned in a triangle waveform (Figure 1.7). Voltage limits are chosen such that oxidation and reduction of the analyte of interest occur within the potential window. The fast scan rates result in large background currents associated with charging of the double layer capacitance. Fortunately, these background currents are stable over short time periods, allowing the use of digital background subtraction to reveal the comparatively small Faradaic current resulting from oxidation and reduction of the analyte (Howell et al., 1986). The current amplitude is directly proportional to the local concentration of analyte at the electrode surface, with FSCV at carbon-fiber microelectrodes demonstrating nanomolar limits of detection (Cahill et al., 1996). The background-subtracted cyclic voltammogram (CV) is characteristic of the detected species, and the positions of the peak currents for oxidation and reduction and the

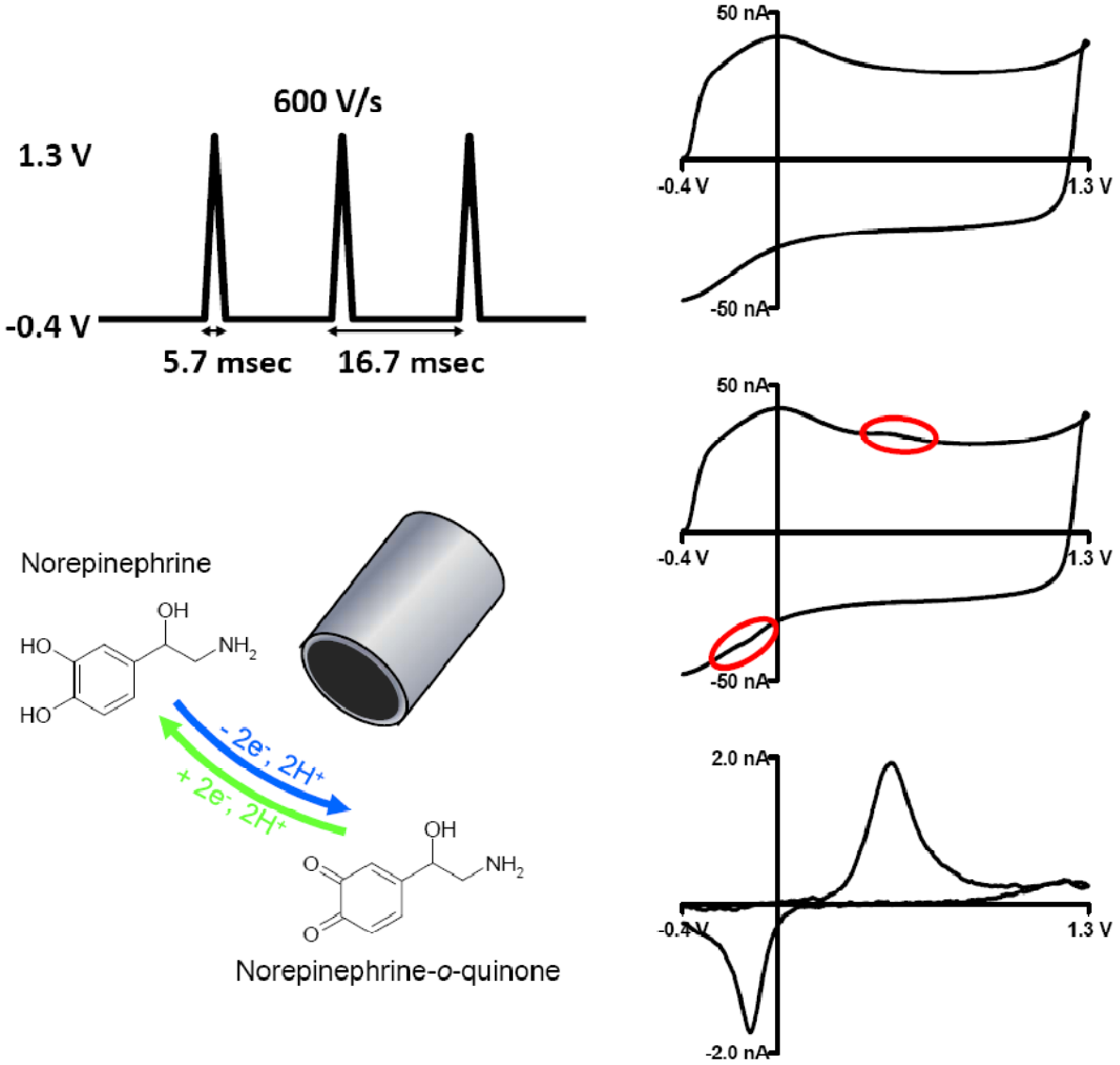

Figure 1.7. Fast scan cyclic voltammetry technique. In FSCV, a triangular waveform is applied to the electrode. In this example, the electrode is ramped linearly from -0.4 V to 1.3 V and back at 600 V/s. The waveform is applied at a frequency of 60 Hz. The analyte (norepinephrine in this case) is oxidized on the positive sweep and reduced on the negative sweep. By scanning at such fast rates, a large charging current is generated (top right). The small Faradaic currents generated from analyte oxidation and reduction are hard to distinguish in the presence of the charging current (middle right, red ovals). However, the charging background is stable over the time course of our experiments, and can be digitally subtracted to give the characteristic CV of the analyte (bottom right).

peak shapes can be used to distinguish between analytes (Heien et al., 2004). This chemical selectivity of FSCV has been exploited in studies of exocytosis at single cells where multiple chemical messengers are released. FSCV at carbon-fiber microelectrodes has been used to discriminate between vesicular release of E and NE at chromaffin cells (Pihel et al., 1994) and to detect release of histamine and serotonin at mast cells (Pihel et al., 1995). The latter providing the first direct evidence for corelease of chemical messengers from a single vesicle.

Figure 1.8 shows an example of the data obtained by monitoring exocytosis at single cells with FSCV. In this example, the potential at the electrode was scanned from -0.4 V to 1.3 V and back at 600 V/s to measure the secretion of NE and E from a chromaffin cell. With this waveform, the CVs for the two catecholamines are indistinguishable and the peak oxidation and reduction currents occur at 0.6 V and -0.2 V, respectively. In order to view multiple CVs simultaneously, FSCV data is generally presented in false color plots (Michael et al., 1998). By extracting the current at the peak oxidation potential from successive CVs, a current vs. time trace very similar to those from amperometric measurements can be obtained. As Figure 1.8 clearly shows, FSCV has sufficient temporal resolution to observe individual exocytotic events. However, when compared to an amperometric trace (Figure 1.5), it is obvious that the resolution is significantly diminished. This, again, is due to the fact that the temporal response in amperometry is limited only by mass transport and electron transfer kinetics. In FSCV, the temporal response is ultimately limited by the frequency at which the waveform is applied to the electrode. In this case, the frequency is 60 Hz, or one data point every 16.7 ms. Despite poorer kinetic information, the advantage to FSCV measurements of exocytosis is that the CV can be used to verify the chemical identity of the secreted species for each vesicular event. Thus, amperometry and FSCV can be viewed as complementary techniques, each vital to the study of exocytosis at single cells.

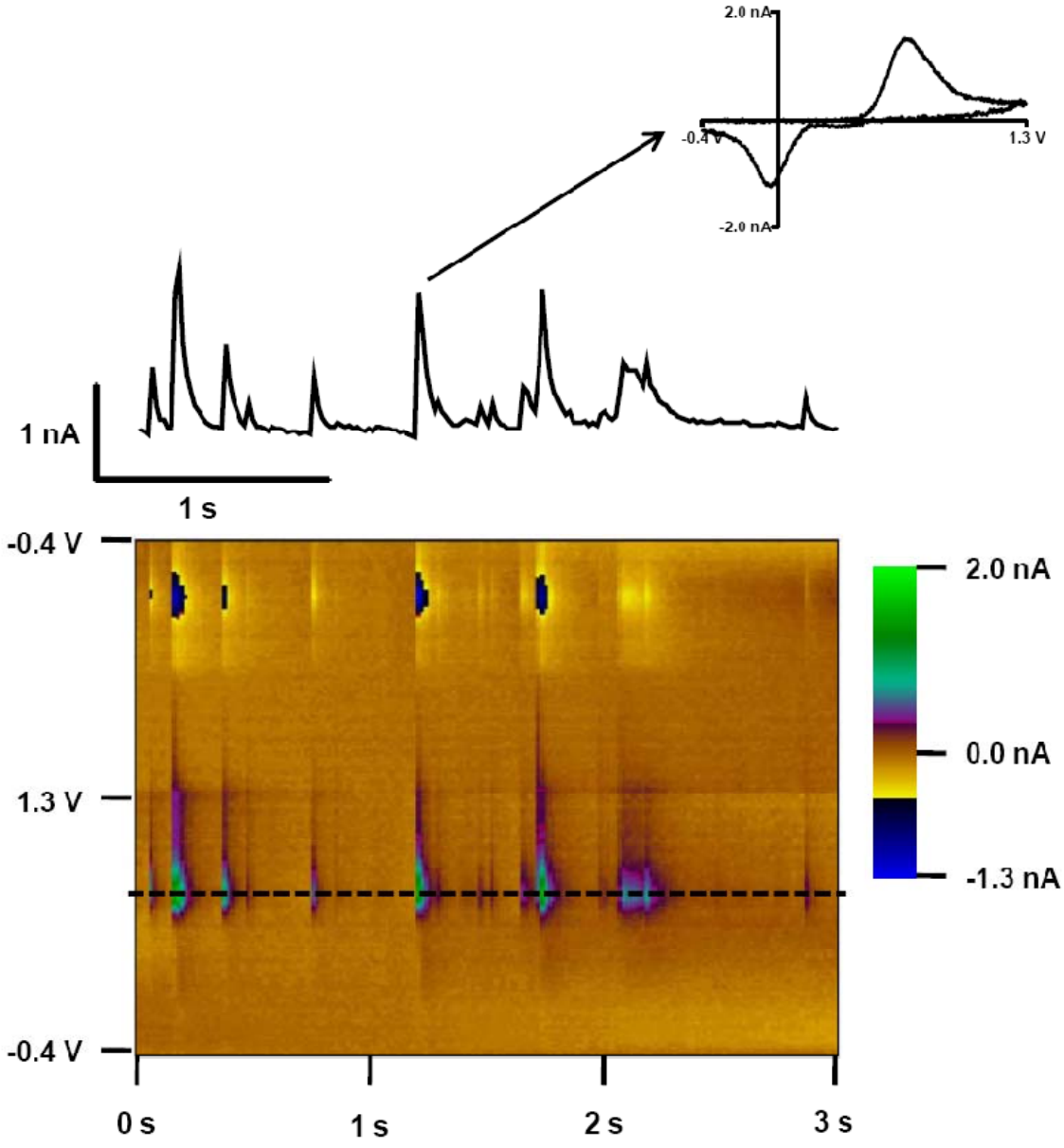

Figure 1.8. FSCV measurements of exocytosis. A 3 s time window of release from a mouse chromaffin cell stimulated with 60 mM K^+ is shown. The color plot (bottom) displays time on the x axis, voltage on the y axis and current in false color. Individual events are detectable by the color changes at the oxidation and reduction potentials of the analytes (in this case the catecholamines epinephrine and norepinephrine). From the color plot, a current versus time trace (top) can be extracted from the peak oxidation potential (dashed black line). CVs for individual events can be used to confirm the identity of the analyte (arrow).

Fluorescent Ca^{2+} Imaging

The fundamental role of Ca^{2+} in vesicular release makes real time monitoring of changes in $[Ca^{2+}]_i$ vital for a complete understanding of exocytosis. The development of the fura family of fluorescent Ca^{2+} indicators in the lab of Dr. Tsien has provided researchers with a simple tool for such measurements (Grynkiewicz et al., 1985). One of the primary advantages of fura dyes is their ability to be prepared as acetoxymethyl ester derivitives, rendering the hydrophillic dyes membrane permeable for easy loading into cells. In the cytosol, endogenous cellular esterases cleave the ester linkages effectively trapping the indicator inside the cell in its active form. Figure 1.9A shows the active forms of fura-2 and fura-FF. The addition of two fluorine atoms produces a near 40-fold decrease in Ca^{2+} affinity for fura-FF relative to fura-2. With Ca^{2+} dissociation constants (K_d) of 0.14 and 5.5 μM, respectively, both fura-2 and fura-FF are suitable for studying the transient changes in $[Ca^{2+}]_i$ accompanying exocytosis, where resting levels near 100 nM are rapidly increased to micromolar levels. However, fura-2 does exhibit limited sensitivity to $[Ca^{2+}]_i$ greater than 1 μM as these concentrations approach the edge of the dye's linear response window (approximately 0.1 to 10 x K_d).

Fura dyes bind Ca^{2+} in a 1:1 manner. The unbound indicator has a peak fluorescence excitation wavelength of 380 nm and a peak fluorescence emission wavelength of 510 nm (Figure 1.9B). Upon Ca^{2+} binding, the dye undergoes an absorption shift to 340 nm, while maintaining peak fluorescence emission at 510 nm (Figure 1.9B). Thus, by rapidly switching the excitation wavelength between 340 and 380 nm and monitoring emission at 510 nm, it is possible to obtain dynamic information on the ratio of bound to unbound dye inside the cell. The ability to perform ratiometric measurements significantly reduces the effects of differing cell thickness, uneven dye loading, dye leakage, photobleaching, and intensity of the excitation source; variables the must be accounted for in dyes utilizing only changes in fluorescence intensity upon binding (Moore et al., 1990).

A

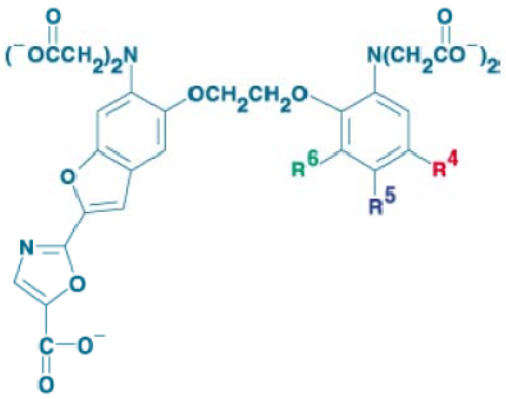

Indicator	$K_d(Ca^{2+})$	R^4	R^5	R^6
Fura-2	0.14 μM	H	CH_3	H
Fura-FF	5.50 μM	H	F	F

B

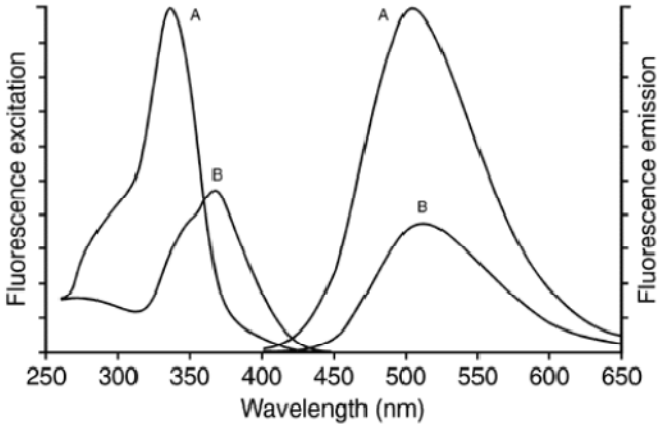

Figure 1.9. Structure and excitation spectra of fura Ca^{2+} dyes. **A.** Molecular structure of the active, cell-impermeant forms of fura-2 and fura-FF. **B.** Fluorescence excitation and emission spectra for fura-2 (fura-FF spectra are identical). Peak excitation wavelength for the Ca^{2+}-bound dye (trace A) is 340 nm. Peak excitation wavelength for the free dye (trace B) is 380 nm. Both species exhibit a peak emission wavelength of 510 nm. Images adapted from product manuals available via the manufacturer's website (http://www.invitrogen.com/site/us/en/home/brands/Molecular-Probes.html).

By calibrating the indicator in solutions of known $[Ca^{2+}]$, experimentally determined ratio values can be calibrated to $[Ca^{2+}]_i$ using the following equation:

$$[Ca^{2+}] = K_d \times \frac{R-R_{min}}{R_{max}-R} \times \frac{F_{380max}}{F_{380min}} \quad (1)$$

where K_d is the dissociation constant, R is the experimentally observed ratio, R_{min} is the ratio measured in a Ca^{2+}-free solution, R_{max} is the ratio measured in a solution of dye-saturating $[Ca^{2+}]$, F_{380max} is the fluorescence observed with 380 nm excitation in a Ca^{2+}-free solution, and F_{380min} is the fluorescence observed with 380 nm excitation in a solution of dye-saturating $[Ca^{2+}]$. This equation assumes that the fluorescent properties and the Ca^{2+} affinity of the dye are similar in both the calibration solutions and the cell cytosol.

Several important limitations have been addressed in the use of fura dyes for measurement of $[Ca^{2+}]_i$ (Roe et al., 1990). These include incomplete hydrolysis of acetoxymethyl ester bonds by cytosolic esterases, sequestration of fura dyes in intracellular organelles, quenching of fluorescence by heavy metals, active and passive dye loss from loaded cells, enhanced cytosolic Ca^{2+} buffering at high concentrations of the dye (≥100 μM), and shifts in the K_d for Ca^{2+} as a function of the viscosity, ionic strength, and temperature of the dye environment. However, through careful control of experimental conditions and dye concentrations, fura dyes can be readily used for accurate determinations of real time changes in $[Ca^{2+}]_i$ during exocytosis.

High Performance Liquid Chromatography

High performance liquid chromatography (HPLC) with electrochemical detection can be used as a valuable supplement to the real time measurement of vesicular release events at single cells with amperometry or FSCV. The high selectivity and sensitivity of this separation method allow for the simultaneous determination of multiple neurotransmitters and metabolites in biologically complex mixtures such as tissue samples, individual cells, and extracellular media. The initial experiments in this field used open tubular liquid

chromatography with electrochemical detection to quantitatively determine the presence of dopamine, serotonin, tyrosine, and tryptophan at the femtomolar level in single cells of the land snail, *Helix aspersa* (Kennedy and Jorgenson, 1989). Further experiments utilized reverse phase HPLC with packed microcolumns to quantitate both the E and NE content of and secretion from individual bovine chromaffin cells and to measure the histamine and serotonin content of single rat peritoneal mast cells (Cooper et al., 1992; Cooper et al., 1994; Pihel et al., 1995). The switch from open tubular columns to packed microcolumns permitted greater retention and separation, of polar compounds like the catecholamines. Combining HPLC determination of cellular neurotransmitter content with amperometric or FSCV measurement of vesicular events at single cells provides a more complete understanding of the related processes of transmitter synthesis, storage, and release by exocytosis.

Dissertation Overview

The following chapters discuss the use of the electrochemical and supporting techniques described above to study exocytosis at single cells. In Chapter 2, amperometry and fluorescent Ca^{2+} imaging at isolated midbrain dopamine neurons were used to examine the cellular mechanisms behind somatodendritic dopamine release. Chapters 3 and 4 both describe collaborative efforts to investigate potential changes in regulated exocytosis at several transgenic mouse lines. FSCV, amperometry, and fluorescent Ca^{2+} imaging were used to characterize biogenic amine release in mice lacking the mitochondrial uncoupling protein UCP2 and in mouse models of obesity and fragile X syndrome. Chapter 5 describes the electrochemistry of three trace amines at carbon-fiber microelectrodes using FSCV. The FSCV techniques developed in Chapter 5 were then employed in Chapter 6 to explore the potential utility of these trace amines as false catecholamine transmitters.

References

Amatore C, Maisonhaute E (2005) When voltammetry reaches nanoseconds. Anal Chem 77:303A-311A.

Amatore C, Arbault S, Guille M, Lemaitre F (2008) Electrochemical monitoring of single cell secretion: vesicular exocytosis and oxidative stress. Chem Rev 108:2585-2621.

Araki S, Kikuchi A, Hata Y, Isomura M, Takai Y (1990) Regulation of reversible binding of smg p25A, a ras p21-like GTP-binding protein, to synaptic plasma membranes and vesicles by its specific regulatory protein, GDP dissociation inhibitor. J Biol Chem 265:13007-13015.

Bahler M, Greengard P (1987) Synapsin I bundles F-actin in a phosphorylation-dependent manner. Nature 326:704-707.

Bath BD, Michael DJ, Trafton BJ, Joseph JD, Runnels PL, Wightman RM (2000) Subsecond adsorption and desorption of dopamine at carbon-fiber microelectrodes. Anal Chem 72:5994-6002.

Becherer U, Moser T, Stuhmer W, Oheim M (2003) Calcium regulates exocytosis at the level of single vesicles. Nat Neurosci 6:846-853.

Bekkers JM, Richerson GB, Stevens CF (1990) Origin of variability in quantal size in cultured hippocampal neurons and hippocampal slices. Proc Natl Acad Sci U S A 87:5359-5362.

Bellocchio EE, Reimer RJ, Fremeau RT, Jr., Edwards RH (2000) Uptake of glutamate into synaptic vesicles by an inorganic phosphate transporter. Science 289:957-960.

Benfenati F, Bahler M, Jahn R, Greengard P (1989a) Interactions of synapsin I with small synaptic vesicles: distinct sites in synapsin I bind to vesicle phospholipids and vesicle proteins. J Cell Biol 108:1863-1872.

Benfenati F, Greengard P, Brunner J, Bahler M (1989b) Electrostatic and hydrophobic interactions of synapsin I and synapsin I fragments with phospholipid bilayers. J Cell Biol 108:1851-1862.

Benfenati F, Valtorta F, Chieregatti E, Greengard P (1992) Interaction of free and synaptic vesicle-bound synapsin I with F-actin. Neuron 8:377-386.

Borst JG, Sakmann B (1996) Calcium influx and transmitter release in a fast CNS synapse. Nature 383:431-434.

Bruns D, Jahn R (1995) Real-time measurement of transmitter release from single synaptic vesicles. Nature 377:62-65.

Burgoyne RD, Cheek TR (1987) Reorganisation of peripheral actin filaments as a prelude to exocytosis. Biosci Rep 7:281-288.

Burgoyne RD, Morgan A (2003) Secretory granule exocytosis. Physiol Rev 83:581-632.

Cahill PS, Walker QD, Finnegan JM, Mickelson GE, Travis ER, Wightman RM (1996) Microelectrodes for the measurement of catecholamines in biological systems. Anal Chem 68:3180-3186.

Chaudhry FA, Edwards RH, Fonnum F (2008) Vesicular neurotransmitter transporters as targets for endogenous and exogenous toxic substances. Annu Rev Pharmacol Toxicol 48:277-301.

Chen TK, Luo G, Ewing AG (1994) Amperometric monitoring of stimulated catecholamine release from rat pheochromocytoma (PC12) cells at the zeptomole level. Anal Chem 66:3031-3035.

Chi P, Greengard P, Ryan TA (2003) Synaptic vesicle mobilization is regulated by distinct synapsin I phosphorylation pathways at different frequencies. Neuron 38:69-78.

Chow RH, von Ruden L, Neher E (1992) Delay in vesicle fusion revealed by electrochemical monitoring of single secretory events in adrenal chromaffin cells. Nature 356:60-63.

Cooper BR, Wightman RM, Jorgenson JW (1994) Quantitation of epinephrine and norepinephrine secretion from individual adrenal medullary cells by microcolumn high-performance liquid chromatography. J Chromatogr B Biomed Appl 653:25-34.

Cooper BR, Jankowski JA, Leszczyszyn DJ, Wightman RM, Jorgenson JW (1992) Quantitative determination of catecholamines in individual bovine adrenomedullary cells by reversed-phase microcolumn liquid chromatography with electrochemical detection. Anal Chem 64:691-694.

De Camilli P, Benfenati F, Valtorta F, Greengard P (1990) The synapsins. Annu Rev Cell Biol 6:433-460.

Deak F, Xu Y, Chang WP, Dulubova I, Khvotchev M, Liu X, Sudhof TC, Rizo J (2009) Munc18-1 binding to the neuronal SNARE complex controls synaptic vesicle priming. J Cell Biol 184:751-764.

Erickson JD, Eiden LE, Hoffman BJ (1992) Expression cloning of a reserpine-sensitive vesicular monoamine transporter. Proc Natl Acad Sci U S A 89:10993-10997.

Erickson JD, Schafer MK, Bonner TI, Eiden LE, Weihe E (1996) Distinct pharmacological properties and distribution in neurons and endocrine cells of two isoforms of the human vesicular monoamine transporter. Proc Natl Acad Sci U S A 93:5166-5171.

Fernandez-Chacon R, Konigstorfer A, Gerber SH, Garcia J, Matos MF, Stevens CF, Brose N, Rizo J, Rosenmund C, Sudhof TC (2001) Synaptotagmin I functions as a calcium regulator of release probability. Nature 410:41-49.

Finnegan JM, Pihel K, Cahill PS, Huang L, Zerby SE, Ewing AG, Kennedy RT, Wightman RM (1996) Vesicular quantal size measured by amperometry at chromaffin, mast, pheochromocytoma, and pancreatic beta-cells. J Neurochem 66:1914-1923.

Fremeau RT, Jr., Troyer MD, Pahner I, Nygaard GO, Tran CH, Reimer RJ, Bellocchio EE, Fortin D, Storm-Mathisen J, Edwards RH (2001) The expression of vesicular

glutamate transporters defines two classes of excitatory synapse. Neuron 31:247-260.

Fremeau RT, Jr., Burman J, Qureshi T, Tran CH, Proctor J, Johnson J, Zhang H, Sulzer D, Copenhagen DR, Storm-Mathisen J, Reimer RJ, Chaudhry FA, Edwards RH (2002) The identification of vesicular glutamate transporter 3 suggests novel modes of signaling by glutamate. Proc Natl Acad Sci U S A 99:14488-14493.

Fujita T (1977) Concept of paraneurons. Arch Histol Jpn 40 Suppl:1-12.

Garcia AG, Garcia-De-Diego AM, Gandia L, Borges R, Garcia-Sancho J (2006) Calcium signaling and exocytosis in adrenal chromaffin cells. Physiol Rev 86:1093-1131.

Grynkiewicz G, Poenie M, Tsien RY (1985) A new generation of Ca2+ indicators with greatly improved fluorescence properties. J Biol Chem 260:3440-3450.

Gunter TE, Pfeiffer DR (1990) Mechanisms by which mitochondria transport calcium. Am J Physiol 258:C755-786.

Hanson PI, Roth R, Morisaki H, Jahn R, Heuser JE (1997) Structure and conformational changes in NSF and its membrane receptor complexes visualized by quick-freeze/deep-etch electron microscopy. Cell 90:523-535.

Harata NC, Aravanis AM, Tsien RW (2006) Kiss-and-run and full-collapse fusion as modes of exo-endocytosis in neurosecretion. J Neurochem 97:1546-1570.

Hata Y, Slaughter CA, Sudhof TC (1993) Synaptic vesicle fusion complex contains unc-18 homologue bound to syntaxin. Nature 366:347-351.

Heien ML, Johnson MA, Wightman RM (2004) Resolving neurotransmitters detected by fast-scan cyclic voltammetry. Anal Chem 76:5697-5704.

Hosaka M, Sudhof TC (1998a) Synapsin III, a novel synapsin with an unusual regulation by Ca2+. J Biol Chem 273:13371-13374.

Hosaka M, Sudhof TC (1998b) Synapsins I and II are ATP-binding proteins with differential Ca2+ regulation. J Biol Chem 273:1425-1429.

Howell JO, Kuhr WG, Ensman RE, Mark Wightman R (1986) Background subtraction for rapid scan voltammetry. Journal of Electroanalytical Chemistry 209:77-90.

Huang L, Shen H, Atkinson MA, Kennedy RT (1995) Detection of exocytosis at individual pancreatic beta cells by amperometry at a chemically modified microelectrode. Proc Natl Acad Sci U S A 92:9608-9612.

Jahn R, Lang T, Sudhof TC (2003) Membrane fusion. Cell 112:519-533.

Johnston PA, Archer BT, 3rd, Robinson K, Mignery GA, Jahn R, Sudhof TC (1991) rab3A attachment to the synaptic vesicle membrane mediated by a conserved polyisoprenylated carboxy-terminal sequence. Neuron 7:101-109.

Kawagoe KT, Zimmerman JB, Wightman RM (1993) Principles of voltammetry and microelectrode surface states. J Neurosci Methods 48:225-240.

Kennedy RT, Jorgenson JW (1989) Quantitative analysis of individual neurons by open tubular liquid chromatography with voltammetric detection. Anal Chem 61:436-441.

Leszczyszyn DJ, Jankowski JA, Viveros OH, Diliberto EJ, Jr., Near JA, Wightman RM (1990) Nicotinic receptor-mediated catecholamine secretion from individual chromaffin cells. Chemical evidence for exocytosis. J Biol Chem 265:14736-14737.

Leszczyszyn DJ, Jankowski JA, Viveros OH, Diliberto EJ, Jr., Near JA, Wightman RM (1991) Secretion of catecholamines from individual adrenal medullary chromaffin cells. J Neurochem 56:1855-1863.

Liu Y, Peter D, Roghani A, Schuldiner S, Prive GG, Eisenberg D, Brecha N, Edwards RH (1992) A cDNA that suppresses MPP+ toxicity encodes a vesicular amine transporter. Cell 70:539-551.

Livett BG (1984) Adrenal medullary chromaffin cells in vitro. Physiol Rev 64:1103-1161.

Llinas R, Sugimori M, Silver RB (1992) Microdomains of high calcium concentration in a presynaptic terminal. Science 256:677-679.

Maycox PR, Deckwerth T, Hell JW, Jahn R (1988) Glutamate uptake by brain synaptic vesicles. Energy dependence of transport and functional reconstitution in proteoliposomes. J Biol Chem 263:15423-15428.

McIntire SL, Reimer RJ, Schuske K, Edwards RH, Jorgensen EM (1997) Identification and characterization of the vesicular GABA transporter. Nature 389:870-876.

Meinrenken CJ, Borst JG, Sakmann B (2003) Local routes revisited: the space and time dependence of the Ca2+ signal for phasic transmitter release at the rat calyx of Held. J Physiol 547:665-689.

Michael D, Travis ER, Wightman RM (1998) Color images for fast-scan CV measurements in biological systems. Anal Chem 70:586A-592A.

Moore ED, Becker PL, Fogarty KE, Williams DA, Fay FS (1990) Ca2+ imaging in single living cells: theoretical and practical issues. Cell Calcium 11:157-179.

Morgan A, Burgoyne RD (1997) Common mechanisms for regulated exocytosis in the chromaffin cell and the synapse. Semin Cell Dev Biol 8:141-149.

Neher E (1998) Vesicle pools and Ca2+ microdomains: new tools for understanding their roles in neurotransmitter release. Neuron 20:389-399.

Perin MS, Fried VA, Mignery GA, Jahn R, Sudhof TC (1990) Phospholipid binding by a synaptic vesicle protein homologous to the regulatory region of protein kinase C. Nature 345:260-263.

Pihel K, Schroeder TJ, Wightman RM (1994) Rapid and Selective Cyclic Voltammetric Measurements of Epinephrine and Norepinephrine as a Method To Measure Secretion from Single Bovine Adrenal Medullary Cells. Analytical Chemistry 66:4532-4537.

Pihel K, Hsieh S, Jorgenson JW, Wightman RM (1995) Electrochemical detection of histamine and 5-hydroxytryptamine at isolated mast cells. Anal Chem 67:4514-4521.

Pothos EN, Davila V, Sulzer D (1998) Presynaptic recording of quanta from midbrain dopamine neurons and modulation of the quantal size. J Neurosci 18:4106-4118.

Pothos EN, Larsen KE, Krantz DE, Liu Y, Haycock JW, Setlik W, Gershon MD, Edwards RH, Sulzer D (2000) Synaptic vesicle transporter expression regulates vesicle phenotype and quantal size. J Neurosci 20:7297-7306.

Rizzoli SO, Betz WJ (2005) Synaptic vesicle pools. Nat Rev Neurosci 6:57-69.

Rizzuto R, Bernardi P, Pozzan T (2000) Mitochondria as all-round players of the calcium game. J Physiol 529 Pt 1:37-47.

Rodriguez Del Castillo A, Lemaire S, Tchakarov L, Jeyapragasan M, Doucet JP, Vitale ML, Trifaro JM (1990) Chromaffin cell scinderin, a novel calcium-dependent actin filament-severing protein. Embo J 9:43-52.

Roe MW, Lemasters JJ, Herman B (1990) Assessment of Fura-2 for measurements of cytosolic free calcium. Cell Calcium 11:63-73.

Roghani A, Feldman J, Kohan SA, Shirzadi A, Gundersen CB, Brecha N, Edwards RH (1994) Molecular cloning of a putative vesicular transporter for acetylcholine. Proc Natl Acad Sci U S A 91:10620-10624.

Rybin V, Ullrich O, Rubino M, Alexandrov K, Simon I, Seabra MC, Goody R, Zerial M (1996) GTPase activity of Rab5 acts as a timer for endocytic membrane fusion. Nature 383:266-269.

Sagne C, El Mestikawy S, Isambert MF, Hamon M, Henry JP, Giros B, Gasnier B (1997) Cloning of a functional vesicular GABA and glycine transporter by screening of genome databases. FEBS Lett 417:177-183.

Schiebler W, Jahn R, Doucet JP, Rothlein J, Greengard P (1986) Characterization of synapsin I binding to small synaptic vesicles. J Biol Chem 261:8383-8390.

Schroeder TJ, Jankowski JA, Senyshyn J, Holz RW, Wightman RM (1994) Zones of exocytotic release on bovine adrenal medullary cells in culture. J Biol Chem 269:17215-17220.

Schroeder TJ, Borges R, Finnegan JM, Pihel K, Amatore C, Wightman RM (1996) Temporally resolved, independent stages of individual exocytotic secretion events. Biophys J 70:1061-1068.

Smith SM, Renden R, von Gersdorff H (2008) Synaptic vesicle endocytosis: fast and slow modes of membrane retrieval. Trends Neurosci 31:559-568.

Sollner T, Whiteheart SW, Brunner M, Erdjument-Bromage H, Geromanos S, Tempst P, Rothman JE (1993) SNAP receptors implicated in vesicle targeting and fusion. Nature 362:318-324.

Squire LR (2008) Fundamental neuroscience, 3rd Edition. Amsterdam ; Boston: Academic Press/Elsevier.

Sudhof TC (2004) The synaptic vesicle cycle. Annu Rev Neurosci 27:509-547.

Takamori S, Rhee JS, Rosenmund C, Jahn R (2000) Identification of a vesicular glutamate transporter that defines a glutamatergic phenotype in neurons. Nature 407:189-194.

Verkhratsky A (2004) Endoplasmic reticulum calcium signaling in nerve cells. Biol Res 37:693-699.

Villanueva M, Thornley K, Augustine GJ, Wightman RM (2006) Synapsin II negatively regulates catecholamine release. Brain Cell Biol 35:125-136.

Wang YM, Gainetdinov RR, Fumagalli F, Xu F, Jones SR, Bock CB, Miller GW, Wightman RM, Caron MG (1997) Knockout of the vesicular monoamine transporter 2 gene results in neonatal death and supersensitivity to cocaine and amphetamine. Neuron 19:1285-1296.

Weber T, Zemelman BV, McNew JA, Westermann B, Gmachl M, Parlati F, Sollner TH, Rothman JE (1998) SNAREpins: minimal machinery for membrane fusion. Cell 92:759-772.

Wightman RM, Jankowski JA, Kennedy RT, Kawagoe KT, Schroeder TJ, Leszczyszyn DJ, Near JA, Diliberto EJ, Jr., Viveros OH (1991) Temporally resolved catecholamine spikes correspond to single vesicle release from individual chromaffin cells. Proc Natl Acad Sci U S A 88:10754-10758.

Xu J, Mashimo T, Sudhof TC (2007) Synaptotagmin-1, -2, and -9: Ca(2+) sensors for fast release that specify distinct presynaptic properties in subsets of neurons. Neuron 54:567-581.

Zhou Z, Misler S (1995) Amperometric detection of stimulus-induced quantal release of catecholamines from cultured superior cervical ganglion neurons. Proc Natl Acad Sci U S A 92:6938-6942.

Chapter 2

Origins of Extrasynaptic Dopamine Release

Introduction

In the classical model of neurotransmission, electrochemical signals are propagated in a unidirectional manner: a neuron receives information from incoming synaptic terminals at its dendrites, processes the information at the cell body, and then passes the information down its axon to terminals that form synapses with the next cell in the pathway. Over the past few decades the classical model has been shown to be incomplete, as a wealth of evidence has accumulated demonstrating that the somatodendritic region of neurons is capable of synthesizing, storing, and releasing chemical neurotransmitters.

As far back as 1975, glyoxylic acid-induced histofluorescence was used to show the accumulation and storage of dopamine in the dendrites of substantia nigra (SN) neurons (Bjorklund and Lindvall, 1975). Similar to the storage of dopamine at axon terminals, this accumulation was blocked by reserpine, an inhibitor of the vesicular monoamine transporter (VMAT2). Shortly thereafter, experiments with radio-labeled dopamine revealed both spontaneous and depolarization-evoked release in the SN from *in vivo* and *in vitro* preparations (Geffen et al., 1976; Nieoullon et al., 1977). More recently, electrochemical techniques have been used to make direct, real-time measurements of dopamine release in somatodendritic regions. Amperometry has been used to detect quantal release events from the cell bodies of SN neurons in slices of rat brain (Jaffe et al., 1998), while fast scan cyclic voltammetry (FSCV) has been used to characterize dopamine release in the ventral

tegmental area (VTA) of anesthetized rats and in the SN and VTA of rodent brain slices (Rice et al., 1994; Rice et al., 1997; John and Jones, 2006; Kita et al., 2009).

Much effort has been put into understanding the mechanisms that control somatodendritic dopamine release. At this point, however, debate remains as to whether the well-studied, Ca^{2+}-dependent exocytotic release of neurotransmitters from axon terminals is also responsible for transmitter release in somatodendritic regions. Compared to axon terminals, the cell bodies and dendrites of dopaminergic neurons contain a sparse number of vesicles (Wilson et al., 1977; Wassef et al., 1981; Groves and Linder, 1983; Nirenberg et al., 1996b, 1997). Somatodendritic dopamine may be stored primarily in the smooth endoplasmic reticulum (SER) (Mercer et al., 1979). Supporting this notion, in dendrites of dopamine neurons VMAT2 has been shown to localize primarily to tubulovesicles resembling saccules of SER and to a lesser extent to synaptic vesicles (Nirenberg et al., 1996b).

At axon terminals, invading axon potentials trigger exocytosis via the opening of voltage-gated calcium channels (VGCCs). Similarly, somatodendritic release of dopamine has been shown to depend on an influx of extracellular Ca^{2+} (Rice et al., 1997; Bergquist et al., 1998; Chen and Rice, 2001; Beckstead et al., 2004). Interestingly though, somatodendritic release persists at low extracellular Ca^{2+} levels insufficient to support release at axon terminals (Hoffman and Gerhardt, 1999; Chen and Rice, 2001). In addition, while dopamine release at axon terminals appears to be mainly dependent on N- and P/Q-type VGCCs, release at dendrites seems to be supported by either R-type or minimal Ca^{2+} entry through multiple VGCCs (Bergquist et al., 1998; Bergquist and Nissbrandt, 2003; Chen et al., 2006). Backpropagation of action potentials through the dendritic tree has been demonstrated for dopaminergic neurons *in vitro* (Hausser et al., 1995), and may serve as the primary trigger for Ca^{2+} influx. However, reports have also shown the existence of Ca^{2+} conductances in dopaminergic dendrites that occur independent of Na^{+} channels opening

(Llinas et al., 1984; Hounsgaard et al., 1992); thus clouding the dependence of somatodendritic release on dopamine neuron firing.

One alternative to a vesicular, Ca^{2+}-mediated mechanism of somatodendritic release is reversal of the dopamine transporter (DAT). DAT has been shown to localize to both the plasma membrane and SER in dendrites of dopamine neurons in the SN (Nirenberg et al., 1996a). Several findings suggest that at least a portion of somatodendritic dopamine release arises from the Ca^{2+}-independent reversal of DAT (Elverfors et al., 1997; Hoffman and Gerhardt, 1999; Falkenburger et al., 2001). However, there are also literature examples showing that inhibition of DAT leads to increased dendritic release of dopamine (Cragg et al., 1997; Hoffman et al., 1998). Furthermore, basal and stimulus-induced dendritic dopamine release has been shown to depend on SNARE proteins (Bergquist et al., 2002; Fortin et al., 2006). SNAREs mediate fusion of intracellular vesicles with the plasma membrane, and their involvement would naturally suggest an exocytotic mechanism as opposed to reversal of DAT.

This chapter describes an investigation of the biochemical origin of somatodendritic dopamine release via amperometric measurements at isolated neurons. To aid in the identification of dopaminergic neurons, cells were harvested from transgenic mice that coexpress enhanced green fluorescent protein (GFP) in all cells that express tyrosine hydroxlase (TH), the rate-limiting enzyme in dopamine synthesis. Amperometric recordings from the cell bodies of acutely dissociated midbrain dopamine neurons revealed discrete current spikes that were dependent on extracellular Ca^{2+}, hallmark indications of exocytosis. Two vesicular populations were observed, with a majority of very rapid quantal events having single rising and falling phases and a minority of broader events sometimes having multiple rising and/or falling phases. Amperometric recordings at chromaffin cells from both wild type (WT) and TH-GFP mice suggest that the exocytotic machinery was not significantly affected by expression of the GFP reporter gene.

Materials and Methods

Animals

Mice were handled in accordance with the guidelines set forth by the Institutional Animal Care and Use Committee (IACUC) at UNC-Chapel Hill. C57BL/6J mice (WT) were obtained from The Jackson Library (Bar Harbor, ME). A TH-GFP breeding pair was generously provided by Dr. Lorraine Iacovitti at Thomas Jefferson University, and a colony was maintained locally. These mice were generated on a C57BL/6J background and coexpress GFP in TH-positive cells (Kessler et al., 2003).

Preparation Acutely Dissociated Midbrain Neurons

Acutely dissociated midbrain dopaminergic neurons were prepared as previously described (Puopolo et al., 2007), with slight modification. A P12-P18 mouse pup was deeply anesthetized with ether, decapitated, and the brain rapidly removed into ice-cold, oxygenated dissociation medium containing (in mM): 82 Na_2SO_4, 30 K_2SO_4, 5 $MgCl_2$, 10 glucose, 10 HEPES, and 0.001 % phenol red, pH adjusted to 7.4 with NaOH. 400 µm thick coronal sections containing the midbrain were obtained using a vibrating tissue slicer (World Precision Instruments, Sarasota, FL). Regions containing the SN and VTA were dissected out, and the pooled tissue was digested for 40 min at 37 ^{o}C in dissociation medium with 3 mg/mL protease type XXIII. Digested tissue was washed and triturated with fire-polished Pasteur pipette tips of decreasing bore size in dissociation medium with 1 mg/mL each BSA and trypsin inhibitor. Cells were pelleted at 1000 rpm for 5 min, resuspended in 300 µL Dulbecco's Modified Eagle's Medium/Nutrient Mixture F-12 Ham (DMEM/F12), and distributed evenly to 3 concanavalin A-coated (1 mg/mL) 25 mm round glass coverslips. After 15 min attachment plates were fed with 2 mL DMEM/F12 and maintained in a humidified, 5 % CO_2 atmosphere at 37 ^{o}C for at least 1 h prior to experimentation. For neuronal preps seeded on glial monolayers, preparation of cortical astrocyte monolayers

was performed as previously described (Pothos et al., 1998). Glial cells were maintained in culture for 2-3 weeks prior to use.

Preparation Adrenal Medullary Chromaffin Cells

Murine chromaffin cells were prepared as previously described (Kolski-Andreaco et al., 2007) with some modifications. A female mouse, 4-8 weeks old, was deeply anesthetized with ether, decapitated, and the adrenal glands rapidly removed into ice-cold, oxygenated Ca^{2+} and Mg^{2+}-free Locke's buffer containing (in mM): 154 NaCl, 3.6 KCl, 5.6 $NaHCO_3$, 5.6 glucose, and 10 HEPES, pH adjusted to 7.2 with NaOH. The medullae were isolated via gentle removal of cortical tissue and digested for 20 min at 37 ^oC in DMEM/F12 with 25 U/mL papain. The digestion media was replaced with a fresh aliquot, followed by a second 20 min digestion period. Digested tissue was washed and triturated with pipette tips of decreasing bore size in 500 µL DMEM/F12 with 10 % fetal bovine serum and 2 % horse serum. The resulting cell suspension was distributed evenly to 3 poly-L-lysine-coated (0.1 mg/mL) 25 mm round glass coverslips. After 15 min attachment plates were fed with 2 mL DMEM/F12 containing 100 U/mL penicillin, 0.1 mg/mL streptomycin, 50 U/mL nystatin, and 40 µg/mL gentamicin. Plates were maintained in a humidified, 5 % CO_2 atmosphere at 37 ^oC for at least 24 h prior to experimentation.

Electrodes and Electrochemistry

Disk carbon-fiber microelectrodes were prepared using T650 carbon fibers (6 µm diameter, Amoco, Greenville, SC) as previously described (Kawagoe et al., 1993). Fibers were aspirated into glass capillaries (A-M Systems, Sequim, WA), and a vertical pipette puller (Narishige, Long Island, NY) was used to seal the glass around the carbon fiber. Carbon fibers were cut at the glass seal, which was then reinforced with epoxy (15 % m-phenylenediamine in Epon 828 resin (Miller-Stephenson, Danbury, CT) heated to between 80 and 90 ^oC). Electrodes were kept at room temperature overnight, and then the epoxy was cured via sequential heating at 100 and 150 ^oC for 8 h and overnight, respectively.

Prior to use, electrodes were beveled at 45 degrees on a diamond dust-embedded polishing wheel (Sutter Instruments, Novato, CA) and soaked in isopropyl alcohol for at least 20 min (Bath et al., 2000).

Amperometric recordings were made using a GeneClamp 500B amplifier (Axon Instruments, Molecular Devices, Union City, CA). Electrodes were held at 0.650 V vs. a Ag/AgCl reference electrode (BASi, West Lafayette, IN), a potential sufficient to oxidize catecholamines. For measurements at neurons, the output current was collected at 100 kHz and filtered at 10 kHz with a low-pass Bessel filter. Post-collection, traces were further digitally filtered using a 3 kHz low-pass Bessel filter. For measurements at chromaffin cells, the output current was collected at 20 kHz and filtered at 5 kHz with a low-pass Bessel filter. Post-collection, traces were further digitally filtered using a 400 Hz low-pass Bessel filter. Data collection and filtering were controlled via the pClamp software provided with the amplifier. Amperometric spike analysis was performed using MiniAnalysis software (Synaptosoft, Decatur, GA). For inclusion, spike amplitude was required to be 5 times greater than the root-mean-squared current noise.

Single Cell Experiments

Glass coverslips containing plated cells were secured in a stainless steel coverslip holder and mounted on the stage of an inverted microscope (Eclipse TE300, Nikon Instruments, Melville, NY). A temperature controller (Warner Instruments, Hamden, CT) connected to the stage maintained cells at 37 ^{o}C throughout the experiments. In all experiments, the extracellular recording buffer contained (in mM): 145 NaCl, 3 KCl, 1.2 $MgCl_2$, 2.4 $CaCl_2$, 1.2 NaH_2PO_4, 11 glucose, and 10 HEPES, pH adjusted to 7.4 with NaOH. Exocytosis/Ca^{2+} influx was triggered via pressure ejection of high K^+ buffer (80 mM for neurons, 60 mM for chromaffin cells) from a stimulating pipette located 20 to 60 μm from the cell. Stimulating pipettes with 6 to 10 μm tip diameters were fabricated using a horizontal pipette puller (Sutter Instruments, Novato, CA) and a microforge (Narishige, Long Island,

NY). Pressure ejection was controlled via a multi-channel Picospritzer (General Valve Corporation, Parker Hannifin, Fairfield, NJ). Positioning of both the electrode and stimulating pipette was controlled using piezoelectric micromanipulators (Burleigh Instruments, Exfo, Plano, TX). For neuronal experiments, GFP-positive dopamine neurons were identified via epifluorescence using a Xe arc lamp and Nikon endow GFP bandpass filter set.

Fluorescent Measurements of Intracellular Ca^{2+}

Intracellular Ca^{2+} dynamics were monitored using the ratiometric dye fura-FF (Invitrogen, Carlsbad, CA). Plated cells were incubated for 20 min at 25 ^{o}C in extracellular recording buffer with 1 µg/mL esterified fura dye and 0.1 % (w/v) BSA, washed twice with buffer without dye, and then incubated for 20 min at 25 ^{o}C in buffer without dye for deesterification. Ca^{2+} bound and unbound dye were excited at 340 and 380 nm, respectively, using a computer-controlled high speed wavelength switcher (Sutter Instruments, Novato, CA). Emission was monitored at 510 nm using a CCD camera and acquisition software (Empix Imaging, Mississauga, ON, Canada).

HPLC Determination of Dopamine Content

Tissue samples were dissected from a slice (300 - 500 µm in thickness) containing the region of interest. The tissue was weighed and homogenized with a wand sonicator (Fisher Scientific, Hampton, NH) in 200 µL 0.1 N perchloric acid spiked with 1 µM hydroquinone (HQ). Following centrifugation at 6,000 rpm for 10 min, the supernatant was removed and filtered with a 0.2 µm syringe filter unit (Millex-LG). Injections (50 µL) were made onto a reverse phase column (C-18, 5 µm, 4.6 x 250 mm, Waters symmetry 300 or Waters Atlantis T3). The mobile phase (prepared in HPLC grade water) contained 0.1 M citric acid, 0.1 mM EDTA, and 1 mM hexyl sodium sulfate, pH 3.5. Methanol was added as the organic modifier at a concentration of 10 % to shorten analyte elution times. Catecholamines were detected with a thin-layer radial electrochemical flowcell (BASi, West

Lafayette, IN), with the working electrode at 700 mV vs. a Ag/AgCl reference electrode (BASi, West Lafayette, IN). The HQ (1 μM) was used as an internal standard for analyte quantification and recovery. All analyte response ratios were taken with respect to the internal standard to account for differential electrode responses. The determination of peak areas for HPLC measurements was performed using custom written Igor programs. These programs were a gift from the Jorgenson lab at UNC-CH. Peak area determination was performed using statistical moments regression theory (Hsieh and Jorgenson, 1996). The peak area of the analyte was taken as a ratio to that of an internal standard at a known concentration, adjusted for differential detector response. The ratio was then used to calculate a mass of analyte in the extraction solution which was normalized by the mass of tissue taken.

Histochemistry

Dopamine neurons were identified by visualization of TH or dopamine. Detection of dopamine was performed using the sucrose-potassium phosphate-glyoxylic acid (SPG) histofluorescence method (De la Torre, 1980). Plates were incubated in ice-cold SPG solution (1 % glyoxylic acid, 6.8 % sucrose, 3.2 % KH_2PO_4, pH 7.4) for 5 min, dried in a laminar flow hood, covered with mineral oil, and heated at 95 ^{o}C for 5 min. Plates were cooled by replacing the mineral oil and visualized with fluorescein epifluorescence. For TH immunohistochemistry, plates were fixed with 3.7 % formaldehyde in PBS for 30 min. Following a 2 h treatment with a pre-blocking solution (1 % BSA, 10 % goat serum, and 0.3 % Triton X-100 in PBS), cells were incubated overnight at 4 ^{o}C in PBS with 5 % goat serum and 1:1000 rabbit anti-TH (Chemicon AB152). Plates were incubated for 1 h in PBS with 5 % goat serum and 5 μg/mL biotinylated goat anti-rabbit (Vector BA-1000), then for 30 min in R.T.U. Horseradish Peroxidase Avidin D (Vector A2704), and visualized with diaminobenzidine (DAB).

Chemicals

Unless noted, all chemicals were purchased from Sigma-Aldrich (St. Louis, MO) and used as received. All solutions were prepared using doubly-distilled, deionized water.

Results

Properties of Acutely Dissociated Midbrain Dopamine Neurons

A procedure for the study of Na^+ and Ca^{2+} currents in isolated SN neurons (Puopolo et al., 2007) was modified to produce acutely dissociated midbrain dopamine neurons from both the SN and VTA. TH staining revealed that 38 % of neurons (31/81) in these preparations were dopaminergic (Figure 2.1A). Consistent with the staining, 35 % of live cells (30/86) harvested from TH-GFP mice demonstrated GFP fluorescence (Figure 2.1B). In contrast to the diverse morphologies and dense axodendritic networks observed in the postnatal midbrain *in vivo* (Domesick et al., 1983; Tepper et al., 1987), acutely dissociated midbrain dopamine neurons resembled the immature shapes of cells cultured from fetal tissue. With no glial scaffold to support process outgrowth and only hours of recovery time, dopaminergic cells generally possessed only a few small neurites at experimentation (Figure 2.1), and on occasion were spherical and devoid of processes.

As an exocytotic mechanism of extrasynaptic dopamine release would be Ca^{2+}-dependent, the dynamics of depolarization-induced $[Ca^{2+}]_i$ changes at cell bodies of dissociated dopamine neurons were monitored with the fluorescent dye fura-FF. GFP fluorescence has been shown to significantly interfere with the use of fura dyes (Bolsover et al., 2001), so measurements were made at cells isolated from WT mice. TH staining was performed after experimentation to identify dopaminergic neurons. Figure 2.2A shows representative $[Ca^{2+}]_i$ responses from the cell body of a dopamine neuron to a 1 s pressure ejection of 80 mM K^+ at both 25 ^oC and 37 ^oC. As expected, cellular Ca^{2+} buffering capacity is enhanced at physiological temperature relative to room temperature recordings. At both temperatures, no detectable increase in $[Ca^{2+}]_i$ was observed upon removal of Ca^{2+} from the

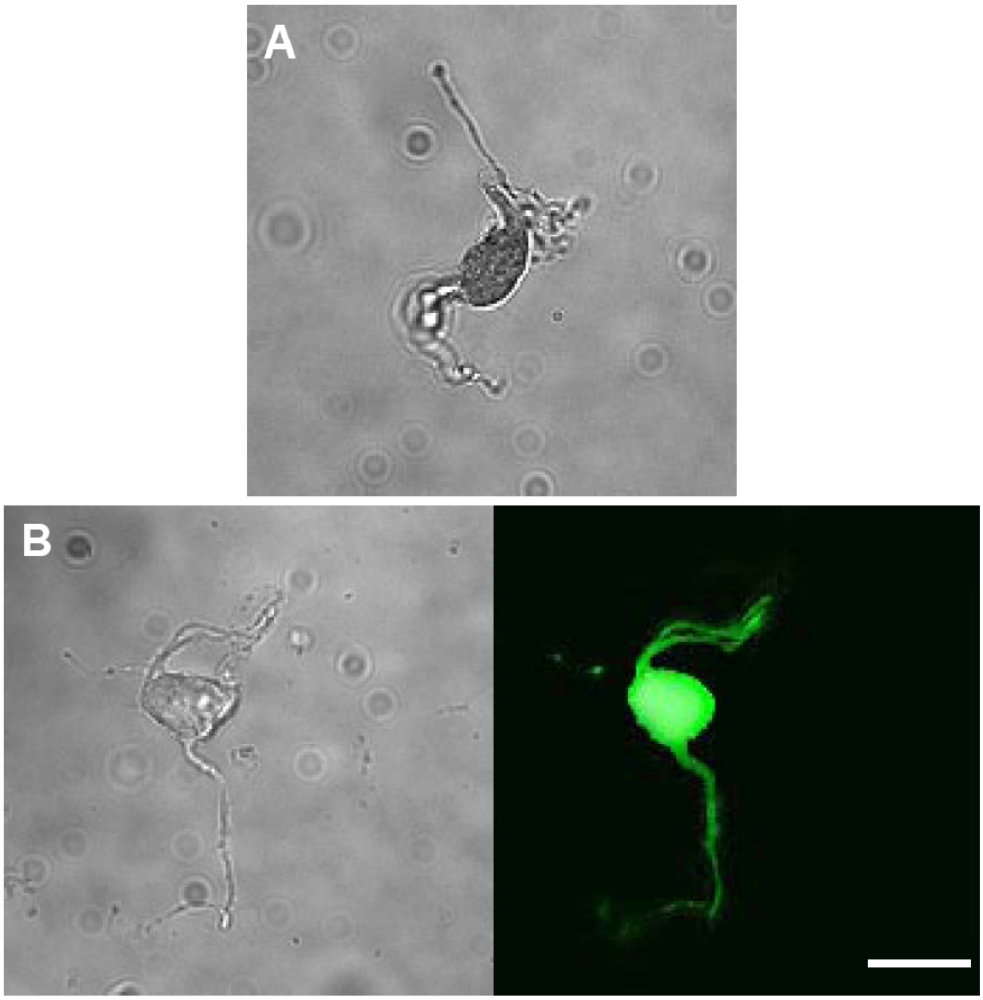

Figure 2.1. Identification of dissociated midbrain dopamine neurons. **(A)** TH labeling of a fixed cell visualized with the peroxidase/DAB method. The characteristic dark brown precipitate is clearly visible at the cell body. **(B)** Brightfield (left panel) and fluorescent (right panel) image of a live cell isolated from a TH-GFP mouse. All images taken at total magnification of 400X. Scale bar = 20 μm.

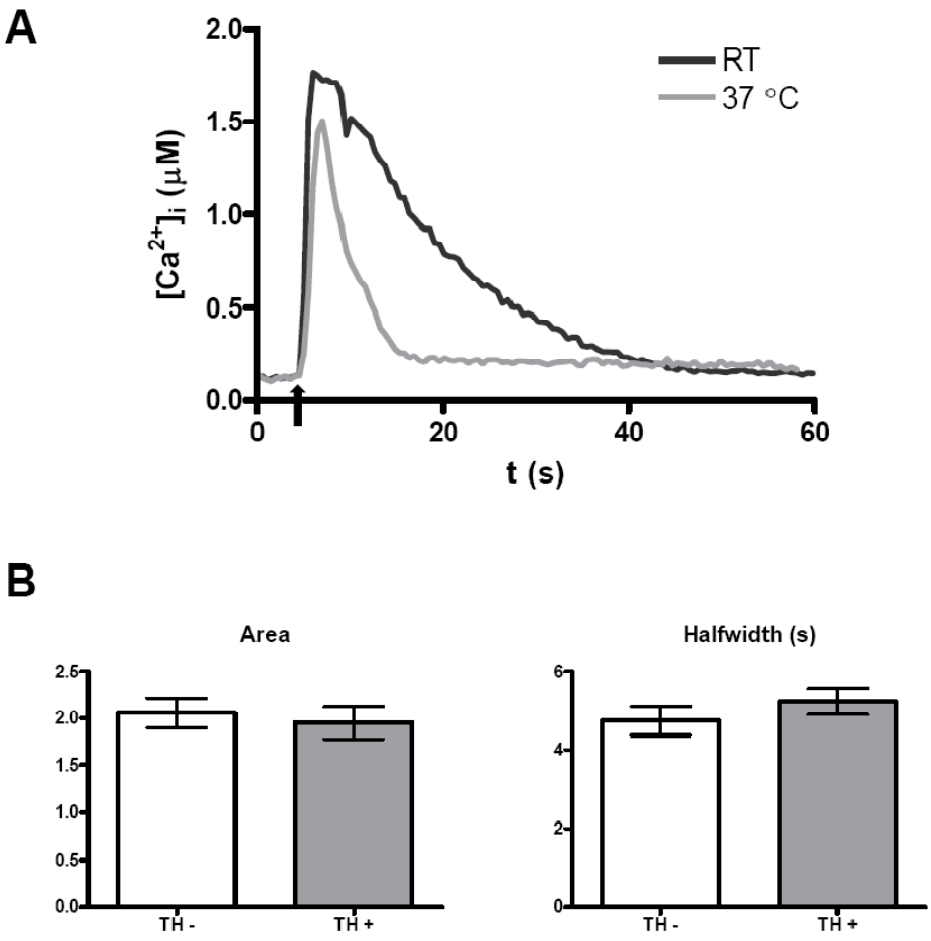

Figure 2.2. Intracellular Ca^{2+} transients at midbrain dopamine neurons. **(A)** Time course of $[Ca^{2+}]_i$ changes measured at the cell body in response to a 1 s stimulation with 80 mM K^+ (arrow). Responses are shown at both room (RT) and physiological temperatures (37 ^oC). **(B)** Comparison of $[Ca^{2+}]_i$ dynamics at the cell body of TH positive (n = 18) and TH negative (n = 21) neurons. No significant difference ($p > 0.05$, Student's t-test) was observed in the area (in arbitrary units) or halfwidth (in s) of the Ca^{2+} transient between cell types at 37 ^oC.

extracellular buffer and stim. The intracellular Ca^{2+} transients measured at TH-positive cells (n = 18) were statistically identical ($p > 0.05$, Student's t-test) to those from TH-negative cells (n = 21) at 37 ^{o}C (Figure 2.2B). The $[Ca^{2+}]_i$ peak had an area of 2.0 ± 0.2 arbitrary units in TH-positive cells, with a halfwidth of 5.2 ± 0.3 s. In TH-negative cells, the $[Ca^{2+}]_i$ spike had an area of 2.1 ± 0.2 arbitrary units and a halfwidth of 4.7 ± 0.4 s.

Vesicular Release at Cell Bodies of Dissociated Midbrain Neurons

Initial amperometric recordings at the cell bodies of acutely dissociated midbrain dopamine neurons revealed no current changes either spontaneously or in response to depolarizing stimulations with 80 mM K^+. To enhance dopamine synthesis, cells were incubated with 100 μM L-3,4-dihydroxy-phenylalanine (L-DOPA) for 30 min at 37 ^{o}C prior to experimentation (Pothos et al., 2000). After incubation, amperometric traces obtained at the cell body of GFP-positive neurons revealed a number of discrete current spikes characteristic of the vesicular release of dopamine (Figure 2.3). These spikes were dependent on the presence of extracellular Ca^{2+} and were only observed if the electrode was held at a potential sufficient to oxidize catecholamines. The frequency of vesicular events was very low, and no spontaneous release was ever observed prior to stimulation. Relative to the fast coupling of depolarization and secretion at chromaffin cells and axon terminals, the latencies between stimulation and the first detectable events were unusually long and variable at dopamine neuron cell bodies, ranging from 5 to 20 s.

In the bottom panel of Figure 2.3, individual amperometric spikes are shown on an expanded time axis. Unlike events recorded at chromaffin cells, the spikes measured at the cell body of acutely dissociated dopamine neurons were not uniform in shape. A subset of spikes (like those labeled 1 and 3) displayed single, rapid rising and falling phases. A second subset (like those labeled 2 and 4) exhibited significantly broader time courses and were occasionally marked by multiple rising and/or falling phases. The distribution of amperometric spike halfwidth ($t_{1/2}$) reinforces the visual classification of events into two

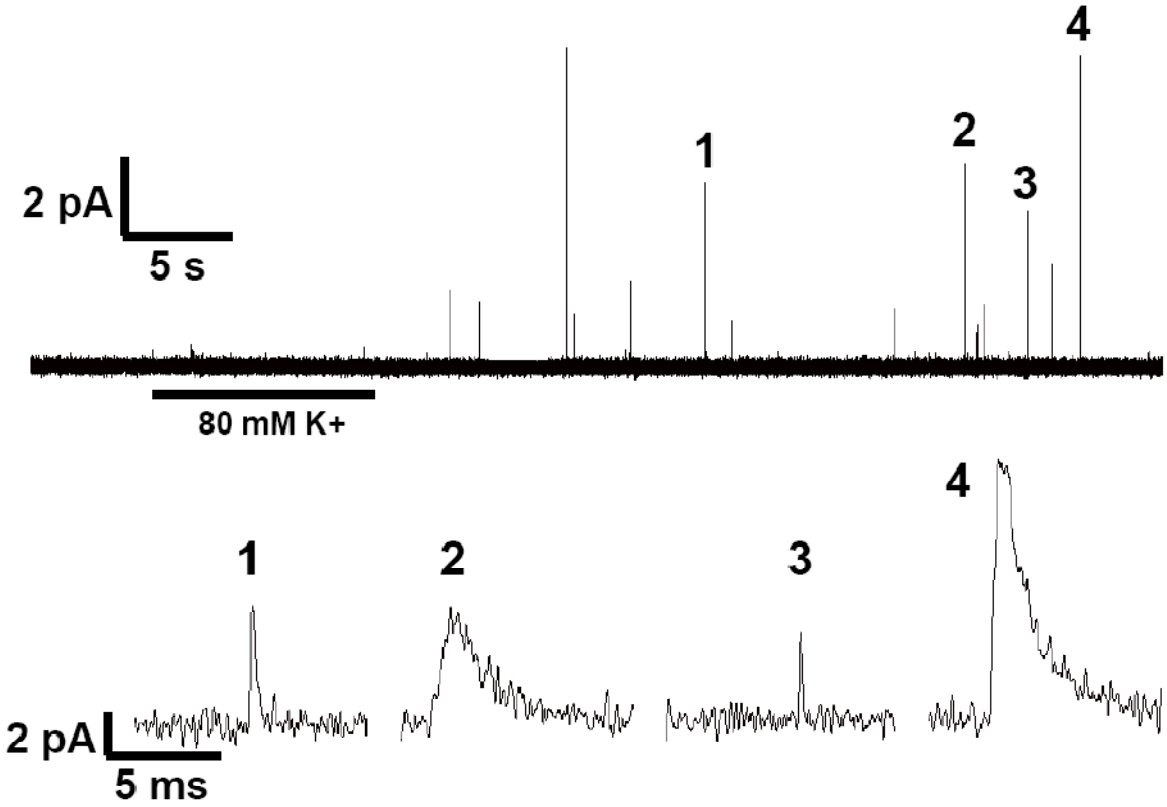

Figure 2.3. Vesicular release of dopamine from the cell body of an acutely dissociated midbrain dopamine neuron. Upper trace shows multiple exocytotic events detected with amperometry following 10 s pressure ejection of high K^+. Individual spikes are shown below on an expanded timescale.

subtypes. Figure 2.4A shows a histogram of the $t_{1/2}$ values, adjusted to normalize the distribution by taking the cube root (Finnegan et al., 1996; Pothos et al., 1998; Villanueva et al., 2006). The plot shows two distinct populations (best fit line is sum of two Gaussians, R^2 = 0.95). Quantal events were officially divided into two subtypes, narrow and wide, based on whether their adjusted halfwidth was below or above, respectively, the population intersection value of 0.8 $ms^{1/3}$. Of the recorded events, 65 % of spikes were classified as narrow, with an average $t_{1/2}$ of 0.19 ± 0.01 ms, and 35 % of spikes were classified as wide, with an average $t_{1/2}$ of 1.33 ± 0.09 ms. On average, the wide subset of events resulted in the release of substantially more dopamine than narrow events (Figure 2.4B). Narrow spikes had an average quantal size (Q) of 5.3 ± 0.6 zmol dopamine (3190 molecules per vesicle), while wide spikes had an average Q of 49 ± 4 zmol dopamine (29500 molecules per vesicle).

Effects of Axodendritic Differentiation on Release at Cell Bodies

To ensure the vesicular release recorded at cell bodies of acutely dissociated midbrain dopamine neurons was not an artifact of the immature cellular morphologies, neurons were seeded on glial monolayers and given a 2 week recovery period prior to amperometric measurements. After 2 weeks, neuronal shapes were consistent with *in vivo* observations, and cells extended vast axodendritic networks (Figure 2.5). The additional recovery period had no effect on the proportion of isolated cells that were dopaminergic, as 37 % of the cells (29/78) on plates from TH-GFP mice were GFP-positive (Figure 2.5B). Glyoxylic acid-induced dopamine histofluorescence was confirmed in 39 % of cells (34/87) as well (Figure 2.5A). As before, amperometric traces obtained at the cell bodies of these neurons displayed a series of discrete current spikes in response to depolarizing stimulation with 80 mM K^+. Release again required preincubation with L-DOPA and was dependent on the presence of extracellular Ca^{2+}. Spikes were only observed with electrode holding potentials sufficient to oxidize catecholamines, confirming the released substance was

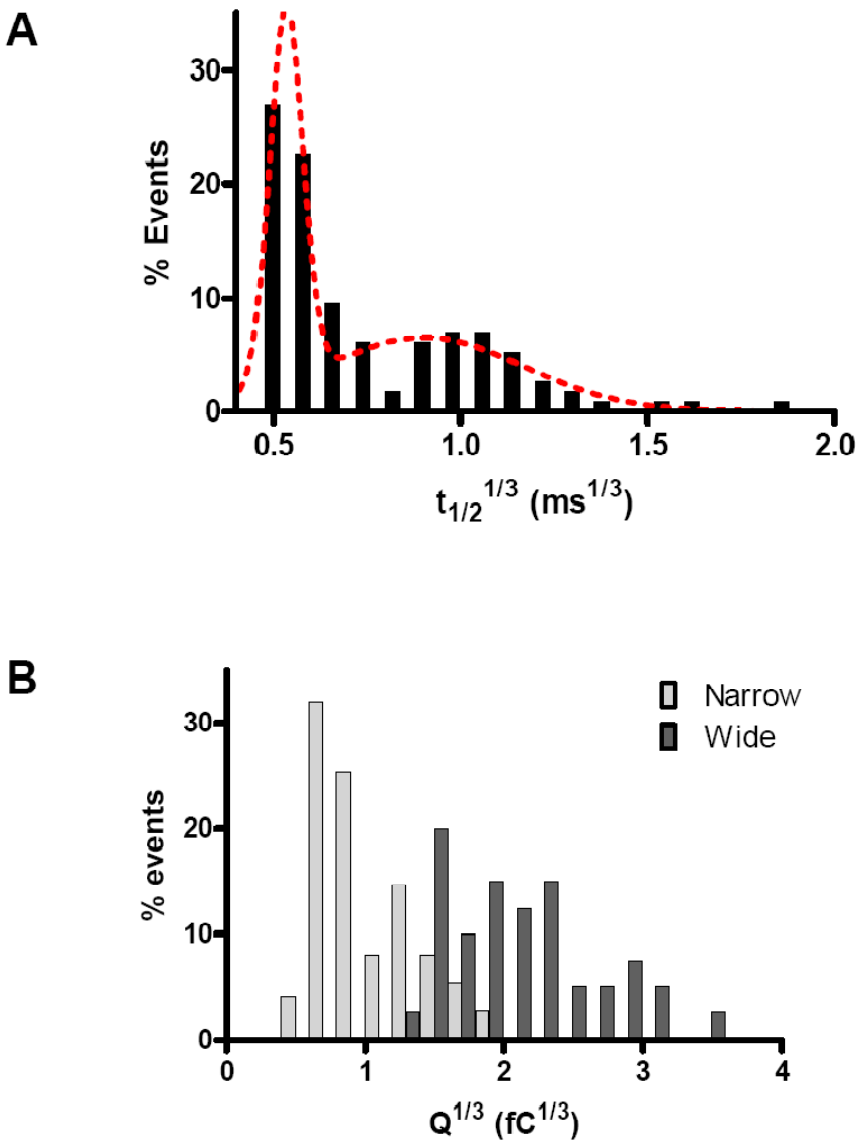

Figure 2.4. Amperometric spike distributions reveal two vesicle pools. **(A)** Distribution of the cube root of $t_{1/2}$. Distribution was best fit by sum of two gaussians (dashed red line). **(B)** Distribution of $Q^{1/3}$. Vesicular events were classified as narrow or wide using a cutoff value of 0.8 $ms^{1/3}$ determined from the $t_{1/2}$ distribution.

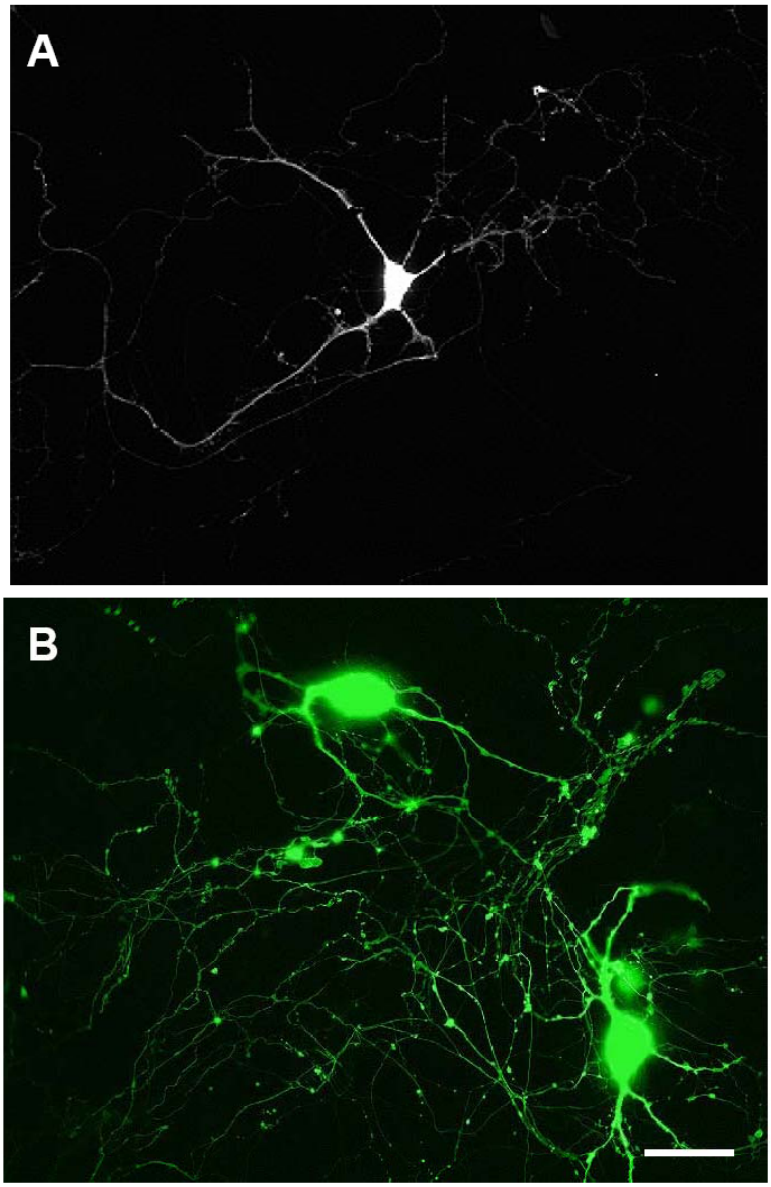

Figure 2.5 Identificaiton of dissociated midbrain dopamine neurons grown on glial monolayers. **(A)** Fixed cell exhibiting glyoxylic acid-induced dopamine histofluoresence. **(B)** Fluorescent image of live cells isolated from a TH-GFP mouse. Both images taken at total magnification of 400X. Scale bar = 20 um.

dopamine. The frequency of events was again very low, and spontaneous events were never recorded. Latencies between stimulation and detected events were still long and variable, ranging from 3 to 20 s.

Visual inspection of the amperometric spikes revealed the same two subtypes: spikes with single, rapid rising and falling phases and broader spikes with occasional multiple rising and/or falling phases. Figure 2.6A shows the adjusted halfwidth distribution, indicating two populations (best fit line is sum of two Gaussians, $R^2 = 0.91$). Events were divided into two subtypes, narrow and wide, based on whether their adjusted halfwidth was below or above, respectively, the population intersection value of 0.9 $ms^{1/3}$. Of the measured events, 76 % of spikes were classified as narrow, with an average $t_{1/2}$ of 0.23 ± 0.02 ms, and 24 % of spikes were classified as wide, with an average $t_{1/2}$ of 1.2 ± 0.1 ms. The wide subset of events resulted, on average, in the release of more dopamine than narrow events (Figure 2.6B). Narrow spikes had an average Q of 9 ± 1 zmol dopamine (5420 molecules per vesicle), while wide spikes had an average Q of 47 ± 6 zmol dopamine (28300 molecules per vesicle). All in all, release measured at the cell bodies of acutely dissociated midbrain dopamine neurons was remarkably similar after allowing time for axodendritic differentiation. Ca^{2+}-dependence, spike frequency, and spike latency were unaffected and two populations of vesicular events were discovered in both preparations. Only minor differences were observed in the percentages of narrow and wide events and the spike characteristics of those events. Figure 2.7 summarizes the $t_{1/2}$ and Q values for spikes recorded from acutely dissociated dopamine neurons with and without a two week recovery on a glial monolayer. The $t_{1/2}$ and Q values for wide events from both preps are the same ($p > 0.05$, Student's t-test). For narrow events, neurons grown on glial monolayers showed a small but statistically significant ($p < 0.05$) increase in $t_{1/2}$ and Q.

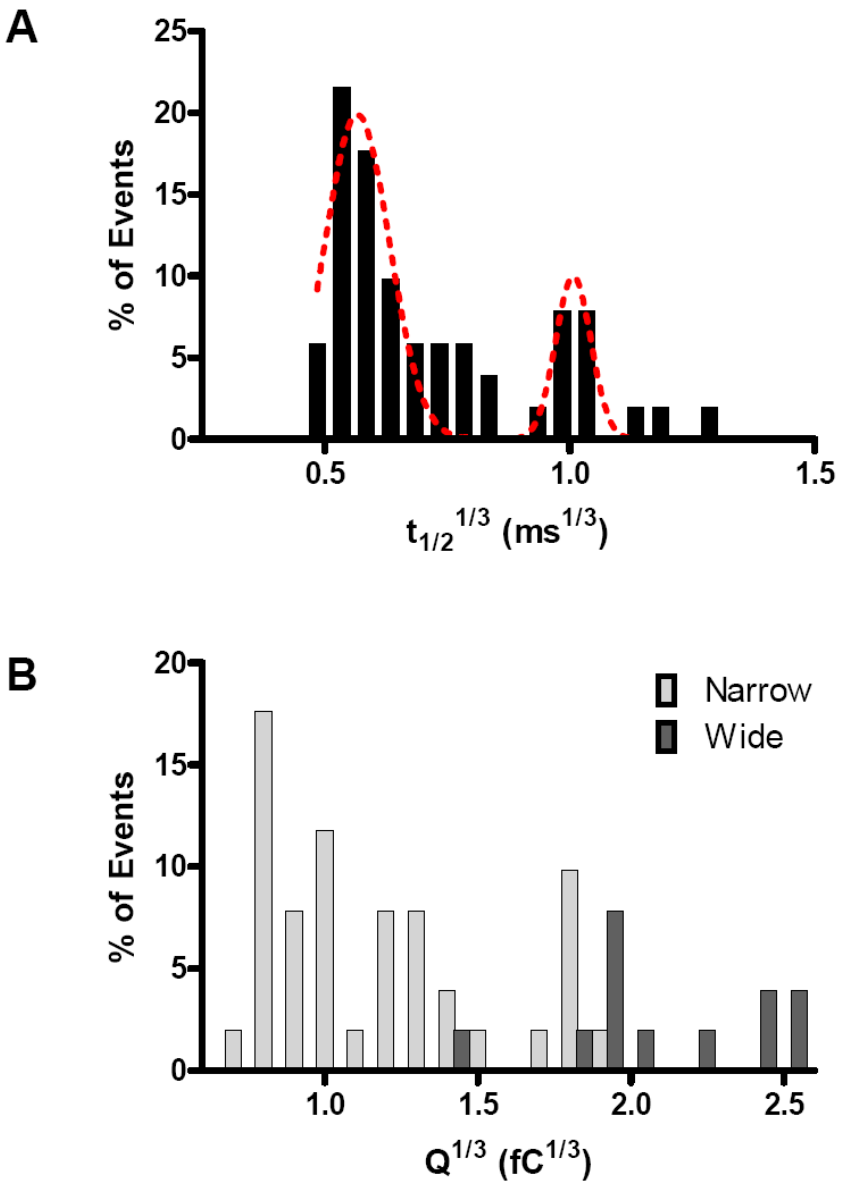

Figure 2.6. Amperometric spike distributions remain bimodal. **(A)** Distribution of the cube root of $t_{1/2}$. Distribution was best fit by sum of two gaussians (dashed red line). **(B)** Distribution of $Q^{1/3}$. Vesicular events were classified as narrow or wide using a cutoff value of 0.9 $ms^{1/3}$ determined from the $t_{1/2}$ distribution.

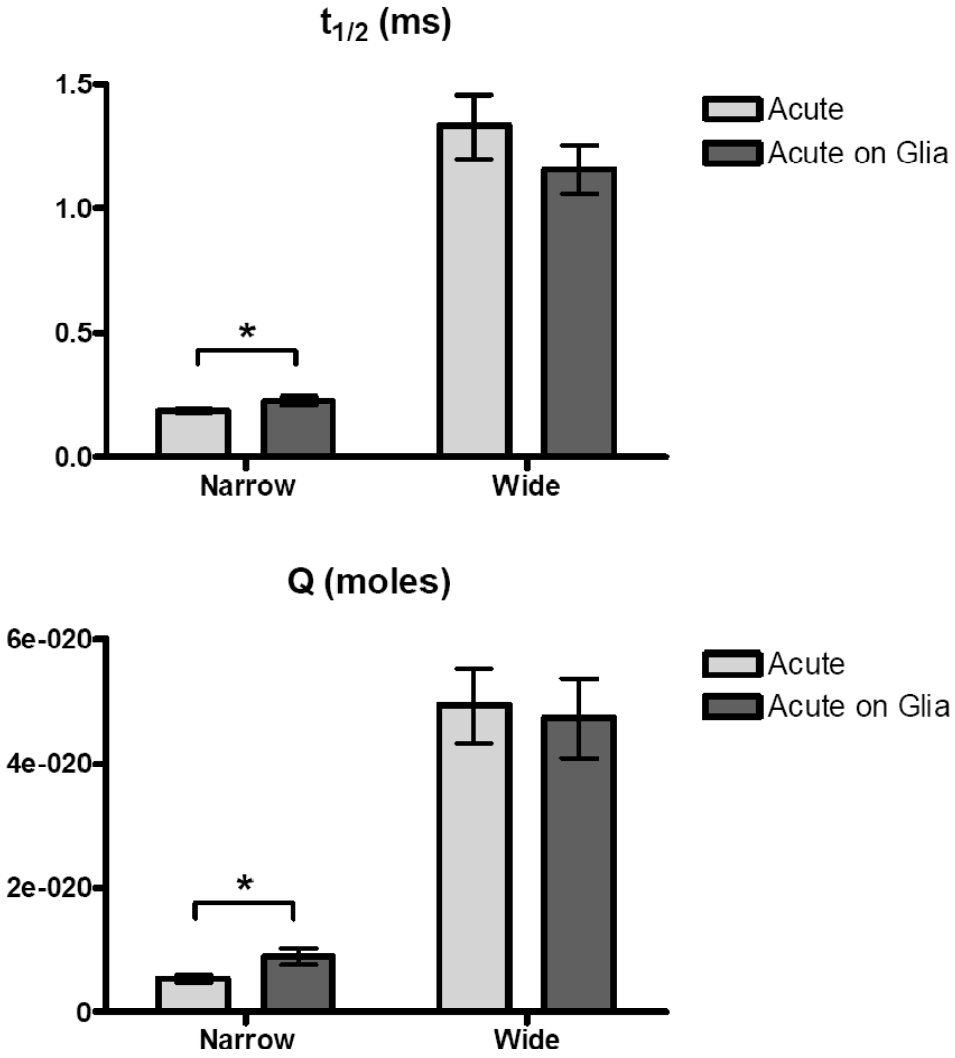

Figure 2.7. Differences in amperometric spike characteristics between neuron isolation procedures. Average $t_{1/2}$ and Q values were compared for acutely dissociated midbrain dopamine neurons and those grown on glial monolayers. Acutely dissociated neurons grown on glial monolayers showed a statistically significant increase (* $p < 0.05$, Student's t-test) in $t_{1/2}$ and Q for spikes classified as narrow, while no significant change ($p > 0.05$) was observed for spikes classified as wide.

TH-GFP Mice as Suitable Models for Midbrain Studies

To assess whether the exocytotic mechanism is affected in the genetically altered TH-GFP mice, vesicular release at murine chromaffin cells was compared for WT and TH-GFP animals. As both dopamine neurons and chromaffin cells express TH, potential side effects of the TH-linked transgene should be similar in these cells. Amperometry was used to record vesicular events at chromaffin cells from both mice following a single 1 s stimulation with 60 mM K^+. The results of these experiments are displayed in Figure 2.8. An average of 38 ± 9 amperometric spikes were detected per stimulation at WT cells (n = 10). These events occurred at a frequency of 8.2 ± 0.9 Hz and had an average $t_{1/2}$ of 5.0 ± 0.2 ms. No significant differences ($p > 0.05$, Student's t-test) in these parameters were observed at TH-GFP cells (n = 22). An average of 32 ± 3 spikes were detected per stimulation. These events occurred at a frequency of 7.2 ± 0.6 Hz and had an average $t_{1/2}$ of 5.4 ± 0.1 ms. Taken together, these results suggest that the size of the readily releasable pool, the efficiency of vesicular docking, and the kinetics of vesicular extrusion are unchanged in TH-GFP mice. One difference was observed, however, between the WT and TH-GFP cells. In WT cells, the average Q was 1.7 ± 0.1 amol catecholamine. TH-GFP cells showed a significant reduction ($p < 0.05$) in quantal size to 1.38 ± 0.06 amol catecholamine.

As a further test of potentially altered dopamine release in TH-GFP mice, HPLC with electrochemical detection was used to determine total dopamine content in the cell body and terminal region of midbrain dopamine neurons for both WT and TH-GFP animals. As can be seen in Table 2.1, dopamine content in the VTA was identical for WT and TH-GFP mice at 0.7 ± 0.1 and 0.7 ± 0.2 µg dopamine/g tissue, respectively. In the caudate putamen, dopamine content was 9.6 ± 1.7 µg/g in WT mice and 7.3 ± 0.8 µg/g in TH-GFP mice. While the difference was not statistically significant ($p > 0.05$), the 24 % decrease in dopamine content in the terminal region of TH-GFP mice relative to WT mice matches in magnitude the 21 % reduction in Q observed at chromaffin cells.

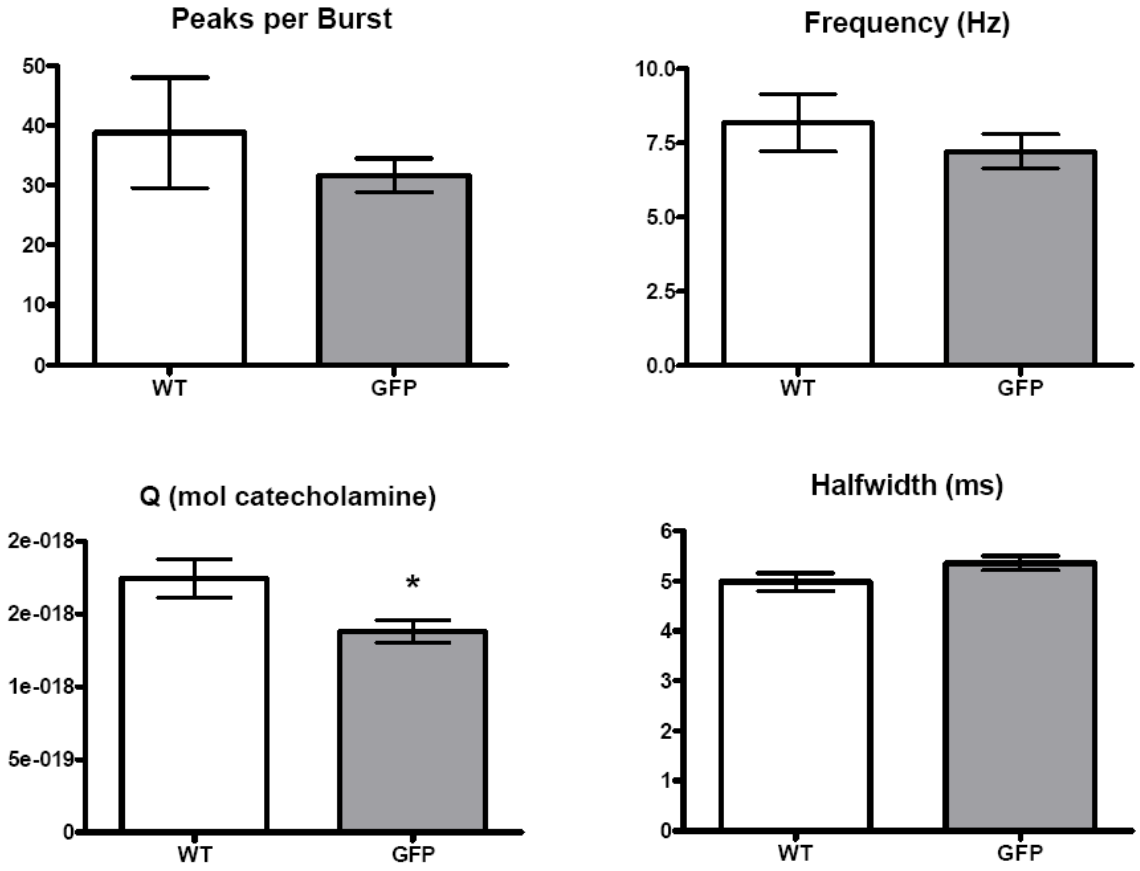

Figure 2.8. Comparison of exocytosis between WT and TH-GFP mice. Vesicular release was recorded at isolated murine chromaffin cells following a 1 s stimulation with 60 mM K^+. Spikes observed at TH-GFP cells (n = 22) showed a statistically significant reduction (* $p < 0.05$, Student's t-test) in Q relative to WT cells (n = 10). No significant difference ($p > 0.05$) was noted in the number of spikes, spike frequency, and average $t_{1/2}$ between cell types.

Table 2.1. Comparison of total dopamine content in WT and TH-GFP mice. HPLC with electrochemical detection was used to evaluate the amount of dopamine per gram of tissue in the caudate putamen and VTA of adult mice. No statistically significant differences ($p > 0.05$, Student's t-test) were detected between WT and TH-GFP mice.

Animal	Brain Region	Dopamine Content (µg/g)
WT	VTA	0.7 ± 0.1
TH-GFP	VTA	0.7 ± 0.2
WT	Caudate Putamen	9.6 ± 1.7
TH-GFP	Caudate Putamen	7.3 ± 0.8

Discussion

The work described here demonstrates the successful development of a procedure for the isolation of mammalian midbrain dopaminergic neurons. Utilizing this technique with TH-GFP mice, freshly dissociated dopamine neurons can be identified *in vitro* for amperometric recordings of dopamine release. In response to depolarizing stimulations of high K^+, amperometric traces from the cell bodies of these neurons displayed a number of current spikes that meet the criteria for exocytosis of dopamine. First, spikes were only observed at TH-positive cells (identified by GFP fluorescence) and only when holding the electrode at a potential sufficient to oxidize catecholamines. Together, these observations are strong evidence that the substance being detected is indeed dopamine. Second, events were only detected in the presence of extracellular Ca^{2+}. While intracellular Ca^{2+} stores may play a role in the release process, the requirement of depolarization-induced influx of extracellular Ca^{2+} as a first step is a consistent marker of vesicular exocytosis across all cell types (Burgoyne and Morgan, 2003). Third, the current spikes were rapid, discrete phenomena consistent with the delivery of individual packets of molecules to the electrode surface. Individual release events demonstrated a rapid outward flux of dopamine (~$3x10^6$ molecules/s), significantly higher than what has been observed experimentally for monoamine transporters (Galli et al., 1998). In sum, the experiments in this work argue strongly that the extrasynaptic release of dopamine occurs through a Ca^{2+}-mediated exocytosis, not reversal of DAT.

One of the more striking features of the extrasynaptic release was the prolonged latency from the onset of depolarization to the first detectable vesicular events (Figure 2.3). This observation establishes an important distinction between synaptic and extrasynaptic transmission in midbrain dopamine neurons. At neuronal synapses, the close physical association of VGCCs and the exocytosis machinery (Ca^{2+} sensors, vesicles, SNARE proteins, etc…) helps establish a very tight correlation between depolarization and vesicular

fusion and release. One potential explanation for the long latencies observed in these experiments could be a less dense population of VGCCs at the cell body. It has previously been observed in neuroendocrine cells that delays between stimulation and secretion can be explained by prolonged Ca^{2+} diffusion (Chow et al., 1996). This diffusional delay could depend not only on VGCC density, but also vesicle location. Unlike nerve terminals, cell bodies lack presynaptic active zones characterized by a pool of vesicles docked at the cell membrane and primed for release. VMAT2 staining of retinal dopamine neurons labeled vesicles that were randomly distributed throughout the cell body (Puopolo et al., 2001). These vesicles were spaced at a considerable distance from each other and the cell membrane. Coincidentally, amperometric measurements at the cell bodies of these cells displayed similar release latencies of 0.5 – 30 s. Therefore, the observed delay in vesicular events could likely stem from the time required to recruit and mobilize vesicles to the plasma membrane for fusion. As the intracellular movement of vesicles is thought to occur via Ca^{2+}-dependent interactions with the cytoskeletal network (Burgoyne and Morgan, 2003), differences in these interactions at the cell body compared to the nerve terminals could also influence the observed delay in amperometric spikes following depolarization.

The vesicular events observed at the cell bodies of midbrain dopamine neurons were heterogeneous in nature. Visually, spikes could easily be separated into two classes based on their time course. While the narrow events always consisted of a single rising and falling phase, the wide events sometimes displayed multiple rising and/or falling phases. Distributions of the raw amperometric $t_{1/2}$ and Q values were broad and skewed to the right, such that the means were greater than the modes. Similar distributions have been previously observed in secretory cells (Finnegan et al., 1996; Pothos et al., 1998; Villanueva et al., 2006). Plotting the cube roots resulted in normalized distributions. The explanation being that vesicle radii are normally distributed, and since the amperometric spike characteristics depend on vesicular volume (r^3) their cube root should also be normally

distributed (Bekkers et al., 1990). Transformed distributions of the extrasynaptic release $t_{1/2}$ and Q values were normalized and the $t_{1/2}$ distribution was described by two Gaussians, consistent with the visual classification of events (Figure 2.4 and Figure 2.6). Individually, both subtypes of events showed amperometric spike characteristics on the same order of magnitude as events previously recorded from other dopamine neuron preparations (Jaffe et al., 1998; Pothos et al., 1998; Puopolo et al., 2001; Kim et al., 2008).

The fundamental question raised by these studies involves the biological origin of the two vesicular populations. Two subpopulations of amperometric spikes have been observed previously in release from the cell body of both the leech Retzius cell and a dopamine neuron in the pond snail (Bruns and Jahn, 1995; Chen and Ewing, 1995). In each case the two populations could be attributed to release from small synaptic vesicles (SSVs) and large dense-core vesicles (LDCVs). VMAT has been localized to numerous intracellular compartments in the somatodendritic region of midbrain dopamine neurons: tubulovesicles resembling saccules of SER, SSVs, LDCVs, and multivesicular bodies (Nirenberg et al., 1996b). Similarly, three types of secretory organelles were observed at the cell body of retinal dopamine neurons, including SSVs and LDCVs (Puopolo et al., 2001). Thus, it's plausible that the two observed vesicular populations arise from the exocytosis of two different secretory organelles. A second possibility is that the two populations correspond to the exocytosis of one type of vesicle, but via two different fusion mechanisms. Amperometric spikes detected at axonal varicosities of midbrain dopamine neurons have shown a bimodal distribution of this type (Staal et al., 2004). Events with single rising and falling phases or with multiple rising and falling phases of decreasing amplitude were attributed to dopamine release through a fusion pore that flickers either once or multiple times in succession. As not all of the wide events from this study exhibited multiple rising and/or falling phases, such a mechanism could not, however, be the sole explanation for the two vesicular populations.

As all of the amperometric measurements were made at cells from transgenic mice, it was necessary to confirm that the genetic manipulations had not resulted in significant deviations from the vesicular release that would have been observed in WT animals. As direct comparisons between neuronal release were unfeasible, a common model cell for neuronal exocytosis was employed: the chromaffin cell. Unlike midbrain dopamine neurons, homogenous populations of morphologically identifiable chromaffin cells can easily be obtained from WT animals. Chromaffin cells are an especially valid model for our experiments, as they express TH. Vesicular release measured at chromaffin cells was predominantly unchanged between WT and TH-GFP mice. The size of the readily releasable pool, efficiency of vesicle docking with the plasma membrane, and kinetics of vesicular extrusion were similar in both animals. One deficiency was observed, though, in the release from TH-GFP cells: a 21 % reduction in vesicular content. As a second check of potential transgenic side effects, total brain dopamine content as determined by HPLC was compared between WT and TH-GFP mice. Dopamine content was statistically equivalent in the cell body and synaptic terminal regions of both mice, although the raw content values for TH-GFP mice were reduced by 24 % at the terminals. Taken with the release data from the MAMC cells, the HPLC analysis suggests that, at worse, the amperometric data obtained from the cell bodies of dopamine neurons is underreporting the average vesicular content by about 20 %. Potential explanations for a lower vesicular content in TH-GFP mice include reduced catecholamine synthesis and impaired vesicular packaging. As the reporter gene in the transgenic mouse is linked to TH expression, reduced synthesis seems the most likely candidate. Insertion of the GFP gene downstream of the TH promoter could negatively impact TH transcription leading to lower protein levels and lower catecholamine synthesis.

References

Bath BD, Michael DJ, Trafton BJ, Joseph JD, Runnels PL, Wightman RM (2000) Subsecond adsorption and desorption of dopamine at carbon-fiber microelectrodes. Anal Chem 72:5994-6002.

Beckstead MJ, Grandy DK, Wickman K, Williams JT (2004) Vesicular dopamine release elicits an inhibitory postsynaptic current in midbrain dopamine neurons. Neuron 42:939-946.

Bekkers JM, Richerson GB, Stevens CF (1990) Origin of variability in quantal size in cultured hippocampal neurons and hippocampal slices. Proc Natl Acad Sci U S A 87:5359-5362.

Bergquist F, Nissbrandt H (2003) Influence of R-type (Cav2.3) and t-type (Cav3.1-3.3) antagonists on nigral somatodendritic dopamine release measured by microdialysis. Neuroscience 120:757-764.

Bergquist F, Niazi HS, Nissbrandt H (2002) Evidence for different exocytosis pathways in dendritic and terminal dopamine release in vivo. Brain Res 950:245-253.

Bergquist F, Jonason J, Pileblad E, Nissbrandt H (1998) Effects of local administration of L-, N-, and P/Q-type calcium channel blockers on spontaneous dopamine release in the striatum and the substantia nigra: a microdialysis study in rat. J Neurochem 70:1532-1540.

Bjorklund A, Lindvall O (1975) Dopamine in dendrites of substantia nigra neurons: suggestions for a role in dendritic terminals. Brain Res 83:531-537.

Bolsover S, Ibrahim O, O'Luanaigh N, Williams H, Cockcroft S (2001) Use of fluorescent Ca2+ dyes with green fluorescent protein and its variants: problems and solutions. Biochem J 356:345-352.

Bruns D, Jahn R (1995) Real-time measurement of transmitter release from single synaptic vesicles. Nature 377:62-65.

Burgoyne RD, Morgan A (2003) Secretory granule exocytosis. Physiol Rev 83:581-632.

Chen BT, Rice ME (2001) Novel Ca2+ dependence and time course of somatodendritic dopamine release: substantia nigra versus striatum. J Neurosci 21:7841-7847.

Chen BT, Moran KA, Avshalumov MV, Rice ME (2006) Limited regulation of somatodendritic dopamine release by voltage-sensitive Ca channels contrasted with strong regulation of axonal dopamine release. J Neurochem 96:645-655.

Chen G, Ewing AG (1995) Multiple classes of catecholamine vesicles observed during exocytosis from the Planorbis cell body. Brain Res 701:167-174.

Chow RH, Klingauf J, Heinemann C, Zucker RS, Neher E (1996) Mechanisms determining the time course of secretion in neuroendocrine cells. Neuron 16:369-376.

Cragg S, Rice ME, Greenfield SA (1997) Heterogeneity of electrically evoked dopamine release and reuptake in substantia nigra, ventral tegmental area, and striatum. J Neurophysiol 77:863-873.

De la Torre JC (1980) An improved approach to histofluorescence using the SPG method for tissue monoamines. J Neurosci Methods 3:1-5.

Domesick VB, Stinus L, Paskevich PA (1983) The cytology of dopaminergic and nondopaminergic neurons in the substantia nigra and ventral tegmental area of the rat: a light- and electron-microscopic study. Neuroscience 8:743-765.

Elverfors A, Jonason J, Jonason G, Nissbrandt H (1997) Effects of drugs interfering with sodium channels and calcium channels on the release of endogenous dopamine from superfused substantia nigra slices. Synapse 26:359-369.

Falkenburger BH, Barstow KL, Mintz IM (2001) Dendrodendritic inhibition through reversal of dopamine transport. Science 293:2465-2470.

Finnegan JM, Pihel K, Cahill PS, Huang L, Zerby SE, Ewing AG, Kennedy RT, Wightman RM (1996) Vesicular quantal size measured by amperometry at chromaffin, mast, pheochromocytoma, and pancreatic beta-cells. J Neurochem 66:1914-1923.

Fortin GD, Desrosiers CC, Yamaguchi N, Trudeau LE (2006) Basal somatodendritic dopamine release requires snare proteins. J Neurochem 96:1740-1749.

Galli A, Blakely RD, DeFelice LJ (1998) Patch-clamp and amperometric recordings from norepinephrine transporters: channel activity and voltage-dependent uptake. Proc Natl Acad Sci U S A 95:13260-13265.

Geffen LB, Jessell TM, Cuello AC, Iversen LL (1976) Release of dopamine from dendrites in rat substantia nigra. Nature 260:258-260.

Groves PM, Linder JC (1983) Dendro-dendritic synapses in substantia nigra: descriptions based on analysis of serial sections. Exp Brain Res 49:209-217.

Hausser M, Stuart G, Racca C, Sakmann B (1995) Axonal initiation and active dendritic propagation of action potentials in substantia nigra neurons. Neuron 15:637-647.

Hoffman AF, Gerhardt GA (1999) Differences in pharmacological properties of dopamine release between the substantia nigra and striatum: an in vivo electrochemical study. J Pharmacol Exp Ther 289:455-463.

Hoffman AF, Lupica CR, Gerhardt GA (1998) Dopamine transporter activity in the substantia nigra and striatum assessed by high-speed chronoamperometric recordings in brain slices. J Pharmacol Exp Ther 287:487-496.

Hounsgaard J, Nedergaard S, Greenfield SA (1992) Electrophysiological localization of distinct calcium potentials at selective somatodendritic sites in the substantia nigra. Neuroscience 50:513-518.

Hsieh S, Jorgenson JW (1996) Preparation and evaluation of slurry-packed liquid chromatography microcolumns with inner diameters from 12 to 33 microns. Anal Chem 68:1212-1217.

Jaffe EH, Marty A, Schulte A, Chow RH (1998) Extrasynaptic vesicular transmitter release from the somata of substantia nigra neurons in rat midbrain slices. J Neurosci 18:3548-3553.

John CE, Jones SR (2006) Exocytotic release of dopamine in ventral tegmental area slices from C57BL/6 and dopamine transporter knockout mice. Neurochem Int 49:737-745.

Kawagoe KT, Zimmerman JB, Wightman RM (1993) Principles of voltammetry and microelectrode surface states. J Neurosci Methods 48:225-240.

Kessler MA, Yang M, Gollomp KL, Jin H, Iacovitti L (2003) The human tyrosine hydroxylase gene promoter. Brain Res Mol Brain Res 112:8-23.

Kim Y, Park MK, Chung S (2008) Voltage-operated Ca2+ channels regulate dopamine release from somata of dopamine neurons in the substantia nigra pars compacta. Biochem Biophys Res Commun 373:665-669.

Kita JM, Kile BM, Parker LE, Wightman RM (2009) In vivo measurement of somatodendritic release of dopamine in the ventral tegmental area. Synapse 63:951-960.

Kolski-Andreaco A, Cai H, Currle DS, Chandy KG, Chow RH (2007) Mouse adrenal chromaffin cell isolation. J Vis Exp:129.

Llinas R, Greenfield SA, Jahnsen H (1984) Electrophysiology of pars compacta cells in the in vitro substantia nigra--a possible mechanism for dendritic release. Brain Res 294:127-132.

Mercer L, del Fiacco M, Cuello AC (1979) The smooth endoplasmic reticulum as a possible storage site for dendritic dopamine in substantia nigra neurones. Experientia 35:101-103.

Nieoullon A, Cheramy A, Glowinski J (1977) Release of dopamine in vivo from cat substantia nigra. Nature 266:375-377.

Nirenberg MJ, Vaughan RA, Uhl GR, Kuhar MJ, Pickel VM (1996a) The dopamine transporter is localized to dendritic and axonal plasma membranes of nigrostriatal dopaminergic neurons. J Neurosci 16:436-447.

Nirenberg MJ, Chan J, Liu Y, Edwards RH, Pickel VM (1996b) Ultrastructural localization of the vesicular monoamine transporter-2 in midbrain dopaminergic neurons: potential sites for somatodendritic storage and release of dopamine. J Neurosci 16:4135-4145.

Nirenberg MJ, Chan J, Liu Y, Edwards RH, Pickel VM (1997) Vesicular monoamine transporter-2: immunogold localization in striatal axons and terminals. Synapse 26:194-198.

Pothos EN, Davila V, Sulzer D (1998) Presynaptic recording of quanta from midbrain dopamine neurons and modulation of the quantal size. J Neurosci 18:4106-4118.

Pothos EN, Larsen KE, Krantz DE, Liu Y, Haycock JW, Setlik W, Gershon MD, Edwards RH, Sulzer D (2000) Synaptic vesicle transporter expression regulates vesicle phenotype and quantal size. J Neurosci 20:7297-7306.

Puopolo M, Raviola E, Bean BP (2007) Roles of subthreshold calcium current and sodium current in spontaneous firing of mouse midbrain dopamine neurons. J Neurosci 27:645-656.

Puopolo M, Hochstetler SE, Gustincich S, Wightman RM, Raviola E (2001) Extrasynaptic release of dopamine in a retinal neuron: activity dependence and transmitter modulation. Neuron 30:211-225.

Rice ME, Cragg SJ, Greenfield SA (1997) Characteristics of electrically evoked somatodendritic dopamine release in substantia nigra and ventral tegmental area in vitro. J Neurophysiol 77:853-862.

Rice ME, Richards CD, Nedergaard S, Hounsgaard J, Nicholson C, Greenfield SA (1994) Direct monitoring of dopamine and 5-HT release in substantia nigra and ventral tegmental area in vitro. Exp Brain Res 100:395-406.

Staal RG, Mosharov EV, Sulzer D (2004) Dopamine neurons release transmitter via a flickering fusion pore. Nat Neurosci 7:341-346.

Tepper JM, Sawyer SF, Groves PM (1987) Electrophysiologically identified nigral dopaminergic neurons intracellularly labeled with HRP: light-microscopic analysis. J Neurosci 7:2794-2806.

Villanueva M, Thornley K, Augustine GJ, Wightman RM (2006) Synapsin II negatively regulates catecholamine release. Brain Cell Biol 35:125-136.

Wassef M, Berod A, Sotelo C (1981) Dopaminergic dendrites in the pars reticulata of the rat substantia nigra and their striatal input. Combined immunocytochemical localization of tyrosine hydroxylase and anterograde degeneration. Neuroscience 6:2125-2139.

Wilson CJ, Groves PM, Fifkova E (1977) Monoaminergic synapses, including dendro-dendritic synapses in the rat substantia nigra. Exp Brain Res 30:161-174.

Chapter 3

Energy Stores in Regulated Exocytosis

Introduction

The hormone leptin operates as a negative feedback signal in the brain, helping to regulate an organism's body weight (specifically, the adipose tissue mass) by modulating the activity of neuronal circuits controlling food intake and energy expenditure (Friedman, 2009). Leptin is a 16 kD protein secreted into the bloodstream primarily by white adipose tissue. The hormone binds to leptin receptors in the arcuate nucleus of the hypothalamus, inhibiting orexigenic neurons that express neuropeptide Y and Agouti gene-related peptide and activating anorexigenic neurons that express pro-opiomelanocortin (Broberger, 2005). Plasma concentrations of leptin have been shown to mimic increases and decreases in adipose tissue (Maffei et al., 1995), and infusions of leptin have reduced food intake and body weight in both normal and obese mice (Halaas et al., 1995). A striking example of leptin's physiological importance is the *ob/ob* mouse, in which a nonsense mutation renders the protein nonfunctional (Ingalls et al., 1950). These animals are grossly obese and exhibit overeating, hypometabolism, and decreased locomotor activity (Coleman, 1978).

Recently, novel roles for leptin regulation outside the hypothalamus have been documented. Leptin-deficient *ob/ob* mice show a substantial decrease in stimulated dopamine release in the nucleus accumbens (NAc) and impaired vesicular somatodendritic dopamine stores in the ventral tegmental area (VTA) and the substantia nigra compacta (SNc) (Fulton et al., 2006; Roseberry et al., 2007). A potential action of leptin on vesicular release from midbrain dopamine neurons is fitting given the well-documented roles they play

in regulating movement and in mediating the rewarding properties of natural stimuli such as food (Roitman et al., 2004). Leptin has also been shown to act outside the central nervous system, as it induces an acute, Ca^{2+}-dependant increase in tyrosine hydroxylase (TH) activity and catecholamine secretion from chromaffin cells (Takekoshi et al., 1999; Takekoshi et al., 2001). Taken together, these findings suggest that one of the pathways through which leptin regulates food intake and energy expenditure could be via a largely unexplored role in the exocytosis of chemical messengers, particularly in catecholaminergic cells.

Uncoupling protein 2 (UCP2) is a carrier protein located at the inner mitochondrial membrane with ubiquitous expression in mammalian tissues (Fleury et al., 1997). UCP2 is one of five UCP homologues that, despite isoform-specific tissue distributions (Alan et al., 2009), all function as dissipaters of the inner mitochondrial membrane potential. This electrochemical potential is generated via the coupling of the electron transport chain to the active pumping of protons from the matrix into the intermembrane space, and serves as the primary driving force for the phosphorylation of ADP by ATP synthase. By leaking protons back into the mitochondrial matrix, UCP2 dissipates the electrochemical gradient and uncouples oxidative phosphorylation (Andrews et al., 2005).

Through disruption of the mitochondrial membrane potential, and its subsequent effect on cellular ATP levels, UCP2 could influence vesicular exocytosis via several mechanisms. The packaging of chemical messengers into vesicles is dependent on an ATP-driven pump that shuttles protons from the cytosol to the vesicle interior (Maycox et al., 1988). In addition, several other steps in exocytosis are ATP-dependent, including the recruitment and mobilization of vesicles to the plasma membrane and the priming of docked vesicles for Ca^{2+}-triggered fusion (Burgoyne and Morgan, 2003; Keating, 2008). Cellular ATP levels can also help shape the intracellular Ca^{2+} signal, which acts as the ultimate trigger for vesicular exocytosis, as ATP-dependent Ca^{2+} pumps on the endoplasmic

reticulum (ER) and plasma membranes help restore cytosolic Ca^{2+} to resting levels (Garcia et al., 2006). Finally, UCP2 can also affect cellular Ca^{2+} handling directly through dissipation of the mitochondrial membrane potential. This potential is the main driving force for clearance of cytosolic Ca^{2+} through the uniporter on the outer mitochondrial membrane (Gunter and Pfeiffer, 1990). An additional, and rather surprising, role for UCP2 in exocytosis has recently been proposed. UCP2 mRNA levels were significantly increased in two models of obesity: WT mice fed a high fat diet and leptin-deficient *ob/ob* mice (Parton et al., 2007). This finding suggests that some of the locomotor activity and transmitter release deficits in *ob/ob* mice could stem from a UCP2-induced decrease in cellular ATP levels.

To investigate the individual roles of leptin and UCP2 in vesicular release a multi-dimensional approach was used to study exocytosis in mice lacking the two proteins. Vesicular release in *ob/ob* and UCP2 KO mice was monitored using fast scan cyclic voltammetry (FSCV) in brain slices and amperometry and fluorescent Ca^{2+} imaging at isolated chromaffin cells. This combinatorial method has been used successfully in this lab to elucidate the mechanism responsible for the impaired dopamine release in a mouse model of Huntington's disease (Johnson et al., 2006; Johnson et al., 2007), and provides a complete description of transmitter release, from release and uptake from multiple exocytosis sites down to the individual vesicular event characteristics. Brain slice measurements in *ob/ob* mice revealed significant decreases in both dopamine release and uptake relative to WT mice. Measurements at individual chromaffin cells suggest the impaired release is due to Ca^{2+}-independent decreases in both vesicle mobilization and packaging. In slices from UCP2 KO mice, dopamine release and uptake were significantly increased compared to WT mice. However, no changes were observed in the individual vesicular events or intracellular Ca^{2+} dynamics at chromaffin cells, hindering identification of the mechanism responsible for the changes observed in slices.

Disclaimer

The experiments on exocytosis in UCP2 KO and *ob/ob* mice were undertaken in collaboration with the lab of Dr. Brad Lowell at Beth Israel Deaconess Hospital at Harvard University. The individual in this lab responsible for providing the genotypes of mice used in the study has recently been removed from his/her position as part of an investigation into academic misconduct. The genotypes of all mice used in this study have since been independently confirmed, and the results presented here are considered valid. However, many of the initial hypotheses driving this collaboration/study were based on data that is now in question. Much care has been taken so that the results and discussions included in this chapter are presented independently of these previous theories.

Materials and Methods

Animals

Mice were handled in accordance with the guidelines set forth by the Institutional Animal Care and Use Committee (IACUC) at UNC-Chapel Hill. UCP2 KO, *ob/ob*, and their littermate WT mice were generously provided by the lab of Dr. Brad Lowell at Harvard Unversity.

Preparation of Adrenal Medullary Chromaffin Cells

Murine chromaffin cells were prepared as previously described (Kolski-Andreaco et al., 2007) with some modifications. Mice were deeply anesthetized with ether, decapitated, and the adrenal glands rapidly removed into ice-cold, oxygenated Ca^{2+} and Mg^{2+}-free Locke's buffer containing (in mM): 154 NaCl, 3.6 KCl, 5.6 $NaHCO_3$, 5.6 glucose, and 10 HEPES, pH adjusted to 7.2 with NaOH. The medullae were isolated via gentle removal of cortical tissue and digested for 20 min at 37 ^{o}C in Dulbecco's Modified Eagle's Medium/Nutrient Mixture F-12 Ham (DMEM/F12) with 25 U/mL papain. The digestion media was replaced with a fresh aliquot, followed by a second 20 min digestion period. Digested tissue was washed and triturated with pipette tips of decreasing bore size in 500 µL

DMEM/F12 with 10 % fetal bovine serum and 2 % horse serum. The resulting cell suspension was distributed evenly to 3 poly-L-lysine-coated (0.1 mg/mL) 25 mm round glass coverslips. After 15 min attachment plates were fed with 2 mL DMEM/F12 containing 100 U/mL penicillin, 0.1 mg/mL streptomycin, 50 U/mL nystatin, and 40 µg/mL gentamicin. Plates were maintained in a humidified, 5 % CO_2 atmosphere at 37 ^oC for at least 24 h prior to experimentation.

Preparation of Brain Slices

Mice were anesthetized with ether and decapitated. The brain was rapidly removed and placed on ice. Coronal brain slices (300 µm thick) containing the caudate putamen or substantia nigra pars reticulata (SNr) were prepared in ice cold artificial cerebral spinal fluid (aCSF) using a Lancer Vibratome (World Precision Instruments, Sarasota, Fl.). The aCSF contained (in mM): 20 HEPES, 2.4 $CaCl_2$, 1.2 $MgCl_2$, 1.2 NaH_2PO_4, 2.45 KCl, 126 NaCl, 11 glucose, and 25 $NaHCO_3$. The pH was adjusted to pH 7.4 and the aCSF was saturated with 95 % O_2/5 % CO_2. Slices were superfused in aCSF at 37 ^oC for 35-40 minutes prior to recording.

Electrodes and Electrochemistry

Carbon-fiber microelectrodes were prepared using T650 carbon fibers (6 µm diameter, Amoco, Greenville, SC) as previously described (Kawagoe et al., 1993). Fibers were aspirated into glass capillaries (A-M Systems, Sequim, WA), and a vertical pipette puller (Narishige, Long Island, NY) was used to seal the glass around the carbon fiber. For cylinder electrodes, the exposed carbon fiber was trimmed to a length of 50 µm. For disk electrodes, the carbon fibers were cut at the glass seal, which was then reinforced with epoxy (15 % m-phenylenediamine in Epon 828 resin (Miller-Stephenson, Danbury, CT) heated to between 80 and 90 ^oC). Electrodes were kept at room temperature overnight, and then the epoxy was cured via sequential heating at 100 and 150 ^oC for 8 h and overnight, respectively. Disks were generated by beveling electrodes at 45 degrees on a diamond

dust-embedded polishing wheel (Sutter Instruments, Novato, CA). Prior to use, all electrodes were soaked in isopropyl alcohol for at least 20 min (Bath et al., 2000).

Amperometric recordings at single cells were made using a GeneClamp 500B amplifier (Axon Instruments, Molecular Devices, Union City, CA). Disk electrodes were held at 0.650 V vs. a Ag/AgCl reference electrode (BASi, West Lafayette, IN), a potential sufficient to oxidize catecholamines. The output current was analog filtered at 5 kHz with a low-pass Bessel filter and acquired at 20 kHz. Post-collection, traces were further digitally filtered using a 400 Hz low-pass Bessel filter. Data collection and filtering were controlled via the pClamp software provided with the amplifier.

Measurements of dopamine and serotonin (5-HT) release in brain slices were made using FSCV at cylinder electrodes. Waveform application, current monitoring, and stimulus application were all controlled by locally written software (Tarheel CV, Labview) through a home built potentiostat (UEI, UNC electronics shop). For dopamine detection, the potential at the electrode was scanned from -0.4 V to 1 V and back at 600 V/s, with the ramp repeated at 60 Hz. For 5-HT, the electrode was scanned from 0.2 V to 1 V down to -0.1 V and back to 0.2 V at 1000 V/s, with the waveform repeated at 10 Hz (Jackson et al., 1995). After an experiment, electrodes were calibrated in a flow injection system with a 1 μM bolus of analyte.

Single Cell Experiments

Glass coverslips containing plated cells were secured in a stainless steel coverslip holder and mounted on the stage of an inverted microscope (Eclipse TE300, Nikon Instruments, Melville, NY). A temperature controller (Warner Instruments, Hamden, CT) connected to the stage maintained cells at 37 ^{o}C throughout the experiments. The extracellular recording buffer contained (in mM): 145 NaCl, 3 KCl, 1.2 $MgCl_2$, 2.4 $CaCl_2$, 1.2 NaH_2PO_4, 11 glucose, and 10 HEPES, pH adjusted to 7.4 with NaOH. Exocytosis was triggered via a 0.5 s pressure ejection of 60 mM K^+ buffer from a stimulating pipette located

30 µm from the cell. Cells were stimmed every 30 s for 10 total stimulations. Stimulating pipettes with 6 to 10 µm tip diameters were fabricated using a horizontal pipette puller (Sutter Instruments, Novato, CA) and a microforge (Narishige, Long Island, NY). Pressure ejection was controlled via a multi-channel Picospritzer (General Valve Corporation, Parker Hannifin, Fairfield, NJ). Positioning of both the electrode and stimulating pipette was controlled using piezoelectric micromanipulators (Burleigh Instruments, Exfo, Plano, TX).

Slice Experiments

Recordings were performed on a microscope (Nikon FN1, Gibraltar Stage) fitted with a slice perfusion chamber (Warner Instruments, Hamden CT). Neurotransmitter release was evoked by local electrical stimulation delivered through a tungsten bipolar stimulating electrode placed on the surface of the slice (Frederick Haer Co., Bowdoinham, ME). The stimulation consisted of a computer generated, biphasic (2 ms per phase), constant-current (350 µA) pulse. A single stimulation pulse was used to evoke striatal dopamine release in the caudate putamen (Jones et al., 1995) and a 20 pulse 100 Hz stimulation train was used to evoke 5-HT release in the SNr (Bunin et al., 1998). The current pulse was optically isolated from the preparation (NL 800, Neurolog, Medical Systems, Great Neck, NY). Stimulations were performed at regular 3-5 min intervals to maintain consistent release. Neurotransmitter release was detected at a microelectrode placed 75-100 µm into the slice at a distance of 100-200 µm from the stimulating electrode.

Data Analysis

Amperometric spike analysis was performed using MiniAnalysis software (Synaptosoft, Decatur, GA). For inclusion, spike amplitude was required to be 5 times greater than the root-mean-squared current noise. Overlapping peaks were included in frequency and foot analysis, but excluded from individual spike analysis. Visual examination of the peaks was used to determine presence of pre- and post-spike feet. For frequency analysis, the first observed spike following stimulation marked the burst start time. Burst

end time was denoted by the first interspike interval > 1s. Individual amperometric spike characteristics such as quantal size (Q), $t_{1/2}$, and amplitude were averaged for an individual cell. The cumulative mean for an experimental group was then determined using the cell averages (Colliver et al., 2000).

Release values reported from the slice experiments are the maximal neurotransmitter concentrations obtained following stimulation. Values were averaged across multiple locations in each slice, and then pooled for each genotype. For determination of kinetic constants such as maximal uptake rate (V_{max}), concentration traces were fit to a Michaelis-Menten-based regression model (Wightman et al., 1988). Kinetic parameters were fixed, creating a simulated trace. This trace is then convoluted by the electrode time constant and compared to the experimental data (Wu et al., 2001).

All data are presented as means ± standard errors of the mean. Statistical comparisons were performed using a one-way ANOVA or a Student's t-test, as appropriate.

Fluorescent Measurements of Intracellular Ca^{2+}

Intracellular Ca^{2+} dynamics were monitored using the ratiometric dye fura-FF (Invitrogen, Carlsbad, CA). Plated cells were incubated for 20 min at 25 ^{o}C in extracellular recording buffer with 1 µg/mL esterified fura dye and 0.1 % (w/v) BSA, washed twice with buffer without dye, and then incubated for 20 min at 25 ^{o}C in buffer without dye for deesterification. Ca^{2+} bound and unbound dye were excited at 340 and 380 nm, respectively, using a computer-controlled high speed wavelength switcher (Sutter Instruments, Novato, CA). Emission was monitored at 510 nm using a CCD camera and acquisition software (Empix Imaging, Mississauga, ON, Canada).

Results

Stimulated Release in Brain Slices from ob/ob Animals

The effect of leptin deficiency on stimulated dopamine release was examined using brain slices containing the caudate putamen from both WT and *ob/ob* mice (Figure 3.1A).

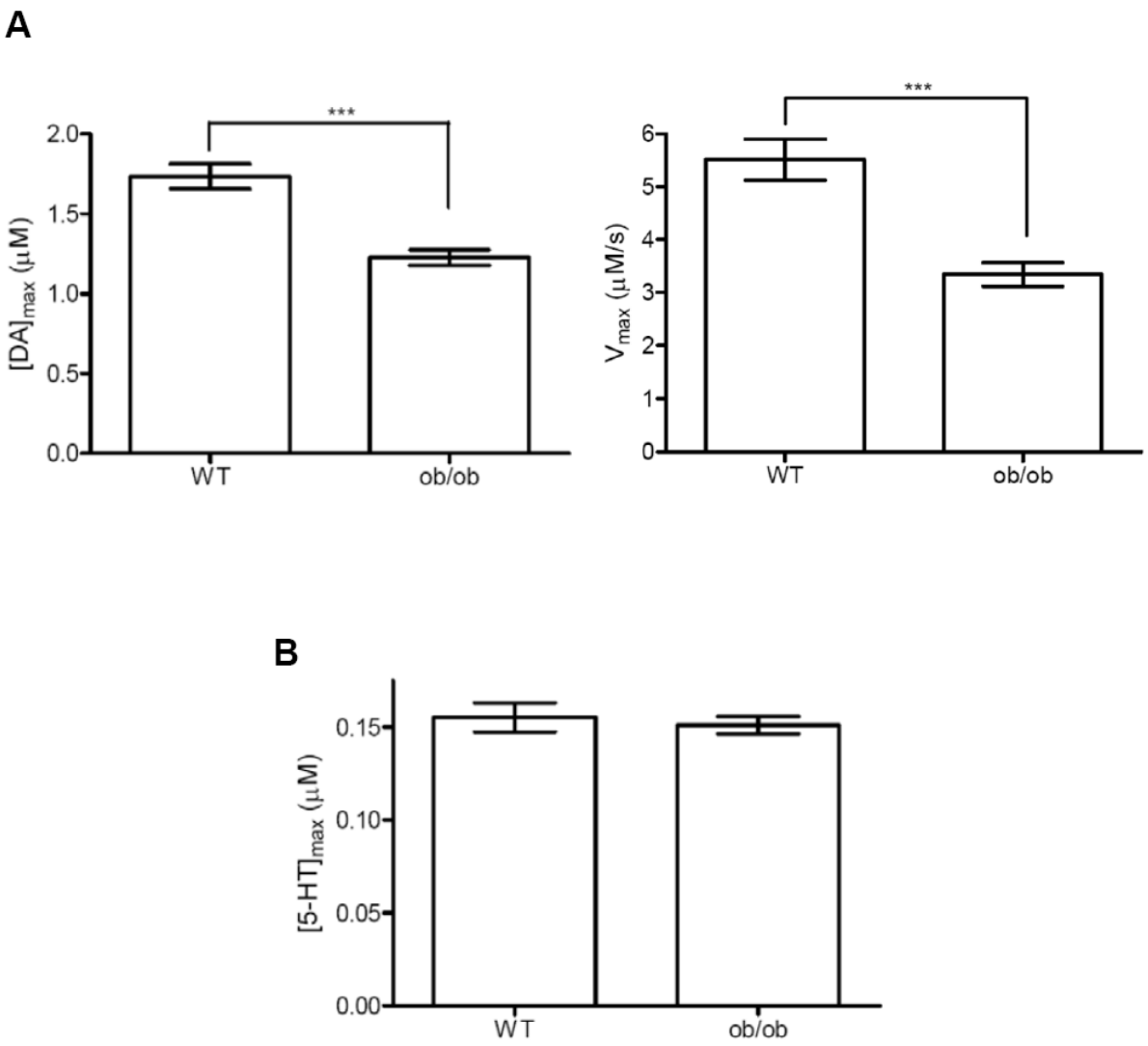

Figure 3.1. Leptin deficiency affects striatal dopamine release but not stimulated 5-HT release in the substantia nigra. **(A)** Stimulated dopamine release in the caudate putamen of *ob/ob* mice is significantly reduced (n = 9, *** $p < 0.001$, one-way ANOVA). Similarly, the V_{max} of dopamine uptake is significantly diminished in *ob/ob* mice compared to WT animals (*** $p < 0.001$, n = 5 both genotypes). **(B)** There is no significant difference in stimulated 5-HT release between WT animals or *ob/ob* animals ($p > 0.05$, n = 9).

Dopamine release was evoked with a single pulse electrical stimulation and detected with FSCV. Leptin deficiency resulted in significantly reduced ($p < 0.001$, one-way ANOVA, $n = 9$ for both genotypes) stimulated dopamine release, with the average maximal dopamine concentration measured at 1.74 ± 0.08 μM in WT slices and 1.23 ± 0.05 μM in *ob/ob* slices. In addition to decreased release of dopamine, clearance of the neurotransmitter was also significantly impaired ($p < 0.001$, $n = 5$ for both genotypes) in the leptin deficient animals, with the average V_{max} observed at 5.5 ± 0.4 μM/s in WT slices and 3.3 ± 0.2 μM/s in *ob/ob* slices. These alterations in transmitter release and uptake appear to be specific to dopamine neurons, as no significant difference ($p > 0.05$, $n = 9$ for both genotypes) was measured in electrically stimulated 5-HT release in the SNr of slices from WT and *ob/ob* mice (Figure 3.1B). Average maximal 5-HT concentrations were an equivalent 155 ± 8 nM and 151 ± 5 nM in WT and *ob/ob* animals, respectively.

Exocytosis at Chromaffin Cells from ob/ob Mice

Amperometric recordings of exocytosis were performed at isolated chromaffin cells from both WT ($n = 18$ cells) and *ob/ob* ($n = 23$ cells) mice. Vesicular release was triggered with a 0.5 s application of 60 mM K^+, spaced every 30 s, for a total of 10 stimulations. Figure 3.2 shows a representative amperometric trace following a single stimulation for both cell types. The amperometric spike characteristics for both genotypes are summarized in Table 3.1. On average, significantly fewer ($p < 0.05$, one-way ANOVA) vesicular events were detected at *ob/ob* cells (240 ± 16) compared to WT (310 ± 20). This difference was due to the frequency of events during each stimulated exocytotic burst, not the length. In WT cells, the average burst was 4.0 ± 0.3 s long with a spike frequency of 7.3 ± 0.4 Hz. In cells from the leptin-deficient mice, the burst length was unchanged ($p > 0.05$) at 3.9 ± 0.2 s, but the frequency of spikes was significantly reduced ($p < 0.001$) to 5.4 ± 0.2 Hz. The diminished spike frequency in *ob/ob* cells indicates an impaired vesicle mobilization process.

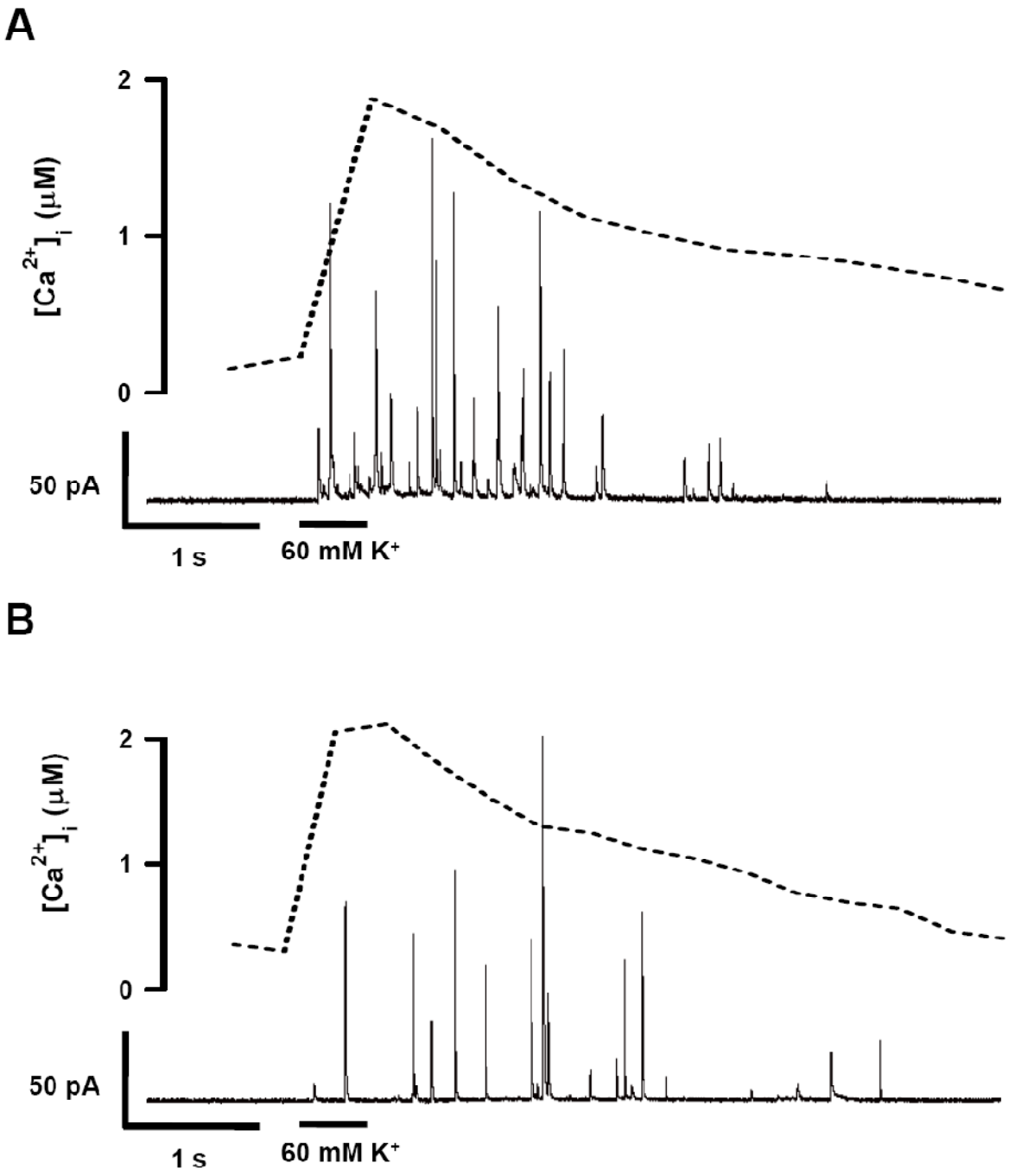

Figure 3.2. Vesicular release at WT and *ob/ob* cells. Representative amperometric traces (lower, solid line) and changes in $[Ca^{2+}]_i$ (upper, dotted line) measured in response to a 0.5 s stimulation with 60 mM K^+ at chromaffin cells from WT **(A)** and *ob/ob* **(B)** mice.

Table 3.1. Amperometric spike characteristics of WT, *ob/ob*, and UCP2 KO mice. Table shows the average number of spikes recorded during a trace (10 stimulations) and the average length of and frequency of spikes within an individual burst of exocytosis following a 0.5 s stimulation with 60 mM K^+. Individual spike characteristics, including % of events with a foot feature, amplitude (I_{max}, in pA), quantal size (Q, in molecules of catecholamine), and halfwidth ($t_{1/2}$, in ms), were averaged over the entire trace. No significant differences were observed between WT and UCP2 KO cells ($p > 0.05$, one-way ANOVA). Several measures of exocytosis were significantly reduced in *ob/ob* cells relative to WT (* = $p < 0.05$, ** = $p < 0.01$, *** = $p < 0.001$).

Cell Type	Total Spikes	Burst Length (s)	Spike Freq (Hz)	% w/ Foot	I_{max} (pA)	Q (molecules)	$t_{1/2}$ (ms)
WT (n = 18)	310 ± 20	4.0 ± 0.3	7.3 ± 0.4	6.5 ± 0.5	62 ± 4	$(8.1 \pm 0.6) \times 10^5$	5.8 ± 0.3
ob/ob (n = 23)	240 ± 16 *	3.9 ± 0.2	5.4 ± 0.2 ***	5.7 ± 0.6	40 ± 4 **	$(5.9 \pm 0.3) \times 10^5$ *	6.3 ± 0.3
UCP2 KO (n = 20)	280 ± 20	4.0 ± 0.2	6.4 ± 0.3	6.4 ± 0.6	55 ± 5	$(8.5 \pm 0.8) \times 10^5$	6.5 ± 0.4

While the mobilization of vesicles was altered in *ob/ob* cells, the efficiency of vesicle docking and the kinetics of catecholamine extrusion following fusion were both unchanged. There was no significant difference ($p > 0.05$) between WT (6.5 ± 0.5 %) and *ob/ob* cells (5.7 ± 0.6 %) in the percentage of events exhibiting a pre- and/or post-spike foot, and the average $t_{1/2}$ for events from WT (5.8 ± 0.3 ms) and *ob/ob* cells (6.3 ± 0.3 ms) was similar. However, the size of individual vesicular events was affected in the leptin-deficient mice. Spike amplitude was significantly reduced ($p < 0.01$) in *ob/ob* cells (40 ± 4 pA) compared to WT (62 ± 4 pA). In addition, the average spike Q was only (5.9 ± 0.3) x 10^5 molecules in *ob/ob* cells, significantly smaller ($p < 0.05$) than the Q of (8.1 ± 0.6) x 10^5 molecules observed in WT cells. The decreased content suggests that leptin-deficient mice have deficits in vesicular packaging, storage, and/or catecholamine synthesis.

As previous reports have implicated leptin acts via a Ca^{2+}-mediated pathway (Takekoshi et al., 2001), the ratiometric dye fura-FF was used to monitor intracellular Ca^{2+} concentrations ($[Ca^{2+}]_i$) in WT (n = 28) and *ob/ob* (n = 21) cells following depolarization with 60 mM K^+. Figure 3.2 shows a representative trace of $[Ca^{2+}]_i$ for each cell type following a single stimulation. The properties of the intracellular Ca^{2+} transient for both genotypes are summarized in Table 3.2. No significant difference ($p > 0.05$, one-way ANOVA) was observed in the $[Ca^{2+}]_i$ response between WT and *ob/ob* cells. The area under the $[Ca^{2+}]_i$ peak was 1.37 ± 0.09 arbitrary units in WT cells and 1.54 ± 0.17 in *ob/ob* cells. The duration of the Ca^{2+} increase was also unchanged, with a $t_{1/2}$ in WT cells of 3.0 ± 0.2 s and a $t_{1/2}$ in *ob/ob* cells of 2.8 ± 0.2 s. These results indicate that the differences in vesicular release in leptin-deficient mice can't be attributed to changes in depolarization-induced Ca^{2+} influx.

Stimulated Release in Brain Slices from UCP2 KO Animals

Potential changes in the release and uptake of dopamine were evaluated in brain slices containing the caudate putamen from both WT and UCP2 KO mice (Figure 3.3A). Dopamine release was evoked with a single pulse electrical stimulation and monitored with

Table 3.2. Intracellular Ca^{2+} dynamics in WT, *ob/ob*, and UCP2 KO mice. Table shows the average area (in arbitrary units), halfwidth ($t_{1/2}$, in s), and decay time (t_d, in s) of the increase in $[Ca^{2+}]_i$ following a 0.5 s stimulation with 60 mM K^+. No significant difference is observed between WT and *ob/ob* or UCP2 KO mice for any of the measures ($p > 0.05$, one-way ANOVA).

Cell Type	Area	$t_{1/2}$ (s)	t_d (s)
WT (n = 28)	1.37 ± 0.09	3.0 ± 0.2	3.7 ± 0.2
ob/ob (n = 21)	1.54 ± 0.17	2.8 ± 0.2	3.9 ± 0.4
UCP2 KO (n = 23)	1.30 ± 0.09	2.9 ± 0.1	3.4 ± 0.2

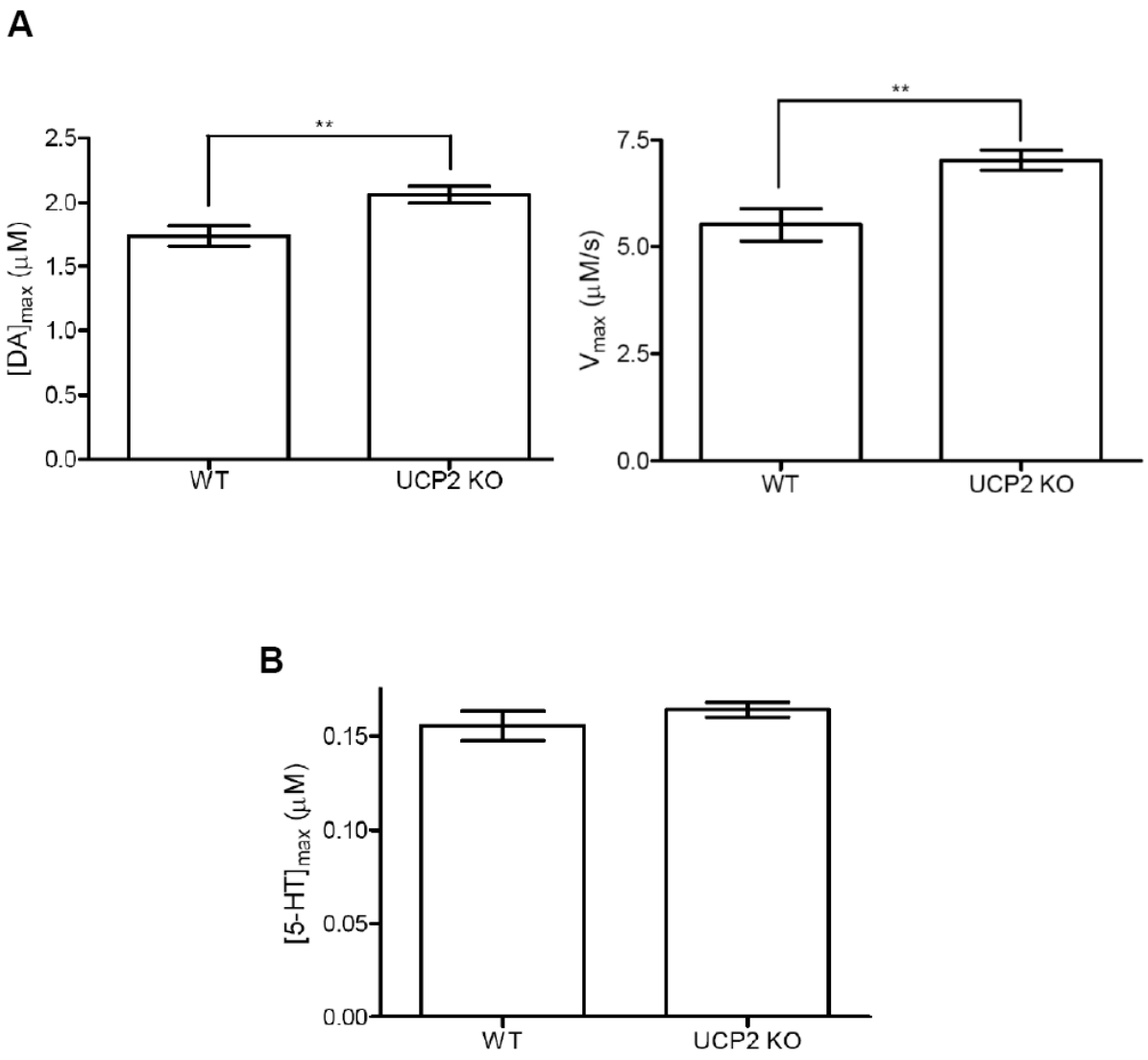

Figure 3.3. Lack of UCP2 affects striatal dopamine release but not stimulated 5-HT release in the substantia nigra. **(A)** Stimulated dopamine release in the caudate putamen of UCP2 KO mice is significantly enhanced relative to WT animals (** $p < 0.01$, one-way ANOVA, $n = 9$ both genotypes). Likewise, the V_{max} of dopamine uptake is significantly increased in UCP2 KO mice compared to WT animals (** $p < 0.01$, $n = 5$ both genotypes). **(B)** There is no significant difference in stimulated 5-HT release between WT animals or UCP2 KO animals ($p > 0.05$, $n \geq 9$, both genotypes).

FSCV. Animals lacking UCP2 demonstrated significantly increased ($p < 0.01$, one-way ANOVA, $n = 9$ for both genotypes) stimulated dopamine release, with average maximal dopamine concentrations of 1.74 ± 0.08 μM in WT slices and 2.06 ± 0.07 μM in UCP2 KO slices. Similar to the *ob/ob* animals, this change in release was mirrored by a corresponding change in uptake. The maximal uptake rate of dopamine was significantly enhanced ($p < 0.01$, $n = 5$ for both genotypes) in UCP2 deficient mice, with an average V_{max} of 5.5 ± 0.4 μM/s in WT slices and 7.0 ± 0.2 μM/s in UCP2 KO mice. These alterations in dopamine signaling are apparently the result of long-term or adaptive changes at the terminals, as attempts to mimic the UCP2 KO phenotype with acute treatment of a UCP2 inhibitor were unsuccessful. A 35 min incubation with 20 μM genipin, which cross-links UCP2 and prevents proton shuttling (Zhang et al., 2006), did not significantly alter ($p > 0.05$, $n = 5$ for both genotypes) the maximal dopamine concentration or uptake rate in WT slices (Figure 3.4). This dosage and time frame had previously been shown to acutely modulate ATP levels in dopamine synaptosomes (Lowell lab, unpublished) and glucose sensing in slices of hypothalamus (Parton et al., 2007). Interestingly, the effects of UCP2 KO appear specific to dopaminergic neurons. No significant difference ($p > 0.05$, $n = 9$ for both genotypes) was observed in electrically stimulated 5-HT release in the SNr, with average maximal 5-HT concentrations of 155 ± 8 nM in WT slices and 164 ± 4 nM in UCP2 KO slices (Figure 3.3B).

Exocytosis at Chromaffin Cells from UCP2 KO Mice

Amperometric recordings of exocytosis were also compared at isolated chromaffin cells from WT ($n = 18$ cells) and UCP2 KO ($n = 20$ cells) mice. As before, vesicular release was triggered with a 0.5 s application of 60 mM K^+, spaced every 30 s, for a total of 10 stimulations. Figure 3.5 shows a representative amperometric trace following a single stimulation for both cell types. The amperometric spike characteristics for both genotypes are summarized in Table 3.1. Despite the ATP-dependence of virtually all phases of the vesicle cycle, vesicular release observed at UCP2 KO cells was completely unaffected ($p >$

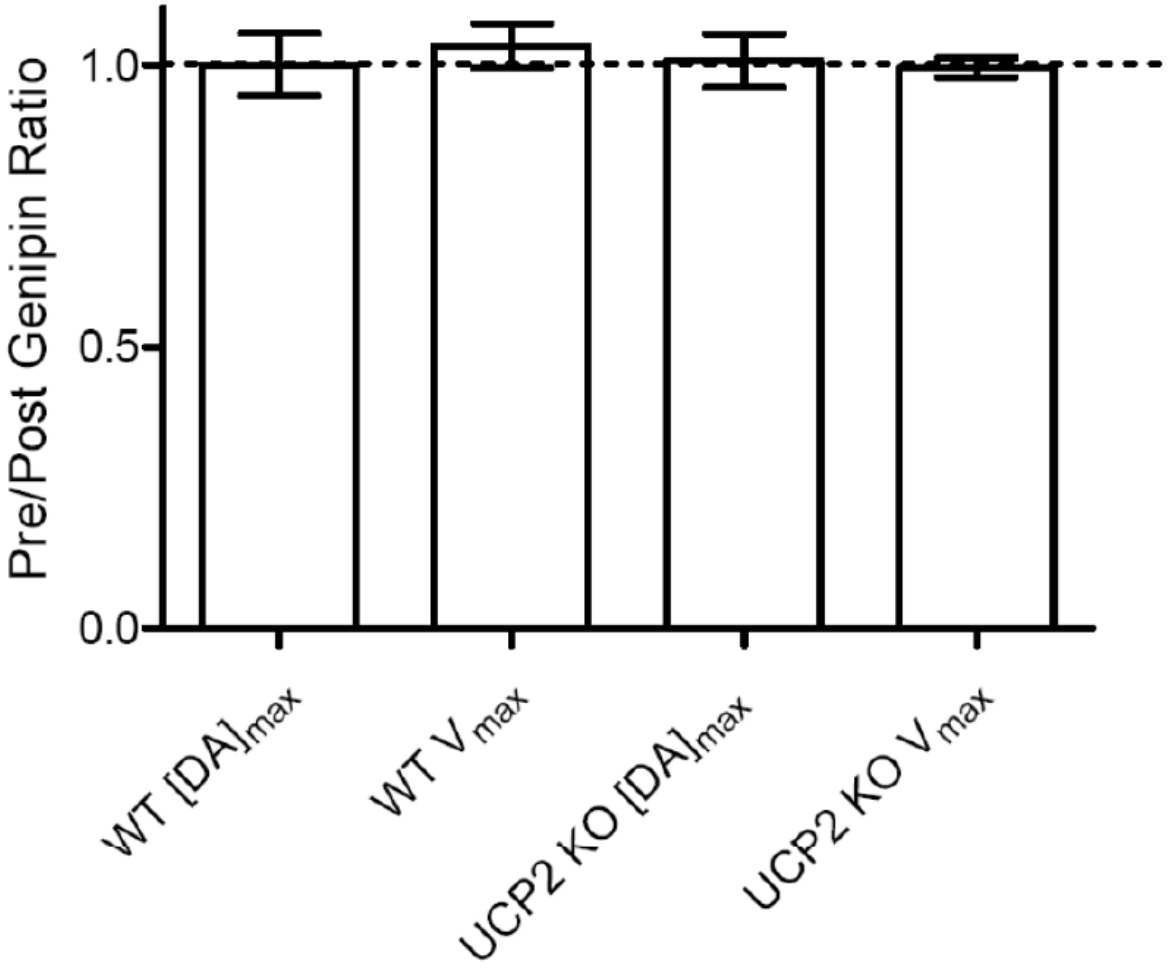

Figure 3.4. Genipin modulation of dopamine release and uptake in mouse brain slices. The addition of 20 μM genipin to striatal brain slices for 35 minutes does not significantly alter ($p > 0.05$, $n = 5$ both genotypes) $[DA]_{max}$ or V_{max} in WT mice when compared to UCP2 KO mice. In this experiment, the UCP2 KO mouse is the control animal because UCP2 KO mice are insensitive to genipin.

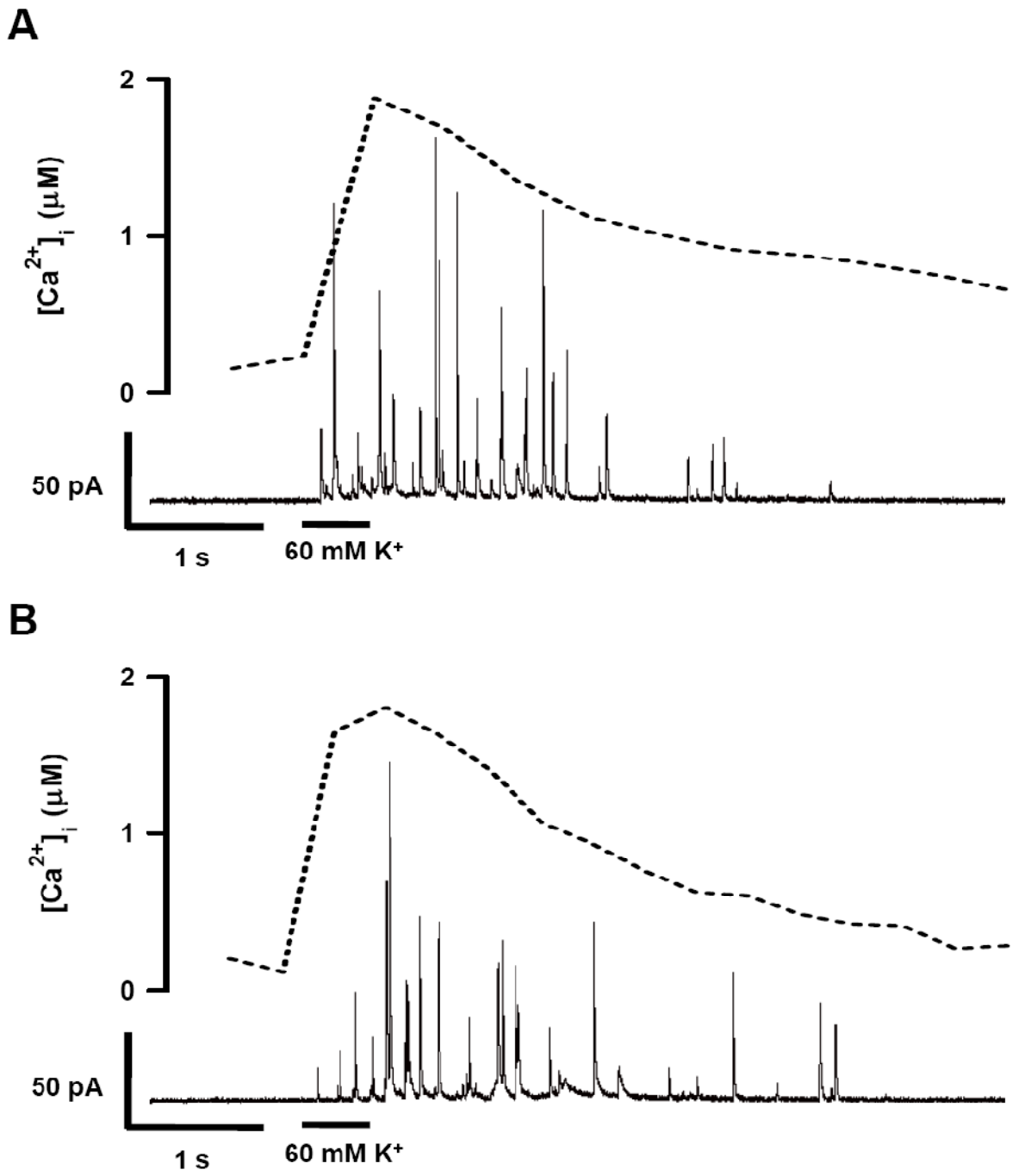

Figure 3.5. Vesicular release at WT and UCP2 KO cells. Representative amperometric traces (lower, solid line) and changes in $[Ca^{2+}]_i$ (upper, dotted line) measured in response to a 0.5 s stimulation with 60 mM K^+ at chromaffin cells from WT **(A)** and UCP2 KO **(B)** mice.

0.05 for all characteristics, one-way ANOVA) in reference to WT cells. An average of 310 ± 20 events were detected at WT cells, with individual bursts lasting 4.0 ± 0.3 s and having a spike frequency of 7.3 ± 0.4 Hz. Similarly, an average of 280 ± 20 events were detected at UCP2 KO cells, with each burst lasting 4.0 ± 0.2 s and having a spike frequency of 6.4 ± 0.3 Hz. The percentage of WT cells exhibiting a pre- and/or post-spike foot was 6.5 ± 0.5 %, equivalent to the 6.4 ± 0.6 % noted for UCP2 KO cells. The average amperometric spike for WT cells had an I_{max} of 62 ± 4 pA, $t_{1/2}$ of 5.8 ± 0.3 ms, and Q of (8.1 ± 0.6) x 10^5 molecules. Likewise, the average spike for UCP2 KO cells had an I_{max} of 55 ± 5 pA, $t_{1/2}$ of 6.5 ± 0.4 ms, and Q of (8.5 ± 0.8) x 10^5 molecules.

As cellular ATP levels and the mitochondrial membrane potential are involved in controlling the clearance of Ca^{2+} from the cytosol, the ratiometric dye fura-FF was used to monitor $[Ca^{2+}]_i$ in WT (n = 28) and UCP2 KO (n = 23) cells following depolarization with 60 mM K^+. Figure 3.5 shows a representative trace of $[Ca^{2+}]_i$ for each cell type following a single stimulation. The properties of the intracellular Ca^{2+} transient for both genotypes are summarized in Table 3.2. Surprisingly, no significant differences ($p > 0.05$, one-way ANOVA) were observed in the $[Ca^{2+}]_i$ response between WT and UCP2 KO cells. The area under the $[Ca^{2+}]_i$ peak was 1.37 ± 0.09 arbitrary units in WT cells and 1.30 ± 0.09 in UCP2 KO cells. The cytosolic Ca^{2+} influx in WT cells had a $t_{1/2}$ of 3.0 ± 0.2 s and took 3.7 ± 0.2 s to return to resting levels from peak $[Ca^{2+}]_i$. In UCP2 KO cells, the cytosolic Ca^{2+} influx had a $t_{1/2}$ of 2.9 ± 0.1 s and took 3.4 ± 0.2 s to return to resting levels from peak $[Ca^{2+}]_i$.

Discussion

FSCV recordings of stimulated neurotransmitter release in brain slices of leptin-deficient animals revealed dopamine-specific alterations in transmission (Figure 3.1). Dopamine release in the caudate putamen was reduced by approximately 30 % in *ob/ob* mice, a finding consistent with previous reports showing decreased dopamine release in the NAc and impaired dopamine stores in the VTA and SNc (Fulton et al., 2006; Roseberry et

al., 2007). This reduction in release was coincident with a near 40 % decrease in the maximal uptake rate, suggesting a natural adaptive mechanism in which the brain attempts to maintain extracellular dopamine tone by modulating uptake in response to release. For a more detailed examination of vesicular release in leptin-deficient animals, single cell studies were also performed. Amperometric measurements of exocytosis at chromaffin cells from *ob/ob* mice showed a 26 % decrease in the frequency of vesicular events and a 27 % reduction in Q, or vesicular catecholamine content (Figure 3.2 and Table 3.1). These results strongly suggest that the observed changes in dopamine release result from impairments in vesicle mobilization upon depolarizing stimulation and either vesicular packaging, storage, or catecholamine synthesis, or some combination thereof. Separate studies have shown that acute leptin application facilitates a Ca^{2+}-dependent increase in catecholamine secretion and TH activity (Takekoshi et al., 1999; Takekoshi et al., 2001). However, the diminished vesicular release observed here was independent of changes in $[Ca^{2+}]_i$ dynamics (Figure 3.2 and Table 3.2), suggesting that the leptin-induced Ca^{2+} currents are not a substantial contributor to the endogenous exocytosis-triggering Ca^{2+} influx. As a whole, these data support a model whereby leptin signaling outside the hypothalamus is important in its regulation of metabolism and energy expenditure. In *ob/ob* animals the absence of basal leptin tone results in reduced catecholaminergic transmission. One component of this reduction is a decrease in vesicular catecholamine stores, which current evidence suggests could be due to a depressed state of synthesis via TH (Takekoshi et al., 2001).

One final but crucial point to make in regards to leptin deficiency is the inherent complexity in analyzing the phenotype of the *ob/ob* mouse. The genetic loss of a functional leptin protein leads to behaviors that make the animals grossly obese. The obese state itself is associated with wide-ranging deficits in physiological function. Thus, while the results reported here are consistent with a leptin effect, it's impossible to separate the hormone deficit from the obesity and assign a direct causal relationship. Illustrating this

difficulty, work on a separate mouse model of obesity also observed impairments in tyrosine hydroxylase expression and K^+-stimulated catecholamine secretion in chromaffin cells (Martins et al., 2004). In addition, high fat diet-induced obesity has been shown to reduce dopamine transporter density in the caudate putamen (South and Huang, 2008), consistent with the decrease in V_{max} observed in this study. Future experiments in WT mice fed an obesity-inducing, high fat diet could help illuminate the true origin of these alterations in catecholamine exocytosis.

By dissipating the proton gradient across the inner mitochondrial membrane, UCP2 effectively limits the maximal rate of cellular ATP production. UCP2 KO animals would then be expected to exist in a hyperenergetic state. Increased cellular ATP levels would exert competing effects on vesicular release through several ATP-dependent processes. Packaging of transmitters through vesicular transporters, mobilization of vesicles to plasma membrane, and priming of docked vesicles would theoretically be facilitated (Burgoyne and Morgan, 2003; Keating, 2008). However, clearance of cytosolic Ca^{2+} by pumps on the plasma and ER membranes would also be facilitated, limiting the elevations in $[Ca^{2+}]_i$ that trigger exocytosis (Garcia et al., 2006). In brain slices of UCP2 KO mice, FSCV recordings in the caudate putamen suggest that, at least for dopamine release, the facilitation of steps in the vesicle cycle overrides the increase in Ca^{2+} clearance (Figure 3.3A). Dopamine release is enhanced by approximately 20 % in UCP2 KO animals, and accompanied by a similar 27 % increase in maximal uptake rate. The time course necessary for increased ATP production to impact exocytosis is apparently greater than 35 min, as acute blockade of UCP2 with genipin did not alter dopamine release (Figure 3.4). By contrast, 5-HT release in the SNr was completely unaffected by UCP2 removal (Figure 3.3B); somewhat surprising given the multitude of potential ATP effects. However, this null result was repeated in studies of exocytosis at single chromaffin cells. Amperometric measurements showed no changes in frequency of spikes or average vesicular content (Figure 3.5 and Table 3.1),

indicating no increase in vesicular packaging, mobilization, or priming. The size and duration of the depolarization-induced intracellular Ca^{2+} transient were equal in both cell types (Figure 3.5 and Table 3.2), indicating no alterations in cytosolic Ca^{2+} clearance through ATP-driven Ca^{2+} pumps or uptake via the mitochondrial uniporter.

The varied effects observed in the vesicular release of chemical messengers in UCP2 KO mice prevent a straightforward description of the protein's role in exocytosis. One partial explanation for these contradictory results is that the uncoupling mechanism of UCP2 isn't constitutively active. A recently emerging hypothesis proposes that UCP2 does not contribute to a basal proton conductance, but is activated by reactive oxygen species generated by the leak of electrons from the electron transport chain (Cannon et al., 2006; Echtay, 2007). The activity-dependent uncoupling of oxidative phosphorylation would then protect the cell from damage. Such a mechanism would help explain the absence of significant changes in individual vesicular events and Ca^{2+} handling at chromaffin cells, in 5-HT release in brain slices containing the SNr, and in dopamine release in the caudate putamen following acute inhibition of UCP2 with genipin. However, the enhanced dopamine release and uptake in UCP2 KO animals doesn't fit with this explanation. A protective role for UCP2 in response to reactive oxygen species would predict either no effect on dopamine release in UCP2 KO mice or a decrease in release owing to greater dopaminergic cell degeneration. A second possible reason for the diverse responses could be cell-type specific differences in the expression of UCP2 or in the endogenous activity of the protein. The release measurements would indicate that, relative to 5-HT neurons and chromaffin cells, dopamine neurons express either a greater amount of UCP2 or a variant with higher basal proton conductance. Although, the failure of genipin to acutely alter dopamine release would argue that even with higher expression/activity UCP2 does not effectively couple vesicular release to short term changes in oxidative phosphorylation. Future measurements of exocytosis from WT and UCP2 KO cells/slices under conditions of oxidative stress and

extension of the genipin treatment to SNr slices and chromaffin cells could help elucidate the function of UCP2 in regulating vesicular release.

References

Alan L, Smolkova K, Kronusova E, Santorova J, Jezek P (2009) Absolute levels of transcripts for mitochondrial uncoupling proteins UCP2, UCP3, UCP4, and UCP5 show different patterns in rat and mice tissues. J Bioenerg Biomembr 41:71-78.

Andrews ZB, Diano S, Horvath TL (2005) Mitochondrial uncoupling proteins in the CNS: in support of function and survival. Nat Rev Neurosci 6:829-840.

Bath BD, Michael DJ, Trafton BJ, Joseph JD, Runnels PL, Wightman RM (2000) Subsecond adsorption and desorption of dopamine at carbon-fiber microelectrodes. Anal Chem 72:5994-6002.

Broberger C (2005) Brain regulation of food intake and appetite: molecules and networks. J Intern Med 258:301-327.

Bunin MA, Prioleau C, Mailman RB, Wightman RM (1998) Release and uptake rates of 5-hydroxytryptamine in the dorsal raphe and substantia nigra reticulata of the rat brain. J Neurochem 70:1077-1087.

Burgoyne RD, Morgan A (2003) Secretory granule exocytosis. Physiol Rev 83:581-632.

Cannon B, Shabalina IG, Kramarova TV, Petrovic N, Nedergaard J (2006) Uncoupling proteins: a role in protection against reactive oxygen species--or not? Biochim Biophys Acta 1757:449-458.

Coleman DL (1978) Obese and diabetes: two mutant genes causing diabetes-obesity syndromes in mice. Diabetologia 14:141-148.

Colliver TL, Hess EJ, Pothos EN, Sulzer D, Ewing AG (2000) Quantitative and statistical analysis of the shape of amperometric spikes recorded from two populations of cells. J Neurochem 74:1086-1097.

Echtay KS (2007) Mitochondrial uncoupling proteins--what is their physiological role? Free Radic Biol Med 43:1351-1371.

Fleury C, Neverova M, Collins S, Raimbault S, Champigny O, Levi-Meyrueis C, Bouillaud F, Seldin MF, Surwit RS, Ricquier D, Warden CH (1997) Uncoupling protein-2: a novel gene linked to obesity and hyperinsulinemia. Nat Genet 15:269-272.

Friedman JM (2009) Leptin at 14 y of age: an ongoing story. Am J Clin Nutr 89:973S-979S.

Fulton S, Pissios P, Manchon RP, Stiles L, Frank L, Pothos EN, Maratos-Flier E, Flier JS (2006) Leptin regulation of the mesoaccumbens dopamine pathway. Neuron 51:811-822.

Garcia AG, Garcia-De-Diego AM, Gandia L, Borges R, Garcia-Sancho J (2006) Calcium signaling and exocytosis in adrenal chromaffin cells. Physiol Rev 86:1093-1131.

Gunter TE, Pfeiffer DR (1990) Mechanisms by which mitochondria transport calcium. Am J Physiol 258:C755-786.

Halaas JL, Gajiwala KS, Maffei M, Cohen SL, Chait BT, Rabinowitz D, Lallone RL, Burley SK, Friedman JM (1995) Weight-reducing effects of the plasma protein encoded by the obese gene. Science 269:543-546.

Ingalls AM, Dickie MM, Snell GD (1950) Obese, a new mutation in the house mouse. J Hered 41:317-318.

Jackson BP, Dietz SM, Wightman RM (1995) Fast-scan cyclic voltammetry of 5-hydroxytryptamine. Anal Chem 67:1115-1120.

Johnson MA, Rajan V, Miller CE, Wightman RM (2006) Dopamine release is severely compromised in the R6/2 mouse model of Huntington's disease. J Neurochem 97:737-746.

Johnson MA, Villanueva M, Haynes CL, Seipel AT, Buhler LA, Wightman RM (2007) Catecholamine exocytosis is diminished in R6/2 Huntington's disease model mice. J Neurochem 103:2102-2110.

Jones SR, Garris PA, Wightman RM (1995) Different effects of cocaine and nomifensine on dopamine uptake in the caudate-putamen and nucleus accumbens. J Pharmacol Exp Ther 274:396-403.

Kawagoe KT, Zimmerman JB, Wightman RM (1993) Principles of voltammetry and microelectrode surface states. J Neurosci Methods 48:225-240.

Keating DJ (2008) Mitochondrial dysfunction, oxidative stress, regulation of exocytosis and their relevance to neurodegenerative diseases. J Neurochem 104:298-305.

Kolski-Andreaco A, Cai H, Currle DS, Chandy KG, Chow RH (2007) Mouse adrenal chromaffin cell isolation. J Vis Exp:129.

Maffei M, Halaas J, Ravussin E, Pratley RE, Lee GH, Zhang Y, Fei H, Kim S, Lallone R, Ranganathan S, et al. (1995) Leptin levels in human and rodent: measurement of plasma leptin and ob RNA in obese and weight-reduced subjects. Nat Med 1:1155-1161.

Martins AC, Souza KL, Shio MT, Mathias PC, Lelkes PI, Garcia RM (2004) Adrenal medullary function and expression of catecholamine-synthesizing enzymes in mice with hypothalamic obesity. Life Sci 74:3211-3222.

Maycox PR, Deckwerth T, Hell JW, Jahn R (1988) Glutamate uptake by brain synaptic vesicles. Energy dependence of transport and functional reconstitution in proteoliposomes. J Biol Chem 263:15423-15428.

Parton LE, Ye CP, Coppari R, Enriori PJ, Choi B, Zhang CY, Xu C, Vianna CR, Balthasar N, Lee CE, Elmquist JK, Cowley MA, Lowell BB (2007) Glucose sensing by POMC neurons regulates glucose homeostasis and is impaired in obesity. Nature 449:228-232.

Roitman MF, Stuber GD, Phillips PE, Wightman RM, Carelli RM (2004) Dopamine operates as a subsecond modulator of food seeking. J Neurosci 24:1265-1271.

Roseberry AG, Painter T, Mark GP, Williams JT (2007) Decreased vesicular somatodendritic dopamine stores in leptin-deficient mice. J Neurosci 27:7021-7027.

South T, Huang XF (2008) High-fat diet exposure increases dopamine D2 receptor and decreases dopamine transporter receptor binding density in the nucleus accumbens and caudate putamen of mice. Neurochem Res 33:598-605.

Takekoshi K, Ishii K, Kawakami Y, Isobe K, Nanmoku T, Nakai T (2001) Ca(2+) mobilization, tyrosine hydroxylase activity, and signaling mechanisms in cultured porcine adrenal medullary chromaffin cells: effects of leptin. Endocrinology 142:290-298.

Takekoshi K, Motooka M, Isobe K, Nomura F, Manmoku T, Ishii K, Nakai T (1999) Leptin directly stimulates catecholamine secretion and synthesis in cultured porcine adrenal medullary chromaffin cells. Biochem Biophys Res Commun 261:426-431.

Wightman RM, Amatore C, Engstrom RC, Hale PD, Kristensen EW, Kuhr WG, May LJ (1988) Real-time characterization of dopamine overflow and uptake in the rat striatum. Neuroscience 25:513-523.

Wu Q, Reith ME, Wightman RM, Kawagoe KT, Garris PA (2001) Determination of release and uptake parameters from electrically evoked dopamine dynamics measured by real-time voltammetry. J Neurosci Methods 112:119-133.

Zhang CY, Parton LE, Ye CP, Krauss S, Shen R, Lin CT, Porco JA, Jr., Lowell BB (2006) Genipin inhibits UCP2-mediated proton leak and acutely reverses obesity- and high glucose-induced beta cell dysfunction in isolated pancreatic islets. Cell Metab 3:417-427.

Chapter 4

Exocytosis in a Mouse Model of Fragile X Syndrome

Introduction

Fragile X syndrome (FXS) is the most commonly inherited form of mental retardation, often presenting as an autism spectrum disorder (Garber et al., 2008). FXS is an X chromosome-linked disorder with an unusual inheritance pattern, in which intellectually normal male carriers pass the relevant alleles through their unaffected carrier daughters and on to their affected sons (Sherman et al., 1985). The gene responsible for FXS is Fragile X Mental Retardation 1 gene (*Fmr1*), which encodes an mRNA-binding protein termed fragile X mental retardation protein (FMRP) (Verkerk et al., 1991; Ashley et al., 1993). FMRP selectively binds about 4 % of the mRNA in the mammalian brain, and is hypothesized to play a role in synaptic plasticity through negative regulation of local protein synthesis at the synapse (Bassell and Warren, 2008). In FXS, expansion of a CGG repeat in the 5'-untranslated region of *Fmr1* leads to hypermethylation-induced silencing of the gene and the absence of FMRP (Sutcliffe et al., 1992; Coffee et al., 1999).

A common phenotype of human FXS patients and a mouse model of the disease, in which the *Fmr1* gene is knocked out (1994), is the prevalence of long, thin dendritic spines of immature morphology (Comery et al., 1997; Irwin et al., 2000). Naturally, most investigations of the role of FMRP in FXS have thus focused on a postsynaptic mechanism. These studies suggest that the cognitive deficits in FXS arise from excess protein synthesis in the basal state and a loss of stimulus-induced translation upon activation of metabotropic glutamate receptors (Muddashetty et al., 2007). Dysregulation of mRNA translation at the

synapse would have significant consequences on dendritic spine development and long-term synaptic plasticity, processes crucial to learning and memory. While most work to date has focused on the postsynaptic role of FMRP, evidence for a presynaptic mechanism has also surfaced. Cortical neurons in *Fmr1* KO mice show diminished levels of several presynaptic proteins associated with the exocytotic machinery, including Rab and synaptotagmin isoforms and Munc-13 (Liao et al., 2008). The putative down regulation of Rab isoforms in FXS is particularly compelling as Rab3A has been shown to be essential for the expression of LTP in the hippocampus (Castillo et al., 1997). Further evidence for presynaptic mechanisms in FXS comes from observed deficiencies in the release of neuropeptides from large dense core vesicles (LDCVs) in *Fmr1* KO mice (Dr. Jonathan Sweedler, personal communication). Additionally, impairments in object recognition have been noted in *Fmr1* KO mice (Ventura et al., 2004). These impairments were coincident with lower basal levels of dopamine in the caudate putamen and altered amphetamine-induced dopamine release in the prefrontal cortex and caudate putamen.

This chapter explores a potential presynaptic role of FMRP in regulating exocytosis by studying vesicular release in *Fmr1* KO mice in two complementary preparations: fast scan cyclic voltammetry (FSCV) monitoring of transmitter release in brain slices and amperometric recordings at isolated chromaffin cells. Measurements at single cells allow for characteristics of individual exocytotic events to be evaluated while measurements in the intact tissue slices can probe the summated release from multiple exocytosis sites as well as the diffusion, uptake, and receptor interactions of neurotransmitters following release. Together, these two techniques have previously been utilized in this lab to attribute the diminished dopamine release in a mouse model of Huntington's disease to impaired vesicle packaging (Johnson et al., 2006; Johnson et al., 2007). Presently, both techniques were unable to detect any alterations in the presynaptic release of chemical messengers in *Fmr1* KO mice, supporting a role for FMRP that is predominantly postsynaptic.

Materials and Methods

Animals

Mice were handled in accordance with the guidelines set forth by the Institutional Animal Care and Use Committee (IACUC) at UNC-Chapel Hill. *Fmr1* KO mice and their littermate WT mice were provided by the lab of Jonathan Sweedler at the University of Illinois at Urbana Champaign.

Preparation of Adrenal Medullary Chromaffin Cells

Murine chromaffin cells were prepared as previously described (Kolski-Andreaco et al., 2007) with some modifications. Mice were deeply anesthetized with ether, decapitated, and the adrenal glands rapidly removed into ice-cold, oxygenated Ca^{2+} and Mg^{2+}-free Locke's buffer containing (in mM): 154 NaCl, 3.6 KCl, 5.6 $NaHCO_3$, 5.6 glucose, and 10 HEPES, pH adjusted to 7.2 with NaOH. The medullae were isolated via gentle removal of cortical tissue and digested for 20 min at 37 ^{o}C in Dulbecco's Modified Eagle's Medium/Nutrient Mixture F-12 Ham (DMEM/F12) with 25 U/mL papain. The digestion media was replaced with a fresh aliquot, followed by a second 20 min digestion period. Digested tissue was washed and triturated with pipette tips of decreasing bore size in 500 µL DMEM/F12 with 10 % fetal bovine serum and 2 % horse serum. The resulting cell suspension was distributed evenly to 3 poly-L-lysine-coated (0.1 mg/mL) 25 mm round glass coverslips. After 15 min attachment plates were fed with 2 mL DMEM/F12 containing 100 U/mL penicillin, 0.1 mg/mL streptomycin, 50 U/mL nystatin, and 40 µg/mL gentamicin. Plates were maintained in a humidified, 5 % CO_2 atmosphere at 37 ^{o}C for at least 24 h prior to experimentation.

Preparation of Brain Slices

Mice were anesthetized with ether and decapitated. The brain was rapidly removed and placed on ice. Coronal brain slices (300 µm thick) containing the caudate putamen, substantia nigra pars reticulata (SNr), or ventral bed nucleus of the stria terminalis (*v*BNST)

were prepared in ice cold artificial cerebral spinal fluid (aCSF) using a Lancer Vibratome (World Precision Instruments, Sarasota, Fl.). The aCSF contained (in mM): 20 HEPES, 2.4 $CaCl_2$, 1.2 $MgCl_2$, 1.2 NaH_2PO_4, 2.45 KCl, 126 NaCl, 11 glucose, and 25 $NaHCO_3$. The pH was adjusted to pH 7.4 and the aCSF was saturated with 95 % O_2/5 % CO_2. Slices were superfused in aCSF at 37 ^oC for 35-40 minutes prior to recording.

Electrodes and Electrochemistry

Carbon-fiber microelectrodes were prepared using T650 carbon fibers (6 µm diameter, Amoco, Greenville, SC) as previously described (Kawagoe et al., 1993). Fibers were aspirated into glass capillaries (A-M Systems, Sequim, WA), and a vertical pipette puller (Narishige, Long Island, NY) was used to seal the glass around the carbon fiber. For cylinder electrodes, the exposed carbon fiber was trimmed to a length of 50 µm. For disk electrodes, the carbon fibers were cut at the glass seal, which was then reinforced with epoxy (15 % m-phenylenediamine in Epon 828 resin (Miller-Stephenson, Danbury, CT) heated to between 80 and 90 ^oC). Electrodes were kept at room temperature overnight, and then the epoxy was cured via sequential heating at 100 and 150 ^oC for 8 h and overnight, respectively. Disks were generated by beveling electrodes at 45 degrees on a diamond dust-embedded polishing wheel (Sutter Instruments, Novato, CA). Prior to use, all electrodes were soaked in isopropyl alcohol for at least 20 min (Bath et al., 2000).

Amperometric recordings at single cells were made using a GeneClamp 500B amplifier (Axon Instruments, Molecular Devices, Union City, CA). Disk electrodes were held at 0.650 V vs. a Ag/AgCl reference electrode (BASi, West Lafayette, IN), a potential sufficient to oxidize catecholamines. The output current was analog filtered at 5 kHz with a low-pass Bessel filter and acquired at 20 kHz. Post-collection, traces were further digitally filtered using a 400 Hz low-pass Bessel filter. Data collection and filtering were controlled via the pClamp software provided with the amplifier.

Measurements of dopamine, norepinephrine (NE) and serotonin (5-HT) release in brain slices were made using FSCV at cylinder electrodes. Waveform application, current monitoring, and stimulus application were all controlled by locally written software (Tarheel CV, Labview) through a home built potentiostat (UEI, UNC electronics shop). For dopamine and NE detection, the potential at the electrode was scanned from -0.4 V to 1 V and back at 600 V/s, with the ramp repeated at 60 Hz. For 5-HT, the electrode was scanned from 0.2 V to 1 V down to -0.1 V and back to 0.2 V at 1000 V/s, with the waveform repeated at 10 Hz (Jackson et al., 1995). After an experiment, electrodes were calibrated in a flow injection system with a 1 µM bolus of analyte.

Single Cell Experiments

Glass coverslips containing plated cells were secured in a stainless steel coverslip holder and mounted on the stage of an inverted microscope (Eclipse TE300, Nikon Instruments, Melville, NY). A temperature controller (Warner Instruments, Hamden, CT) connected to the stage maintained cells at 37 ^{o}C throughout the experiments. The extracellular recording buffer contained (in mM): 145 NaCl, 3 KCl, 1.2 $MgCl_2$, 2.4 $CaCl_2$, 1.2 NaH_2PO_4, 11 glucose, and 10 HEPES, pH adjusted to 7.4 with NaOH. Exocytosis was triggered via a 0.5 s pressure ejection of 60 mM K^+ buffer from a stimulating pipette located 30 µm from the cell. Cells were stimmed every 30 s for 10 total stimulations. Stimulating pipettes with 6 to 10 µm tip diameters were fabricated using a horizontal pipette puller (Sutter Instruments, Novato, CA) and a microforge (Narishige, Long Island, NY). Pressure ejection was controlled via a multi-channel Picospritzer (General Valve Corporation, Parker Hannifin, Fairfield, NJ). Positioning of both the electrode and stimulating pipette was controlled using piezoelectric micromanipulators (Burleigh Instruments, Exfo, Plano, TX).

Slice Experiments

Recordings were performed on a microscope (Nikon FN1, Gibraltar Stage) fitted with a slice perfusion chamber (Warner Instruments, Hamden CT). Neurotransmitter release

was evoked by local electrical stimulation delivered through a tungsten bipolar stimulating electrode placed on the surface of the slice (Frederick Haer Co., Bowdoinham, ME). The stimulation consisted of a computer generated, biphasic (2 ms per phase), constant-current (350 µA) pulse. A single stimulation pulse was used to evoke striatal dopamine release in the caudate putamen (Jones et al., 1995), a 20 pulse 100 Hz stimulation train was used to evoke 5-HT release in the SNr (Bunin et al., 1998), and a 60 pulse 60 Hz stimulation was used to evoke NE release in the vBNST (Miles et al., 2002). The current pulse was optically isolated from the preparation (NL 800, Neurolog, Medical Systems, Great Neck, NY). Stimulations were performed at regular 3-5 min intervals to maintain consistent release. Neurotransmitter release was detected at a microelectrode placed 75-100 µm into the slice at a distance of 100-200 µm from the stimulating electrode.

Data Analysis

Amperometric spike analysis was performed using MiniAnalysis software (Synaptosoft, Decatur, GA). For inclusion, spike amplitude was required to be 5 times greater than the root-mean-squared current noise. Overlapping peaks were included in frequency and foot analysis, but excluded from individual spike analysis. Visual examination of the peaks was used to determine presence of pre- and post-spike feet. For frequency analysis, the first observed spike following stimulation marked the burst start time. Burst end time was denoted by the first interspike interval > 1s. Individual amperometric spike characteristics such as quantal size (Q), $t_{1/2}$, and amplitude were averaged for an individual cell. The cumulative mean for an experimental group was then determined using the cell averages (Colliver et al., 2000). Release values reported from the slice experiments are the maximal neurotransmitter concentrations obtained following stimulation. Values were averaged across multiple locations in each slice, and then pooled for each genotype. All data are presented as means ± standard errors of the mean. Statistical comparisons were performed using a Student's t-test.

Results

Presynaptic Release of Biogenic Amines in Brain Slices

Possible presynaptic alterations in FXS were evaluated using brain slices containing the caudate putamen, *v*BNST, or SNr from both WT and *Fmr1* KO mice (n = 6 animals for both genotypes) (Figure 4.1). No discernible deficits in the presynaptic release mechanism were observed as electrically stimulated neurotransmitter release monitored by FSCV was unchanged in *Fmr1* KO mice when compared to WT mice ($p > 0.05$ for all three regions, Student's t-test). The maximum dopamine concentration measured in the caudate following stimulation was 1.50 ± 0.08 µM in WT slices and 1.61 ± 0.09 µM in *Fmr1* KO slices. NE release in the *v*BNST was equivalent in slices from WT and *Fmr1* KO mice at 0.95 ± 0.14 µM and 1.02 ± 0.14 µM, respectively. Additionally, no differences were detected in the SNr, where electrically stimulated 5-HT release reached a maximal concentration of 133 ± 9 nM in WT slices and 127 ± 6 nM in *Fmr1* KO slices.

Vesicular Release at Chromaffin Cells

To further investigate the role of FMRP in modulating presynaptic secretory proteins, the vesicular release machinery was examined in isolated chromaffin cells from WT (n = 53 cells) and *Fmr1* KO (n = 43 cells) mice. Amperometry was used to measure the exocytosis stimulated by 10 successive 0.5 s applications of 60 mM K^+, spaced 30 s apart. Figure 4.2 shows a representative amperometric trace following a single stimulation for both cell types. The amperometric spike characteristics for both genotypes are summarized in Table 4.1. The mouse model of FXS showed no effects on the exocytotic protein machinery as vesicular release observed at *Fmr1* KO cells was unchanged ($p > 0.05$ for all characteristics, Student's t-test) compared to WT cells. An average of 310 ± 20 events were detected at WT cells, with individual bursts lasting 3.4 ± 0.2 s and having a spike frequency of 8.4 ± 0.3 Hz. Similarly, an average of 320 ± 20 events were detected at *Fmr1* KO cells, with each burst lasting 3.5 ± 0.2 s and having a spike frequency of 9.1 ± 0.4 Hz. The percentage of WT and

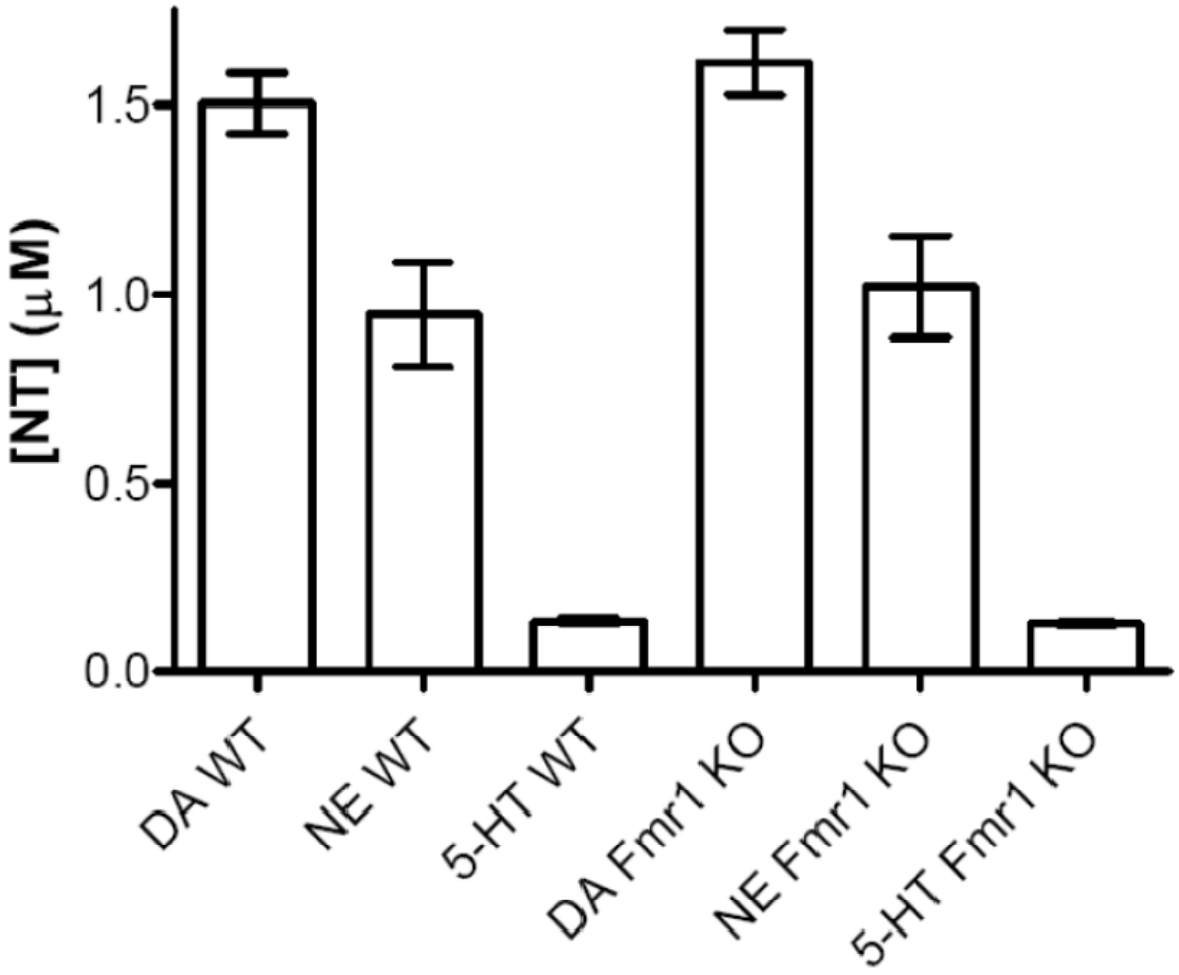

Figure 4.1. Stimulated neurotransmitter release in three regions of the adult mouse brain. Brain slices containing the caudate putamen, vBNST, or SNr were taken from WT mice and *Fmr1* KO mice. Dopamine release evoked by a single pulse electrical stimulation was unchanged in *Fmr1* KO mice compared to WT mice ($p > 0.05$, $n = 6$ both genotypes). The same can be said for 5-HT release evoked by a 20 pulse 100 Hz stimulation in the SNr and NE release evoked by a 60 pulse 60 Hz stimulation in the vBNST ($p > 0.05$, $n = 6$ both genotypes).

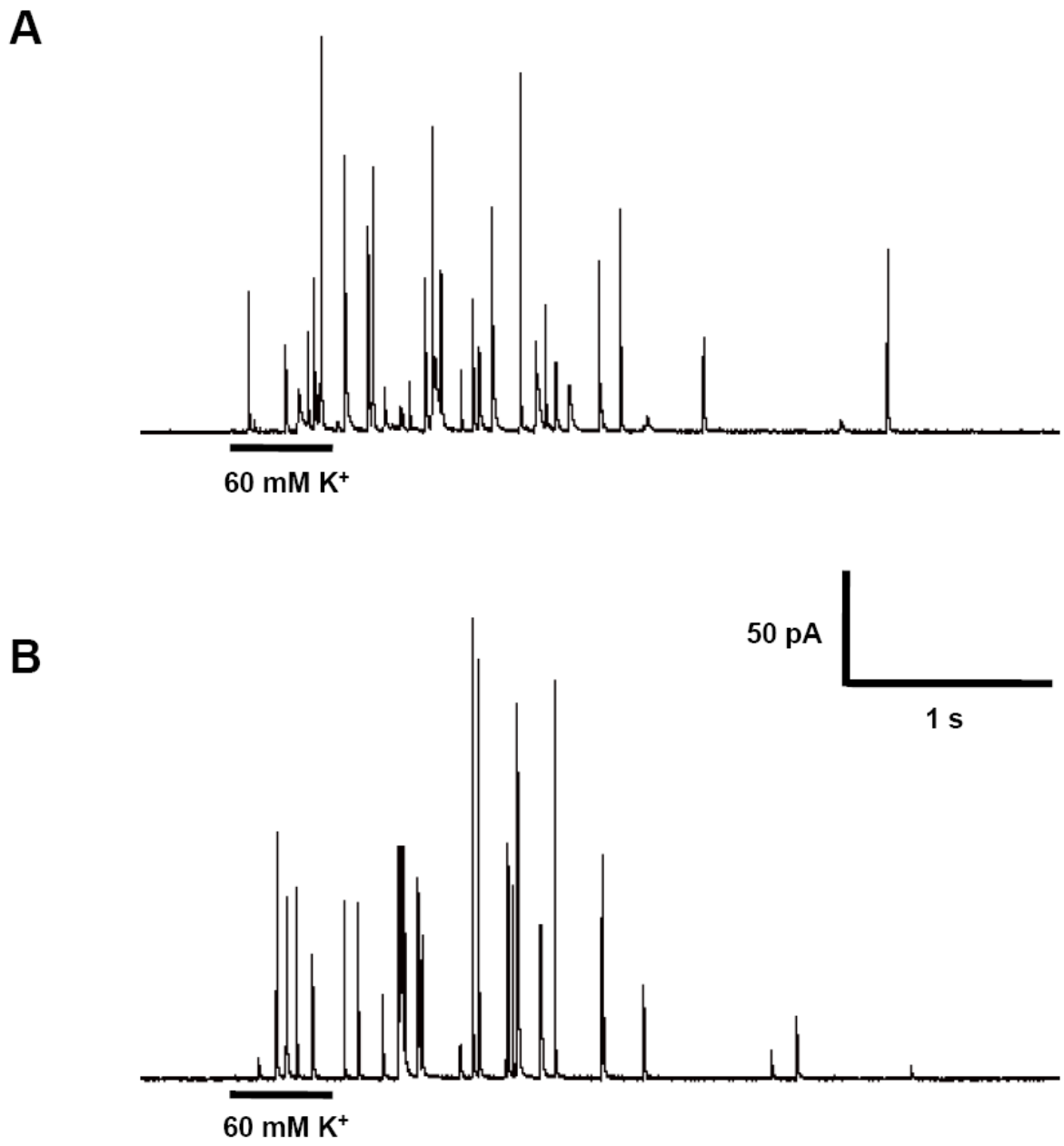

Figure 4.2. Vesicular release at WT and *Fmr1* KO cells. Representative amperometric traces measured in response to a 0.5 s stimulation with 60 mM K^+ at chromaffin cells from WT **(A)** and *Fmr1* KO **(B)** mice.

Table 4.1. Amperometric spike characteristics of WT and *Fmr1* KO mice. Table shows the average number of spikes recorded during a trace (10 stimulations) and the average length of and frequency of spikes within an individual burst of exocytosis following a 0.5 s stimulation with 60 mM K^+. Individual spike characteristics, including % of events with a foot feature, amplitude (I_{max}, in pA), quantal size (Q, in molecules of catecholamine), and halfwidth ($t_{1/2}$, in ms), were averaged over the entire trace. No significant differences were observed between WT and *Fmr1* KO cells ($p > 0.05$, one-way ANOVA).

Cell Type	Total Spikes	Burst Length (s)	Spike Freq (Hz)	% w/ Foot	I_{max} (pA)	Q (molecules)	$t_{1/2}$ (ms)
WT (n = 53)	310 ± 20	3.4 ± 0.2	8.4 ± 0.3	11.1 ± 0.4	76 ± 4	$(8.0 \pm 0.4) \times 10^5$	5.3 ± 0.2
Fmr1 KO (n = 43)	320 ± 20	3.5 ± 0.2	9.1 ± 0.4	11.1 ± 0.4	78 ± 4	$(8.9 \pm 0.6) \times 10^5$	5.5 ± 0.2

Fmr1 cells exhibiting a pre- and/or post-spike foot was an identical 11.1 ± 0.4 %. The average amperometric spike for WT cells had an I_{max} of 76 ± 4 pA, $t_{1/2}$ of 5.3 ± 0.2 ms, and Q of (8.0 ± 0.4) x 10^5 molecules. Likewise, the average spike for *Fmr1* KO cells had an I_{max} of 78 ± 4 pA, $t_{1/2}$ of 5.5 ± 0.2 ms, and Q of (8.9 ± 0.6) x 10^5 molecules.

Discussion

Of the many mRNA cargoes of FMRP, several presynaptic proteins involved in the secretory pathway have been identified (Brown et al., 2001; Miyashiro et al., 2003). In the brains of *Fmr1* KO mice, the lack of FMRP is associated with the down regulation of numerous presynaptic proteins linked to vesicle exocytosis (Liao et al., 2008). Most notable among the mRNA and protein targets is Rab3A, a small GTPase implicated in the GTP-dependent docking and fusion of vesicles with the plasma membrane (Geppert et al., 1997; Leenders et al., 2001). Dysregulation of Rab3A expression, and that of other presynaptic mRNA cargoes of FMRP, is proposed to contribute to the observed mental deficits in FXS through alterations in the vesicular release of neurotransmitters. This theorized link has recently been observed. Cortical synaptoneurosomes from *Fmr1 KO* mice exhibit a 90 % reduction in stimulation-dependent release of neuropeptides from LDCVs (Dr. Jonathan Sweedler, personal communication). This deficit in exocytosis was coincident with a 50 % decrease in Rab3A expression.

To further examine the role of FMRP in regulating the presynaptic release of chemical messengers, electrochemical monitoring of neurotransmitter release with FSCV and amperometry has been performed in *Fmr1 KO* animals. Electrically stimulated dopamine release in the caudate putamen, NE release in the *v*BNST, and 5-HT release in the SNr are all unchanged in brain slices from *Fmr1* KO mice relative to WT mice (Figure 4.1). Similarly, no significant differences were measured in the frequency of vesicular events or individual amperometric spike characteristics between WT and *Fmr1* KO chromaffin cells (Figure 4.2 and Table 4.1). Taken together, these results suggest that

presynaptic regulation of biogenic amine release is largely intact in *Fmr1* KO mice. In light of the evidence for vesicular release deficiencies discussed above, these results imply that the presynaptic regulation of exocytosis by FMRP may be specific to cortical brain regions or to the release of neuropeptides. Future experiments assessing the presynaptic release mechanism in different brain locations or of other neurotransmitters could help elucidate the function of FMRP in the expression of FXS symptoms.

References

(1994) Fmr1 knockout mice: a model to study fragile X mental retardation. The Dutch-Belgian Fragile X Consortium. Cell 78:23-33.

Ashley CT, Jr., Wilkinson KD, Reines D, Warren ST (1993) FMR1 protein: conserved RNP family domains and selective RNA binding. Science 262:563-566.

Bassell GJ, Warren ST (2008) Fragile X syndrome: loss of local mRNA regulation alters synaptic development and function. Neuron 60:201-214.

Bath BD, Michael DJ, Trafton BJ, Joseph JD, Runnels PL, Wightman RM (2000) Subsecond adsorption and desorption of dopamine at carbon-fiber microelectrodes. Anal Chem 72:5994-6002.

Brown V, Jin P, Ceman S, Darnell JC, O'Donnell WT, Tenenbaum SA, Jin X, Feng Y, Wilkinson KD, Keene JD, Darnell RB, Warren ST (2001) Microarray identification of FMRP-associated brain mRNAs and altered mRNA translational profiles in fragile X syndrome. Cell 107:477-487.

Bunin MA, Prioleau C, Mailman RB, Wightman RM (1998) Release and uptake rates of 5-hydroxytryptamine in the dorsal raphe and substantia nigra reticulata of the rat brain. J Neurochem 70:1077-1087.

Castillo PE, Janz R, Sudhof TC, Tzounopoulos T, Malenka RC, Nicoll RA (1997) Rab3A is essential for mossy fibre long-term potentiation in the hippocampus. Nature 388:590-593.

Coffee B, Zhang F, Warren ST, Reines D (1999) Acetylated histones are associated with FMR1 in normal but not fragile X-syndrome cells. Nat Genet 22:98-101.

Colliver TL, Hess EJ, Pothos EN, Sulzer D, Ewing AG (2000) Quantitative and statistical analysis of the shape of amperometric spikes recorded from two populations of cells. J Neurochem 74:1086-1097.

Comery TA, Harris JB, Willems PJ, Oostra BA, Irwin SA, Weiler IJ, Greenough WT (1997) Abnormal dendritic spines in fragile X knockout mice: maturation and pruning deficits. Proc Natl Acad Sci U S A 94:5401-5404.

Garber KB, Visootsak J, Warren ST (2008) Fragile X syndrome. Eur J Hum Genet 16:666-672.

Geppert M, Goda Y, Stevens CF, Sudhof TC (1997) The small GTP-binding protein Rab3A regulates a late step in synaptic vesicle fusion. Nature 387:810-814.

Irwin SA, Galvez R, Greenough WT (2000) Dendritic spine structural anomalies in fragile-X mental retardation syndrome. Cereb Cortex 10:1038-1044.

Jackson BP, Dietz SM, Wightman RM (1995) Fast-scan cyclic voltammetry of 5-hydroxytryptamine. Anal Chem 67:1115-1120.

Johnson MA, Rajan V, Miller CE, Wightman RM (2006) Dopamine release is severely compromised in the R6/2 mouse model of Huntington's disease. J Neurochem 97:737-746.

Johnson MA, Villanueva M, Haynes CL, Seipel AT, Buhler LA, Wightman RM (2007) Catecholamine exocytosis is diminished in R6/2 Huntington's disease model mice. J Neurochem 103:2102-2110.

Jones SR, Garris PA, Wightman RM (1995) Different effects of cocaine and nomifensine on dopamine uptake in the caudate-putamen and nucleus accumbens. J Pharmacol Exp Ther 274:396-403.

Kawagoe KT, Zimmerman JB, Wightman RM (1993) Principles of voltammetry and microelectrode surface states. J Neurosci Methods 48:225-240.

Kolski-Andreaco A, Cai H, Currle DS, Chandy KG, Chow RH (2007) Mouse adrenal chromaffin cell isolation. J Vis Exp:129.

Leenders AG, Lopes da Silva FH, Ghijsen WE, Verhage M (2001) Rab3a is involved in transport of synaptic vesicles to the active zone in mouse brain nerve terminals. Mol Biol Cell 12:3095-3102.

Liao L, Park SK, Xu T, Vanderklish P, Yates JR, 3rd (2008) Quantitative proteomic analysis of primary neurons reveals diverse changes in synaptic protein content in fmr1 knockout mice. Proc Natl Acad Sci U S A 105:15281-15286.

Miles PR, Mundorf ML, Wightman RM (2002) Release and uptake of catecholamines in the bed nucleus of the stria terminalis measured in the mouse brain slice. Synapse 44:188-197.

Miyashiro KY, Beckel-Mitchener A, Purk TP, Becker KG, Barret T, Liu L, Carbonetto S, Weiler IJ, Greenough WT, Eberwine J (2003) RNA cargoes associating with FMRP reveal deficits in cellular functioning in Fmr1 null mice. Neuron 37:417-431.

Muddashetty RS, Kelic S, Gross C, Xu M, Bassell GJ (2007) Dysregulated metabotropic glutamate receptor-dependent translation of AMPA receptor and postsynaptic density-95 mRNAs at synapses in a mouse model of fragile X syndrome. J Neurosci 27:5338-5348.

Sherman SL, Jacobs PA, Morton NE, Froster-Iskenius U, Howard-Peebles PN, Nielsen KB, Partington MW, Sutherland GR, Turner G, Watson M (1985) Further segregation analysis of the fragile X syndrome with special reference to transmitting males. Hum Genet 69:289-299.

Sutcliffe JS, Nelson DL, Zhang F, Pieretti M, Caskey CT, Saxe D, Warren ST (1992) DNA methylation represses FMR-1 transcription in fragile X syndrome. Hum Mol Genet 1:397-400.

Ventura R, Pascucci T, Catania MV, Musumeci SA, Puglisi-Allegra S (2004) Object recognition impairment in Fmr1 knockout mice is reversed by amphetamine:

involvement of dopamine in the medial prefrontal cortex. Behav Pharmacol 15:433-442.

Verkerk AJ, Pieretti M, Sutcliffe JS, Fu YH, Kuhl DP, Pizzuti A, Reiner O, Richards S, Victoria MF, Zhang FP, et al. (1991) Identification of a gene (FMR-1) containing a CGG repeat coincident with a breakpoint cluster region exhibiting length variation in fragile X syndrome. Cell 65:905-914.

Chapter 5

Fast Scan Cyclic Voltammetry of Trace Amines

Introduction

The trace amines are a family of endogenous amines closely related in structure and metabolism to the classical monoamine neurotransmitters (Philips et al., 1974; Axelrod and Saavedra, 1977). As the name suggests, these compounds are present at trace amounts (0.1 – 100 ng/g tissue) in the mammalian brain, several hundred-fold lower than the classical monoamines (Berry, 2004). Trace amines are distributed heterogeneously in the brain, although this distribution closely mimics the cell body and projection regions of the dopamine, norepinephrine (NE), and serotonin systems (Philips, 1984). Synthesis and turnover rates for the trace amines are equivalent or greater than those for dopamine and NE (Durden and Philips, 1980; Durden et al., 1988), with oxidative deamination by the monoamine oxidase enzymes primarily responsible for the high turnover rates (Philips and Boulton, 1979). Though initially considered simple metabolic byproducts of the classical monoamine transmitters, renewed interest in the physiological role of these compounds was triggered by discovery of a family of mammalian trace amine receptors (Borowsky et al., 2001). As summarized in recent reviews, current opinion holds that trace amines function mainly as modulators of monoamine neurotransmission, affecting both presynaptic release and uptake and postsynaptic sensitivity. (Berry, 2004; Burchett and Hicks, 2006).

Although the label extends to derivatives of L-phenylalanine and L-tryptophan as well, this work will focus only on those trace amines derived from the precursor amino acid L-tyrosine: tyramine, octopamine, and synephrine. These molecules are structurally similar

to dopamine, NE, and epinephrine (E), respectively, but are phenolamines rather than catecholamines (Figure 5.1). Over the years, several methods have been employed for the detection and quantification of trace amines including radioenzymatic assays (Axelrod and Saavedra, 1977), immunohistochemistry (Kitahama et al., 2005), mass spectrometry (Philips et al., 1974), and high performance liquid chromatography (D'Andrea et al., 2003). However, none of these methods permit measurement of concentration changes on the subsecond time scale of vesicular release of monoamine transmitters in the brain. Fast scan cyclic voltammetry (FSCV) at carbon-fiber microelectrodes is one technique that would provide the necessary temporal resolution for real-time measurements while still maintaining the sensitivity required to monitor such low concentrations (Robinson et al., 2008). To date though, little is known about the electrochemistry of phenolamines at carbon-fiber microelectrodes. The electrochemistry of tyramine has been investigated at gold, platinum, and graphite electrodes (Tenreiro et al., 2007; de Castro et al., 2008; Luczak, 2008), but at scan rates significantly lower than those used for FSCV recordings of neurotransmission. Like other phenols, these studies show that oxidation of tyramine produces phenoxy radicals that react with other tyramine molecules to yield a para-linked dimer. Subsequent oxidation leads to polymerization, which could form a passivating, insulating film on the electrode surface. The electrochemistry of octopamine and synephrine is likely very similar, and the potential fouling of the electrode through film formation will need to be addressed for the electrochemical detection of phenolamines to prove viable.

This chapter reports the development of FSCV techniques for the real-time monitoring of tyramine, octopamine, and synephrine concentration changes. The electrochemistry of the trace amines is described using two FSCV waveforms. While the generation of polymerized films was diminished with higher holding potentials, no significant evidence for fouling was observed with either waveform. Both waveforms qualitatively distinguish trace amines from their catecholamine counterparts, but show a limited time

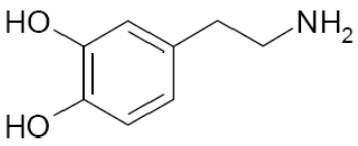

Dopamine

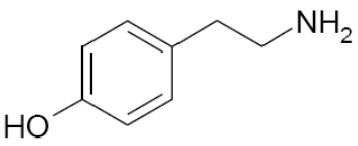

Tyramine

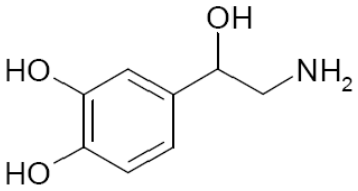

Norepinephrine

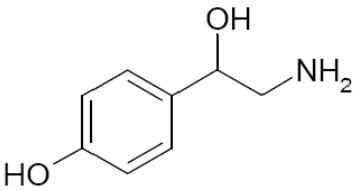

Octopamine

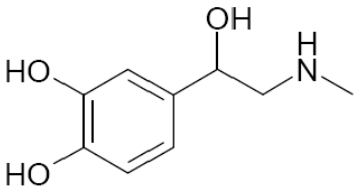

Epinephrine

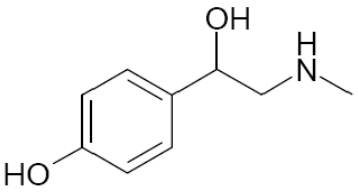

Synephrine

Figure 5.1. Chemical structures of the catecholamines and trace amines. Left hand column shows the classical catecholamine transmitters derived from the precursor amino acid l-tyrosine. Right hand column shows the structurally related trace amines. These compounds are also derived from l-tyrosine, but as phenolamines possess only one ring hydroxyl group.

course for simultaneous quantitative measurements. These techniques could serve as valuable tools for future studies of trace amine modulation of the classical monoamine neurotransmitters.

Materials and Methods

Electrodes and Electrochemistry

Carbon-fiber microelectrodes were prepared using P55 carbon fibers (10 µm diameter, Amoco, Greenville, SC) as previously described (Kawagoe et al., 1993). Fibers were aspirated into glass capillaries (A-M Systems, Sequim, WA), and a vertical pipette puller (Narishige, Long Island, NY) was used to seal the glass around the carbon fiber. Carbon fibers were cut at the glass seal, which was then reinforced with epoxy (15 % m-phenylenediamine in Epon 828 resin (Miller-Stephenson, Danbury, CT) heated to between 80 and 90 ^{o}C). Electrodes were kept at room temperature overnight, and then the epoxy was cured via sequential heating at 100 and 150 ^{o}C for 8 h and overnight, respectively. Prior to use, electrodes were beveled at 45 degrees on a diamond dust-embedded polishing wheel (Sutter Instruments, Novato, CA) and soaked in isopropyl alcohol for at least 20 min (Bath et al., 2000). FSCV measurements were made using an EI-400 biopotentiostat (ESA, Chelmsford, MA). Waveform application, data acquisition, and post-collection digital filtering at 2 kHz were controlled by locally written software (Tarheel CV, Labview). A Ag/AgCl reference electrode (BASi, West Lafayette, IN) was used for all experiments.

Flow Injection Experiments

Carbon-fiber disk microelectrodes were situated in an electrochemical cell at the output of a flow injection system (Kristensen et al., 1986; Zachek et al., 2008). A six-port high performance liquid chromatography injection valve (Upchurch Scientific, Oak Harbor, WA) was mounted on a two-position pneumatic actuator (Rheodyne, Rohnert Park, CA). The actuator was used in conjunction with a 12 V solenoid valve kit (Rheodyne) at 50 psi to precisely control the introduction of analytes to the electrode surface. Solvent flow (2

mL/min) was driven with a variable-resistance infusion pump (Harvard Apparatus, Holliston, MA) through the valve and into the electrochemical cell.

Chemicals

All chemicals were purchased from Sigma Aldrich (St. Louis, MO) and used as received. Aqueous solutions were prepared in doubly-distilled, deionized water. The running buffer for flow injection experiments contained (in mM): 140 NaCl, 4 KCl, 1 $MgCl_2$, 2 $CaCl_2$, 10 glucose, and 20 Tris-HCl, pH adjusted to 7.4 with NaOH. Stock solutions of catecholamines and trace amines were prepared in 0.1 N $HClO_4$ and diluted in running buffer on the day of each experiment. All solutions were deoxygenated prior to use with at least 20 min of N_2 bubbling.

Results

Characterization of Trace Amine Electrochemistry

For catecholamine detection in brain slices, the potential at the carbon-fiber microelectrode is generally scanned from -0.4 V to 1.0 V and back at 600 V/s, with the ramp repeated at 60 Hz (see Chapters 3 and 4). As the oxidation potentials of the trace amines were predicted to be higher than those of the catecholamines (de Castro et al., 2008; Luczak, 2008), the switching potential was increased to 1.3 V (referred to hereafter as the extended waveform). Application of the extended waveform to a disk carbon-fiber microelectrode during a 1 s flow injection of 10 µM tyramine, octopamine, or synephrine resulted in the background-subtracted cyclic voltammograms (CVs) and current versus time traces shown in Figure 5.2. The CVs for all three trace amines were largely similar. A main oxidation peak was observed at 0.98 ± 0.02 V for tyramine, 1.03 ± 0.02 V for octopamine, and 1.02 ± 0.02 V for synephrine (n = 3 electrodes for all compounds). Initially, the main oxidation peak was the primary feature of the CV, along with a small reduction peak at -0.2 V and a small oxidative current near the switching potential (Figure 5.2A-C). However, a second oxidation peak at 0.6 V slowly grew in over the time course of the injection and was

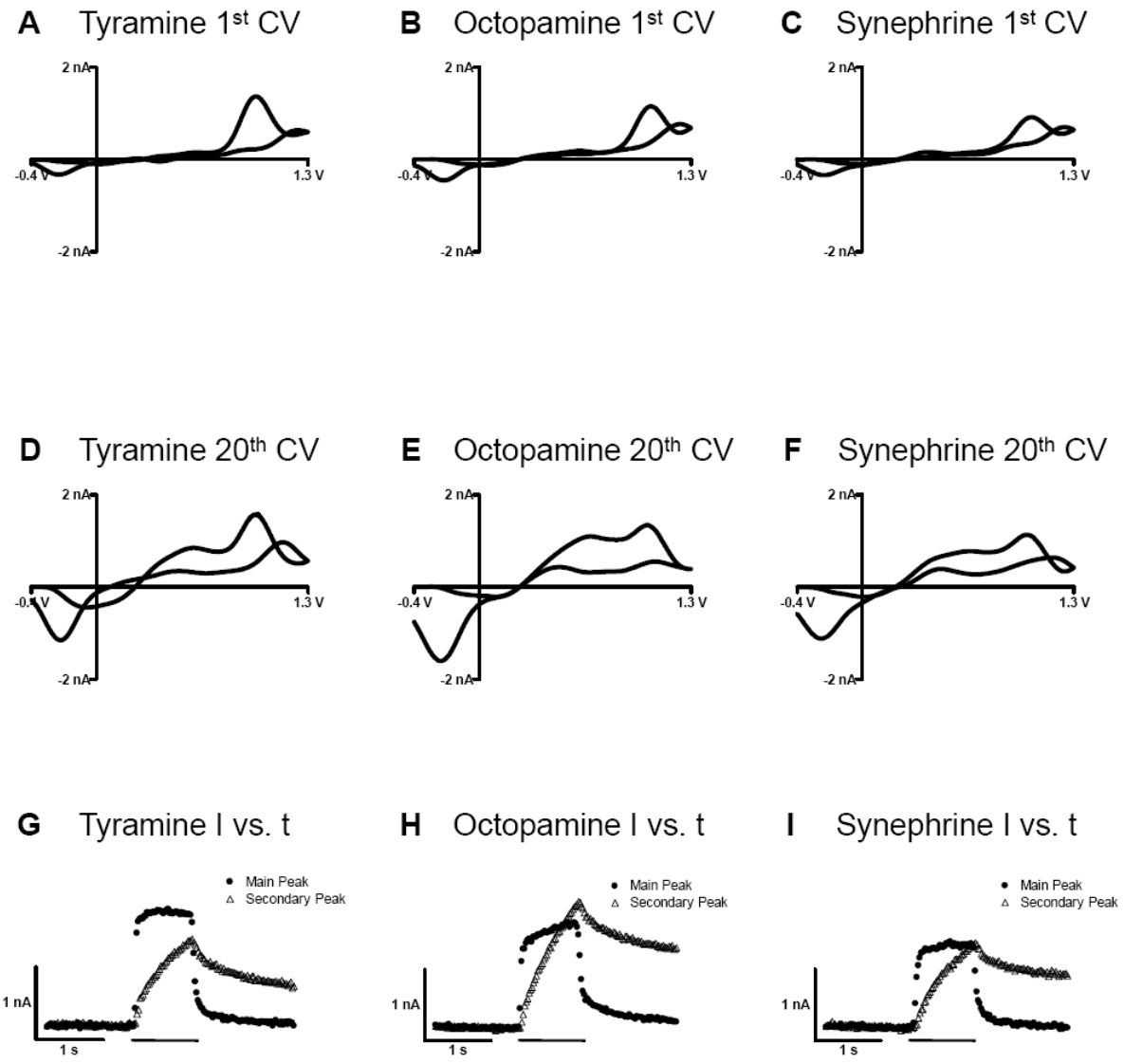

Figure 5.2. Electrochemical characterization of tyramine, octopamine, and synephrine with the extended waveform. Top panel **(A, B, C)** shows the first background-subtracted cyclic voltammogram (CV) obtained after exposure to 10 µM tyramine, octopamine, or synephrine. All three compounds exhibit a main oxidation peak around 1.0 V. Middle panel **(D, E, F)** shows the 20th CV of the injection, approximately 0.33 s after initial exposure to the trace amine. All three compounds now exhibit a pronounced secondary oxidation peak around 0.6 V. The bottom panel **(G, H, I)** shows the current (I) measured at the electrode as a function of time (t) at the potential of both the main (filled circles) and secondary (open triangles) oxidation peaks. The bar indicates when the electrode was exposed to each compound.

clearly visible after only 0.33 s of exposure (Figure 5.2D-F). The growth of this oxidation peak coincided with an increase in the size of the reduction peak at -0.2 V. Additionally, the oxidative current near the switching potential increased with time, but only for tyramine. The current versus time traces show that the secondary oxidation peak continued to increase in current throughout the 1 s injection and returned to baseline much slower than the main peak after the trace amine had been washed out of the flow cell (Figure 5.2G-I). For tyramine, this secondary peak reached 76 ± 2 % of the amplitude of the main oxidation peak by the end of the injection. For octopamine it reached 120 ± 4 % of the amplitude and for synephrine 105 ± 3 %.

FSCV detection with the extended waveform displayed minimal sensitivity differences for the three trace amines. On average, peak currents of 1.56 ± 0.07 nA, 1.48 ± 0.02 nA, and 1.22 ± 0.07 nA were observed for the main oxidation peak of 10 µM tyramine, octopamine, and synephrine, respectively. The square pulse of analyte resulted in a square current response at the main oxidation peak (Figure 5.2G-I), suggesting no short-term fouling of the electrode surface. There was also no evidence for long-term fouling of the electrode. No decrease was observed in the measured current at the main oxidation potential during six successive flow injections of the three trace amines. Further, the electrode response to a 10 µM injection of NE was unaltered ($p > 0.05$, Student's t-test) following exposure to trace amine. After six successive tyramine injections the current measured in response to NE oxidation was 103 ± 4 % of pre-exposure levels. After octopamine exposure the response was 99 ± 5 % of pre-exposure levels and for synephrine 103 ± 3 %.

Discrimination from Catecholamines with the Extended Waveform

With use of the extended waveform, the CVs for dopamine, NE, and E are indistinguishable. The catecholamines all exhibit an oxidation peak at 0.6 V and a reduction peak at -0.2 V. Unfortunately, these potentials are identical to those of the secondary peak

and reduction peak that arise during oxidation of the trace amines. As such, the extended waveform had a limited time window for distinguishing catecholamine and phenolamine species. Flow cell injection of mixtures containing 10 µM NE and 10 µM tyramine, octopamine, or synephrine are summarized in Figure 5.3. The first CVs collected upon exposure to these mixtures showed an oxidation peak at 0.6 V that can be attributed solely to the presence of NE (Fig 5.3A-C). The magnitude of the current at this potential was significantly increased ($p < 0.05$, Student's t-test, $n = 3$ electrodes) within 3 to 5 CVs from the initial scan for all three trace amines, owing to the appearance of the secondary oxidation peak. These data suggest that simultaneous measures of catecholamine and trace amine concentration can only be made accurately for very brief exposures (less than 100 ms) using the extended waveform.

The Effect of Holding Potential on the Secondary Oxidation Peak

The lag between trace amine washout and the current at the secondary oxidation potential returning to baseline indicate that this peak stems from a species adsorbed to the electrode surface. Presumably, like the trace amines themselves, these secondary products contain protonated amines at pH 7.4. In an attempt to reduce adsorption of these species, the holding potential of the FSCV waveform was increased from -0.4 V to 0.1 V (referred to hereafter as the short waveform) (Bath et al., 2000). Application of the short waveform to a disk carbon-fiber microelectrode during 1 s flow injections of 10 µM tyramine, octopamine, or synephrine resulted in the CVs and current versus time traces shown in Figure 5.4. Minus the reductive wave, the initial CVs for all three trace amines were nearly identical to those obtained with the extended waveform (Figure 5.4A-C). A main oxidation peak was observed at 0.97 ± 0.02 V for tyramine, 0.99 ± 0.03 V for octopamine, and 0.98 ± 0.03 V for synephrine ($n = 3$ electrodes for all compounds). The small oxidative current near the switching potential was also still present, and again showed an increase in size during the injection that was specific to tyramine oxidation. Though its size was greatly diminished, the

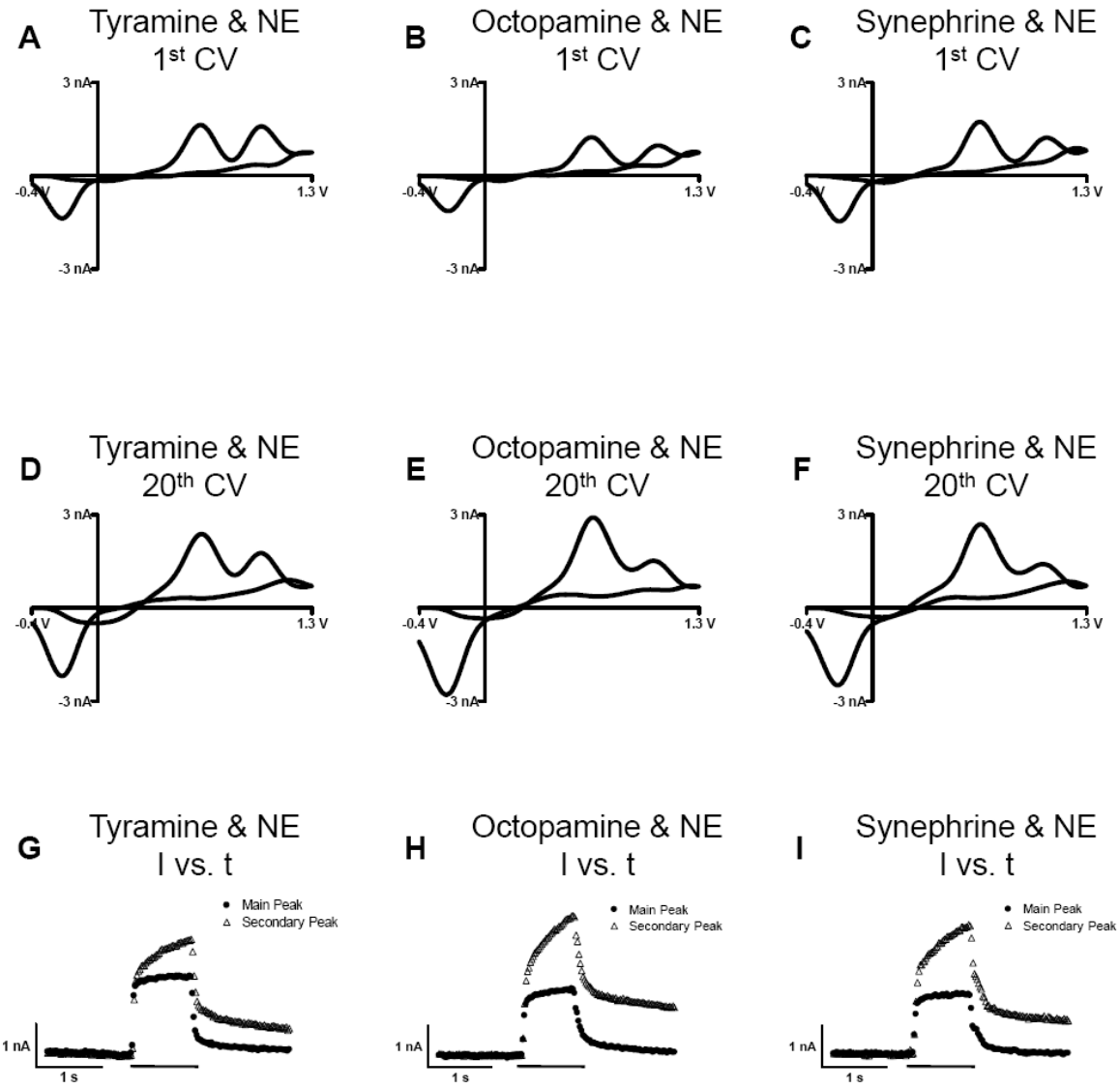

Figure 5.3. Discrimination of catecholamines and trace amines with the extended waveform. Top panel **(A, B, C)** shows the first background-subtracted cyclic voltammogram (CV) obtained after exposure to a mixture of 10 µM norepinephrine (NE) and 10 µM tyramine, octopamine, or synephrine. Two oxidation peaks are clearly visible: one for the trace amine around 1.0 V and one for NE around 0.6 V. Middle panel **(D, E, F)** shows the 20th CV of the injection, approximately 0.33 s after initial exposure to the mixture. The secondary oxidation peak for the trace amines overlaps with the NE oxidation peak, leading to an increase in signal as it grows in. The bottom panel **(G, H, I)** shows the current (I) measured at the electrode as a function of time (t) at the potential of both the main (filled circles) and secondary (open triangles) oxidation peaks. The bar indicates when the electrode was exposed to the mixture.

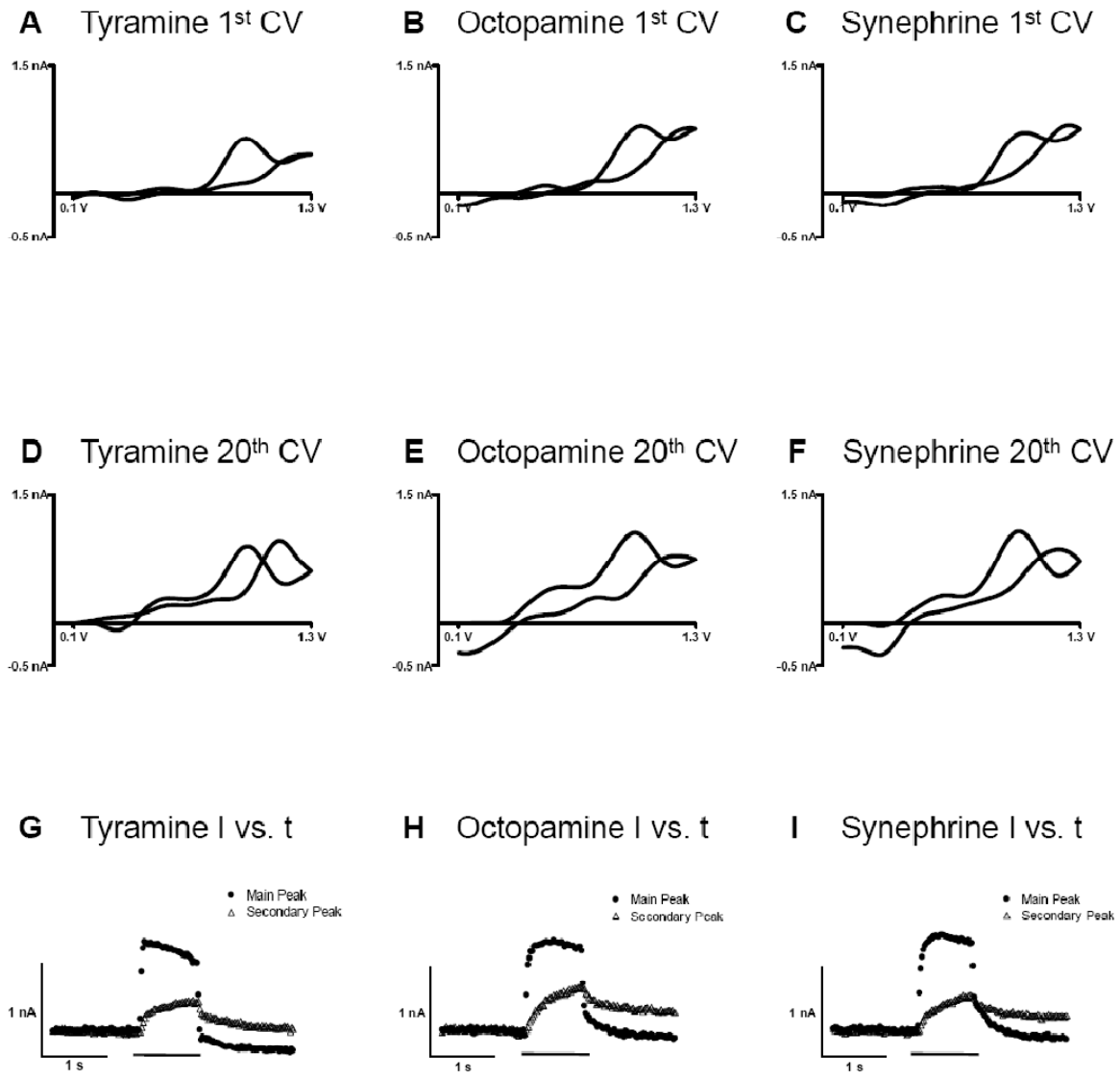

Figure 5.4. Electrochemical characterization of tyramine, octopamine, and synephrine with the short waveform. Top panel **(A, B, C)** shows the first background-subtracted cyclic voltammogram (CV) obtained after exposure to 10 µM tyramine, octopamine, or synephrine. All three compounds exhibit a main oxidation peak around 1.0 V. Middle panel **(D, E, F)** shows the 20th CV of the injection, approximately 0.33 s after initial exposure to the trace amine. While still present, the secondary oxidation peak around 0.6 V is significantly reduced compared to the extended waveform. The bottom panel **(G, H, I)** shows the current (I) measured at the electrode as a function of time (t) at the potential of both the main (filled circles) and secondary (open triangles) oxidation peaks. The bar indicates when the electrode was exposed to each compound.

secondary oxidation peak persisted with application of the short waveform and was readily identifiable within 0.33 s of exposure to trace amine (Figure 5.4D-F). The shape of the current response at the secondary oxidation potential was unchanged, exhibiting a slow, continual increase in current throughout the 1 s injection and a prolonged return to baseline (Figure 5.4G-I). For tyramine, the secondary peak reached 33 ± 2 % of the amplitude of the main oxidation peak by the end of the injection. For octopamine it reached 51 ± 4 % of the amplitude and for synephrine 38 ± 3 %.

Increasing the holding potential diminished the electrode sensitivity for the three trace amines. On average, peak currents of 1.00 ± 0.02 nA, 1.01 ± 0.03 nA, and 1.06 ± 0.02 nA were observed for the main oxidation peak of 10 μM tyramine, octopamine, and synephrine, respectively. The square pulse of analyte resulted in a square current response at the main oxidation peak for octopamine and synephrine (Figure 5.4H,I), suggesting no short-term fouling of the electrode surface. For tyramine injection, a gradual decrease in peak current was observed (Figure 5.4G), indicating a small but immediate loss of sensitivity during exposure. This change in sensitivity was temporary, as both the background and peak currents fully recovered by the next injection. Similarly, no decrease was observed in the measured current at the main oxidation potential during six successive flow injections of octopamine and synephrine. As with the extended waveform, the electrode response to a 10 μM injection of NE was unaltered ($p > 0.05$, Student's t-test) following exposure to trace amine. After six successive tyramine injections the current measured in response to NE oxidation was 94 ± 5 % of pre-exposure levels. After octopamine exposure the response was 97 ± 2 % of pre-exposure levels and for synephrine 97 ± 3 %.

Discrimination from Catecholamines with the Short Waveform

With the continued presence of the secondary oxidation peak, the short waveform is subject to comparable time limitations as the extended waveform when it comes to distinguishing catecholamines from phenolamines. Flow cell injection of mixtures containing

10 μM NE and 10 μM tyramine, octopamine, or synephrine are summarized in Figure 5.5. As before, the first CVs collected upon exposure to these mixtures show an oxidation peak at 0.6 V that can be attributed solely to the presence of NE (Fig 5.5A-C). Owing to the reduced size of the secondary oxidation peak, the magnitude of the current at this potential increases slower than was observed with the extended waveform, with the current response at 0.6 V for tyramine even staying flat throughout the injection (Figure 5.5D-I). The peak current during octopamine and synephrine injection was still significantly increased ($p < 0.05$, Student's t-test, $n = 3$ electrodes) within 5 CVs of the initial scan, suggesting quantitative measures of catecholamine and trace amine concentration would remain limited to very brief exposures (less than 100 ms).

Discussion

The electrochemistry of the trace amines tyramine, octopamine, and synephrine at disk carbon-fiber microelectrodes has been described using two FSCV waveforms. With both the extended and the short waveforms, all three trace amines exhibit a primary oxidation wave around 1.0 V. In contrast, the primary oxidation wave for catecholamines with these waveforms occurs at 0.6 V, demonstrating a higher energy barrier for electron removal from the phenol moiety. While the oxidation potentials of the catecholamines and trace amines are sufficiently resolved from each other by FSCV, selective detection of individual trace amines is not feasible due to their nearly identical CVs (Figure 5.2A-C and Figure 5.4A-C). Thus, like the catecholamines, positive analyte identification of an unknown trace amine cannot be performed solely by electrochemistry. Other analytical or pharmacological approaches would be necessary for confirmation.

In addition to displaying analogous CV shapes, the trace amines also demonstrated similar sensitivities for detection at the electrode surface. With the extended waveform, peak currents at the primary oxidation potential were equal for 10 μM tyramine and octopamine injections, and those for synephrine injections were only slightly lower (Figure

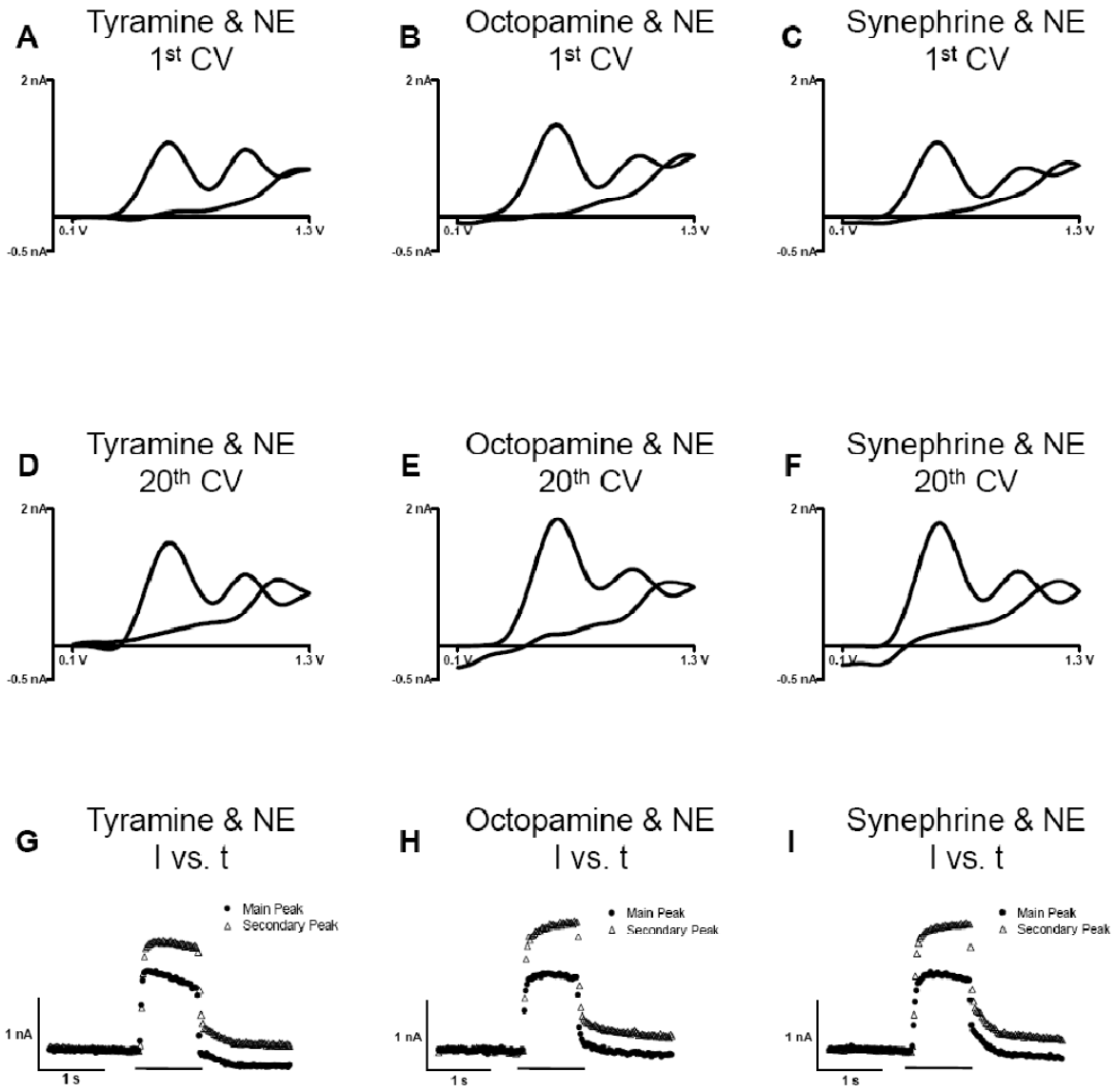

Figure 5.5. Discrimination of catecholamines and trace amines with the short waveform. Top panel **(A, B, C)** shows the first background-subtracted cyclic voltammogram (CV) obtained after exposure to a mixture of 10 µM norepinephrine (NE) and 10 µM tyramine, octopamine, or synephrine. Two oxidation peaks are clearly visible: one for the trace amine around 1.0 V and one for NE around 0.6 V. Middle panel **(D, E, F)** shows the 20th CV of the injection, approximately 0.33 s after initial exposure to the mixture. The increase in the NE signal at 0.6 V is less pronounced than with the extended waveform, owing to a decrease in formation of the trace amine secondary oxidation product. The bottom panel **(G, H, I)** shows the current (I) measured at the electrode as a function of time (t) at the potential of both the main (filled circles) and secondary (open triangles) oxidation peaks. The bar indicates when the electrode was exposed to the mixture.

5.2G-I). By shifting the holding potential from a negative to a positive value, the short waveform resulted in diminished sensitivities for all three compounds (Figure 5.4G-I). This decrease could result from less adsorption of the trace amines, with their positively charged amine groups, to the electrode surface during the time between voltage scans (Bath et al., 2000). The adsorption deficits are evidently greater for primary amines, as synephrine sensitivity was equal to that of tyramine and octopamine when using the short waveform.

It is well documented that tyramine, like other phenols, polymerizes following oxidation, generating a film on electrode surfaces (Pham et al., 1982; Tenreiro et al., 2007; de Castro et al., 2008). The electrodeposition of polytyramine films by cyclic voltammetry has even been used to immobilize enzymes for the fabrication of enzyme-modified electrodes (Manihar et al., 2001). As the polymerization reaction is driven by formation of phenoxy radicals, it is predicted that octopamine and synephrine would behave similarly. The formation of these films is generally observed as electrode passivation and the disappearance of tyramine oxidative currents over successive scans. In one instance, however, the deposited film was electroactive and accompanied by the appearance of a broad oxidative current between 0.2 and 0.7 V and a corresponding reduction peak (de Castro et al., 2008). This finding is in line with the electrochemistry observed during the present experiments. With the extended waveform, trace amine oxidation results in the formation of a secondary product from side reactions of the initial oxidized species. Generation of the secondary product is measured as a slow, continual increase in oxidative current at 0.6 V throughout the injection and coincides with the growth of a reduction peak at -0.2 V (Figure 5.2D-I). This trend is repeated with the short waveform, although the potential window precludes observation of the reduction peak (Figure 5.4D-I). Considering the identical oxidation potentials, the secondary products could be catechol molecules generated from side reactions of the phenoxy radicals. However, both the previous literature reports and the persistence of the secondary peak oxidation current after the end

of the injection strongly support that these oxidative and reductive waves correspond to an electroactive film at the electrode surface resulting from polymerization of the trace amines.

The rates of polymerization differed between the three trace amines, but were consistent under both waveforms. The current at the secondary oxidation peak grew in fastest for octopamine, followed by synephrine, then tyramine (Figure 5.2G-I and Figure 5.4G-I). The extent of polymerization was significantly diminished upon shift of the holding potential from -0.4 to 0.1 V, as evident from the sharp decrease in current response at the secondary peak. This result is consistent with the proposed oxidation and polymerization schemes for tyramine (Pham et al., 1984; Tenreiro et al., 2007), and suggests that adsorption of the monomeric and polymeric species to the electrode surface via electrostatic interactions with the protonated free amino groups may provide a significant driving force for film formation at physiological pH. At the end of trace amine injection, the current at the secondary oxidation peak begins a prolonged return to baseline. Though the time course is slow (30 – 60 s), the current returning to pre-exposure levels suggests that, at least under these FSCV conditions, either the polymerization mechanism or attachment of the film to the electrode surface is reversible and dependent on continued oxidation of the trace amine. This would help explain why no evidence for long-term fouling of the electrode was observed during successive trace amine injections or for NE sensitivity following trace amine exposure. Additionally, no evidence for short-term fouling of the electrode during actual trace amine injection and film formation was noted in all but one case. This is not surprising, as the permeability of thin polytyramine films has been demonstrated (Situmorang et al., 1998; Zhou et al., 2009). For tyramine injections monitored with the short waveform, where a gradual decrease in current of the primary oxidation peak was observed, an additional feature is noted on the CV: an increase in the oxidative current near the switching potential (Figure 5.4D). This current response could represent the generation of additional side products or alternate polymer structures that do affect electrode sensitivity. However, this

same feature can be seen during tyramine injections monitored with the extended waveform (Figure 5.2D), where no change in current of the primary oxidation peak was observed throughout exposure.

As the trace amines are thought to act predominantly as modulators of monoamine neurotransmission (Berry, 2004; Burchett and Hicks, 2006), the ideal FSCV waveform would be able to simultaneously detect both classes of compound. The short and extended waveforms described in this chapter would allow for the qualitative distinction between experimental measurements in the presence of catecholamines or trace amines alone and those in the presence of both catecholamines and trace amines (Figure 5.3 and 5.5). Both waveforms would also allow real-time monitoring of concentration changes for either catecholamines or trace amines. However, quantitative measurements of catecholamine concentration changes when both species are present are temporally limited to a very brief window (100 ms) due to the overlapping trace amine secondary oxidation peak at 0.6 V. While this timescale would be sufficient for the observation of individual vesicular events at single cells, it is most likely too brief for *in vivo* or brain slice recordings. Of course, this limit is derived from mixtures of equal concentration. In the mammalian brain, endogenous concentrations of trace amines are over a hundred-fold lower than the catecholamines (Berry, 2004). The oxidative current from the electroactive trace amine films could prove negligible in these conditions, permitting accurate measurements over greater timescales.

One approach for improving the utility of these FSCV techniques could be through lowering the repetition rate. During collection of the data presented in this chapter, a paper was published on the electrochemistry of tyramine and octopamine at cylindrical carbon-fiber microelectrodes (Cooper and Venton, 2009). Using identical waveforms, only with a repetition rate of 10 Hz instead of 60 Hz, the authors obtained virtually the same results described here. Polymerization of tyramine and octopamine at the electrode surface coincided with the growth of an oxidation current at 0.5 V and a reduction current at -0.2 V.

This film was associated with only a minimal loss of tyramine sensitivity after successive injections (12%). However, at 10 Hz, raising the holding potential from -0.4 to 0.1 V completely eliminated the secondary oxidation peak rather than just diminishing the amplitude. Though the authors did not extend their studies to trace amine and catecholamine discrimination, by preventing generation of the polymer film they developed a technique that would allow for simultaneous and accurate measures of concentration changes for both species. In sum, the findings from both this chapter and the recent publication establish FSCV at carbon-fiber microelectrodes as a viable technique for monitoring real-time changes in trace amine concentration and as a tool that should prove useful in future experiments exploring the role trace amines play in neurotransmission.

References

Axelrod J, Saavedra JM (1977) Octopamine. Nature 265:501-504.

Bath BD, Michael DJ, Trafton BJ, Joseph JD, Runnels PL, Wightman RM (2000) Subsecond adsorption and desorption of dopamine at carbon-fiber microelectrodes. Anal Chem 72:5994-6002.

Berry MD (2004) Mammalian central nervous system trace amines. Pharmacologic amphetamines, physiologic neuromodulators. J Neurochem 90:257-271.

Borowsky B, Adham N, Jones KA, Raddatz R, Artymyshyn R, Ogozalek KL, Durkin MM, Lakhlani PP, Bonini JA, Pathirana S, Boyle N, Pu X, Kouranova E, Lichtblau H, Ochoa FY, Branchek TA, Gerald C (2001) Trace amines: identification of a family of mammalian G protein-coupled receptors. Proc Natl Acad Sci U S A 98:8966-8971.

Burchett SA, Hicks TP (2006) The mysterious trace amines: protean neuromodulators of synaptic transmission in mammalian brain. Prog Neurobiol 79:223-246.

Cooper SE, Venton BJ (2009) Fast-scan cyclic voltammetry for the detection of tyramine and octopamine. Anal Bioanal Chem 394:329-336.

D'Andrea G, Terrazzino S, Fortin D, Farruggio A, Rinaldi L, Leon A (2003) HPLC electrochemical detection of trace amines in human plasma and platelets and expression of mRNA transcripts of trace amine receptors in circulating leukocytes. Neurosci Lett 346:89-92.

de Castro CM, Vieira SN, Goncalves RA, Brito-Madurro AG, Madurro JM (2008) Electrochemical and morphologic studies of nickel incorporation on graphite electrodes modified with polytyramine. Journal of Materials Science 43:475-482.

Durden DA, Philips SR (1980) Kinetic measurements of the turnover rates of phenylethylamine and tryptamine in vivo in the rat brain. J Neurochem 34:1725-1732.

Durden DA, Nguyen TV, Boulton AA (1988) Kinetics of intraventricularly injected trace amines and their deuterated isotopomers. Neurochem Res 13:943-950.

Kawagoe KT, Zimmerman JB, Wightman RM (1993) Principles of voltammetry and microelectrode surface states. J Neurosci Methods 48:225-240.

Kitahama K, Araneda S, Geffard M, Sei H, Okamura H (2005) Tyramine-immunoreactive neuronal structures in the rat brain: abundance in the median eminence of the mediobasal hypothalamus. Neurosci Lett 383:215-219.

Kristensen EW, Wilson RL, Wightman RM (1986) Dispersion in flow injection analysis measured with microvoltammetric electrodes. Analytical Chemistry 58:986-988.

Luczak T (2008) Electrochemical behaviour of benzylamine, 2-phenylethylamine and 4-hydroxyphenylethylamine at gold. A comparative study. Journal of Applied Electrochemistry 38:43-50.

Manihar S, Gooding JJ, Hibbert DB, Donald B (2001) Development of Potentiometric Biosensors Using Electrodeposited Polytyramine as the Enzyme Immobilization Matrix. Electroanalysis 13:1469-1474.

Pham MC, Dubois JE, Lacaze PC (1982) Electrochemically Coated Electrode Surfaces - Voltammetric and Electrical-Properties of Adherent Thin Polytyramine and Polyquinolinol Films Complexed by Transition-Metal Ions. Journal of the Electrochemical Society 129:C136-C136.

Pham MC, Lacaze PC, Dubois JE (1984) Voltammetric and XPS Analysis of Metal-Complexed Polytyramine Films - Geometry-Dependent Electron-Transfer Therein. Journal of the Electrochemical Society 131:777-784.

Philips SR (1984) Analysis of Trace Amines: Endogenous Levels and the Effects of Various Drugs on Tissue Concentrations in the Rate. In: Neurobiology of the Trace Amines: Analytical, Physiological, Pharmacological, Behavioral, and Clinical Aspects (Boulton AA, ed), pp 127-143. Clifton, New Jersey: Humana Press.

Philips SR, Boulton AA (1979) The effect of monoamine oxidase inhibitors on some arylalkylamines in rate striatum. J Neurochem 33:159-167.

Philips SR, Durden DA, Boulton AA (1974) Identification and distribution of p-tyramine in the rat. Can J Biochem 52:366-373.

Robinson DL, Hermans A, Seipel AT, Wightman RM (2008) Monitoring rapid chemical communication in the brain. Chem Rev 108:2554-2584.

Situmorang M, Gooding JJ, Hibbert DB, Barnett D (1998) Electrodeposited polytyramine as an immobilisation matrix for enzyme biosensors. Biosensors & Bioelectronics 13:953-962.

Tenreiro AM, Nabais C, Correia JP, Fernandes F, Romero JR, Abrantes LM (2007) Progress in the understanding of tyramine electropolymerisation mechanism. Journal of Solid State Electrochemistry 11:1059-1069.

Zachek MK, Hermans A, Wightman RM, McCarty GS (2008) Electrochemical Dopamine Detection: Comparing Gold and Carbon Fiber Microelectrodes using Background Subtracted Fast Scan Cyclic Voltammetry. J Electroanal Chem (Lausanne Switz) 614:113-120.

Zhou L, Shang FJ, Pravda M, Glennon JD, Luong JHT (2009) Selective Detection of Dopamine Using Glassy Carbon Electrode Modified by a Combined Electropolymerized Permselective Film of Polytyramine and Polypyrrole-1-propionic Acid. Electroanalysis 21:797-803.

Chapter 6

The Plasticity of Vesicular Content

Introduction

The original recordings of postsynaptic responses at the neuromuscular junction indicated that neurotransmitter release was built upon a fundamental unit, or quantum, of synaptic transmission (Fatt and Katz, 1952; Del Castillo and Katz, 1954). The quantal hypothesis identified single presynaptic vesicles filled with neurotransmitter as these fundamental units (Katz, 1971), and vesicular quantal size (Q) has classically been modeled as invariant. However, considerable evidence has accumulated that indicates the amount of transmitter released per vesicle is not uniform (Edwards, 2007). While Q can be regulated at steps following vesicle fusion (Harata et al., 2006), this chapter will focus on pre-fusion mechanisms that impact the vesicular packing and storage of transmitter.

Chemical messengers are packaged into vesicles via active transport by transporter proteins located on the vesicle membrane. For catecholamines, this packaging is controlled by two differentially expressed isoforms of the vesicular monoamine transporter (VMAT): VMAT1 in chromaffin cells and VMAT2 in neuronal cells (Erickson et al., 1992; Liu et al., 1992). Like all vesicular transporters, the extent to which VMAT loads catecholamines into vesicles is dependent on both an electrochemical proton gradient and the cytoplasmic concentration of substrate (Chaudhry et al., 2008). Thus, the biosynthesis of transmitters is directly tied to Q. For catecholamines, the rate-limiting step in synthesis is the conversion of tyrosine into L-3,4-dihydroxy-phenylalanine (L-DOPA) by tyrosine hydroxylase (TH). Accordingly, bypassing this rate-limiting step in synthesis through the incubation of cells with

L-DOPA has been shown to increase Q in isolated midbrain dopamine neurons (Pothos et al., 1998), rat phaeochromocytoma (PC12) cells (Pothos et al., 1996; Colliver et al., 2000a), and bovine chromaffin cells (Pothos et al., 2002). This effect has not yet been demonstrated in rodent chromaffin cells.

In addition to the extent of catecholamine packaging by VMAT, Q is also dependent on the ability of vesicles to store the loaded transmitters. One class of compounds that has been shown to affect vesicular storage is the amphetamines. In the brain, amphetamine treatment results in the redistribution of vesicular catecholamine to the cytosol, followed by an increase in extracellular catecholamine concentration via reverse transport (Jones et al., 1998). This redistribution of vesicular catecholamine has been shown to decrease Q in both isolated PC12 and bovine chromaffin cells following amphetamine incubation (Sulzer et al., 1995; Mundorf et al., 1999). Though considered to function primarily as neuromodulators of monoamine transmission at their low physiological concentrations (tens of nM), doses of trace amine at levels significantly higher than endogenous concentrations have demonstrated amphetamine-like properties (Berry, 2004; Burchett and Hicks, 2006). Given their amphetamine-like actions on vesicular catecholamine stores, and their activity as substrates for VMAT (Knoth et al., 1984; Romanenko et al., 1998), a potential function for trace amines as false transmitters has been suggested. In this scenario, packaging of trace amines by VMAT would lead to the displacement of catecholamine and the vesicular release of trace amines instead. However, the replacement of catecholamine exocytosis with that of trace amines has not been directly observed.

This chapter describes experiments designed to explore the plasticity of vesicular content at murine chromaffin cells. Amperometric measurements of exocytosis showed no change in Q following preincubation with L-DOPA, norepinephrine (NE), or epinephrine (E). High performance liquid chromatography (HPLC) suggests that despite bypassing the rate-limiting step in catecholamine synthesis, these treatments do not increase cytosolic

concentrations of catecholamine. Fast scan cyclic voltammetry (FSCV) recordings of release after trace amine exposure revealed large deficits in both the size and number of vesicular events. However, no evidence for the exocytosis of these putative false transmitters was detected. HPLC measurements of total cellular catecholamine content indicate that in addition to the redistribution of vesicular stores to the cytoplasm, trace amine treatment also stimulates catecholamine synthesis.

Materials and Methods

Animals

Mice were handled in accordance with the guidelines set forth by the Institutional Animal Care and Use Committee (IACUC) at UNC-Chapel Hill. C57BL/6J mice were obtained from The Jackson Library (Bar Harbor, ME).

Preparation of Adrenal Medullary Chromaffin Cells

Murine chromaffin cells were prepared as previously described (Kolski-Andreaco et al., 2007) with some modifications. A female mouse, 4-8 weeks old, was deeply anesthetized with ether, decapitated, and the adrenal glands rapidly removed into ice-cold, oxygenated Ca^{2+} and Mg^{2+}-free Locke's buffer containing (in mM): 154 NaCl, 3.6 KCl, 5.6 $NaHCO_3$, 5.6 glucose, and 10 HEPES, pH adjusted to 7.2 with NaOH. The medullae were isolated via gentle removal of cortical tissue and digested for 20 min at 37 ^oC in DMEM/F12 with 25 U/mL papain. The digestion media was replaced with a fresh aliquot, followed by a second 20 min digestion period. Digested tissue was washed and triturated with pipette tips of decreasing bore size in 500 µL DMEM/F12 with 10 % fetal bovine serum and 2 % horse serum. The resulting cell suspension was distributed evenly to 3 poly-L-lysine-coated (0.1 mg/mL) 25 mm round glass coverslips. After 15 min attachment plates were fed with 2 mL DMEM/F12 containing 100 U/mL penicillin, 0.1 mg/mL streptomycin, 50 U/mL nystatin, and 40 µg/mL gentamicin. Plates were maintained in a humidified, 5 % CO_2 atmosphere at 37 ^oC. Experiments were carried out the following day.

Electrodes and Electrochemistry

Disk carbon-fiber microelectrodes were prepared using T650 (6 μm diameter, Amoco, Greenville, SC) or P55 carbon fibers (10 μm diameter, Amoco) as previously described (Kawagoe et al., 1993). Fibers were aspirated into glass capillaries (A-M Systems, Sequim, WA), and a vertical pipette puller (Narishige, Long Island, NY) was used to seal the glass around the carbon fiber. Carbon fibers were cut at the glass seal, which was then reinforced with epoxy (15 % m-phenylenediamine in Epon 828 resin (Miller-Stephenson, Danbury, CT) heated to between 80 and 90 ^{o}C). Electrodes were kept at room temperature overnight, and then the epoxy was cured via sequential heating at 100 and 150 ^{o}C for 8 h and overnight, respectively. Prior to use, electrodes were beveled at 45 degrees on a diamond dust-embedded polishing wheel (Sutter Instruments, Novato, CA) and soaked in isopropyl alcohol for at least 20 min (Bath et al., 2000).

Amperometric and FSCV recordings at single cells were made using a GeneClamp 500B amplifier (Axon Instruments, Molecular Devices, Union City, CA). For amperometry, electrodes were held at 0.650 V vs. a Ag/AgCl reference electrode (BASi, West Lafayette, IN), a potential sufficient to oxidize catecholamines. The output current was analog filtered at 5 kHz with a low-pass Bessel filter and acquired at 20 kHz. Post-collection, traces were further digitally filtered using a 400 Hz low-pass Bessel filter. Data collection and filtering were controlled via the pClamp software provided with the amplifier. For FSCV detection of catecholamines, the potential at the electrode was scanned from either -0.4 V or 0.1 V to 1.3 V and back at 600 V/s, with the ramp repeated at 60 Hz. Waveform application and current monitoring were controlled by locally written software (Tarheel CV, Labview).

Single Cell Experiments

Glass coverslips containing plated cells were secured in a stainless steel coverslip holder and mounted on the stage of an inverted microscope (Eclipse TE300, Nikon Instruments, Melville, NY). A temperature controller (Warner Instruments, Hamden, CT)

connected to the stage maintained cells at 37 ^{o}C throughout the experiments. The extracellular recording buffer for amperometry contained (in mM): 145 NaCl, 3 KCl, 1.2 $MgCl_2$, 2.4 $CaCl_2$, 1.2 NaH_2PO_4, 11 glucose, and 10 HEPES, pH adjusted to 7.4 with NaOH. For FSCV, the extracellular recording buffer contained (in mM): 140 NaCl, 4 KCl, 1 $MgCl_2$, 2 $CaCl_2$, 10 glucose, and 20 Tris-HCl, pH adjusted to 7.4 with NaOH. Exocytosis was triggered via pressure ejection of 60 mM K^+ buffer from a stimulating pipette located 30 μm from the cell. Stimulating pipettes with 6 to 10 μm tip diameters were fabricated using a horizontal pipette puller (Sutter Instruments, Novato, CA) and a microforge (Narishige, Long Island, NY). Pressure ejection was controlled via a multi-channel Picospritzer (General Valve Corporation, Parker Hannifin, Fairfield, NJ). Positioning of both the electrode and stimulating pipette was controlled using piezoelectric micromanipulators (Burleigh Instruments, Exfo, Plano, TX).

Data Analysis

FSCV current versus time traces were extracted from the peak catecholamine oxidation potential. Current was converted to concentration by post calibration in a flow injection system with a 10 μM bolus of NE and E. Analysis of amperometric and FSCV traces was performed using MiniAnalysis software (Synaptosoft, Decatur, GA). For inclusion, spike amplitude was required to be 5 times greater than the root-mean-squared current noise. For frequency analysis, the first observed spike following stimulation marked the burst start time. Burst end time was denoted by the first interspike interval > 1s. Individual spike characteristics such as quantal size (Q), amplitude, and $t_{1/2}$ were averaged for an individual cell. The cumulative mean for an experimental group was then determined using the cell averages (Colliver et al., 2000b). All data are presented as means ± standard errors of the mean. Statistical comparisons were performed using a Student's t-test.

HPLC Determination Cellular Catecholamine Content

Total content from all cells on one 25 mm coverslip was extracted via sonication in ice-cold 0.1 N perchloric acid spiked with 1 μM hydroquinone (HQ). The extract was centrifuged at 6,000 rpm for 10 min, and the supernatant was removed and filtered with a 0.2 μm syringe filter unit (Millex-LG). The Lowry assay (Bio-Rad, Hercules, CA) was used to normalize extractions from different cell plates. Injections (50 μL) were made onto a reverse phase column (C-18, 5 μm, 4.6 x 250 mm, Waters symmetry 300 or Waters Atlantis T3). For detection of catecholamines only, the mobile phase (prepared in HPLC grade water) contained 0.1 M citric acid, 0.1 mM EDTA, and 1 mM hexyl sodium sulfate, pH 3.5. Methanol was added as the organic modifier at a concentration of 10 % to shorten analyte elution times. Catecholamines were detected with a thin-layer radial electrochemical flowcell (BASi, West Lafayette, IN), with the working electrode at 700 mV vs. a Ag/AgCl reference electrode (BASi, West Lafayette, IN). For detection of catecholamines and trace amines, the mobile phased contained 7:3 0.02 M citric acid:0.02 M NaH_2PO_4, pH 3 (Pellati and Benvenuti, 2007). The working electrode was held at 1.2 V. The HQ (1 μM) was used as an internal standard for analyte quantification and recovery. All analyte response ratios were taken with respect to the internal standard to account for differential electrode responses. The determination of peak areas for HPLC measurements was performed using custom written Igor programs. These programs were a gift from the Jorgenson lab at UNC-CH. Peak area determination was performed using statistical moments regression theory (Hsieh and Jorgenson, 1996).

Chemicals

All chemicals were purchased from Sigma Aldrich (St. Louis, MO) and used as received. Aqueous solutions were prepared in doubly-distilled, deionized water. Stock solutions of catecholamines and trace amines were prepared in 0.1 N $HClO_4$ and diluted in

buffer on the day of each experiment. All solutions were deoxygenated prior to use with at least 20 min of N_2 bubbling.

Results

Vesicular Loading and Quantal Size at Chromaffin Cells

To examine the flexibility of vesicular Q, amperometric recordings of exocytosis were made at isolated murine chromaffin cells after treatments intended to increase cytosolic concentrations of NE and E. Vesicular release was triggered with a single 3 s application of 60 mM K^+ from cells following a 1 h preincubation of plates at 37 ^oC with extracellular recording buffer or buffer containing 100 μM L-DOPA, NE, or E. The average changes in amperometric spike characteristics are shown in Figure 6.1. Treatment with L-DOPA produced no significant change ($p > 0.05$, Student's t-test) in any of the measures of exocytosis. Events recorded at cells loaded with L-DOPA (n = 18) occurred at a frequency 102 ± 12 % of that at untreated cells (n = 18). Average Q was 97 ± 13 % and average $t_{1/2}$ was 100 ± 5 % of the unloaded levels. Likewise, incubation with NE did not significantly alter ($p > 0.05$) vesicular release. In cells loaded with NE (n = 15), the frequency of amperometric events was 92 ± 9 % of that in unloaded cells (n = 12), and the average Q and $t_{1/2}$ for individual spikes were 100 ± 15 % and 97 ± 7 % of untreated levels, respectively. Finally, cells loaded with E (n = 14) also showed no significant changes ($p > 0.05$), with vesicular events having a frequency at 74 ± 12 %, average Q at 93 ± 16 %, and average $t_{1/2}$ at 107 ± 9 % of values from unloaded cells (n =10).

As L-DOPA, NE, and E loading had no affect on vesicular Q, HPLC with electrochemical detection was used to test if cytosolic concentrations of catecholamine were increasing. Total intracellular NE and E content was determined from plated cells exposed to 50 μM or 100 μM L-DOPA for 1 h at 37 ^oC. Consistent with the amperometric results, no changes were observed in catecholamine concentration after L-DOPA loading (Figure 6.2). Relative to untreated cells (n = 2 plates), NE and E levels were both at 101 % in cells

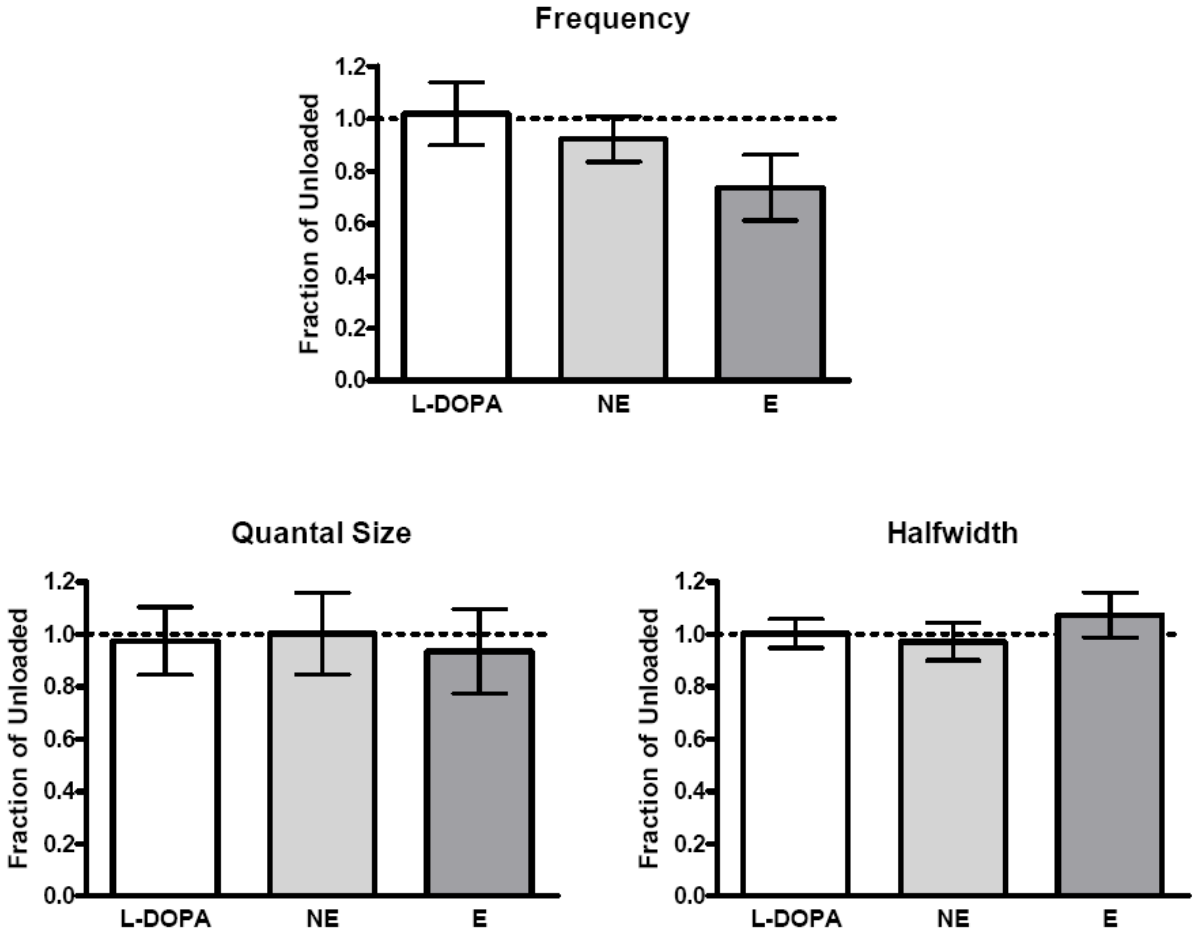

Figure 6.1. Exocytosis following L-DOPA, NE, and E loading. Vesicular release was measured by amperometry at murine chromaffin cells following a 3 s stimulation with 60 mM K^+. Release was measured at untreated cells and cells incubated for 1 h at 37 ^oC in 100 μM L-DOPA (n = 18), NE (n = 15), or E (n = 14). The frequency of events and average spike quantal size and halfwidth after loading are shown as fractions of the unloaded values. After loading, no significant differences ($p > 0.05$, Student's t-test) were observed in any measures of exocytosis for all compounds.

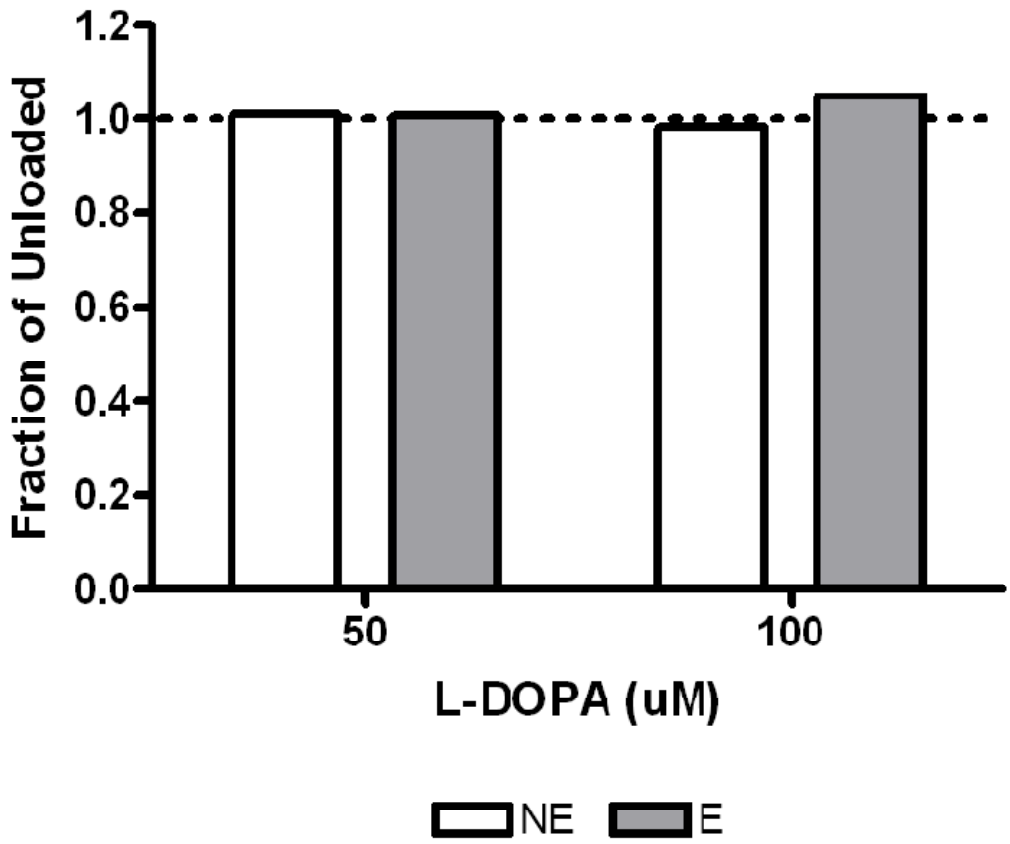

Figure 6.2. Cellular catecholamine content following L-DOPA loading. HPLC with electrochemical detection was used to determine total NE and E content in untreated murine chromaffin cells and cells incubated for 1 h at 37 ^{o}C with 50 μM or 100 μM L-DOPA. Contents measured after loading are shown as a fraction of the unloaded values. Data points are the averages from two 25 mm coverslips, one each from two separate preparations.

treated with 50 μM L-DOPA (n = 2 plates). In cells loaded with 100 μM L-DOPA (n = 2 plates), NE and E concentrations were at 98 % and 105 % of their values from unloaded cells, respectively.

Trace Amines and Vesicular Content at Chromaffin Cells

As high concentrations of trace amine are proposed to displace vesicular catecholamines, FSCV was used to monitor exocytosis at individual chromaffin cells before and after a 20 min exposure at 37 ^{o}C to 1 mM tyramine, 1 mM octopamine, or 100 μM synephrine. Vesicular release was initiated via a 0.5 s pressure ejection of 60 mM K^{+}. Representative color plots and concentration versus time traces from cells incubated with the three trace amines are shown in Figures 6.3 through 6.5. In all three cases, trace amine treatment produced a noticeable decrease in the number and/or size of detectable peaks. As a control, incubations were performed with normal extracellular recording buffer. At these cells (n = 2), the number of peaks observed following treatment was reduced to 72 % of initial values, but peak size was unaffected at 104 %. For cells exposed to tyramine (n = 4), only 34 ± 12 % as many spikes were detected after incubation, with average amplitudes 56 ± 16 % of pre-exposure values. Similar decreases were seen for treatment with octopamine, where peak number and size were reduced to 39 ± 4 % and 61 ± 11 % of original levels, respectively. Unlike tyramine and octopamine, synephrine incubation (n = 4 cells) did not affect a greater reduction in observed spikes (63 ± 27 %) than control conditions, but did show a marked decrease in spike amplitude (41 ± 15 %). Despite the obvious effects of trace amine treatment on the catecholamine content of vesicles, no evidence was observed for their replacement of catecholamines and subsequent vesicular release. Examination of the cyclic voltammograms (CVs) recorded during the concentration spikes following incubation revealed no measurable currents at the characteristic trace amine oxidation potential of 1.0 V.

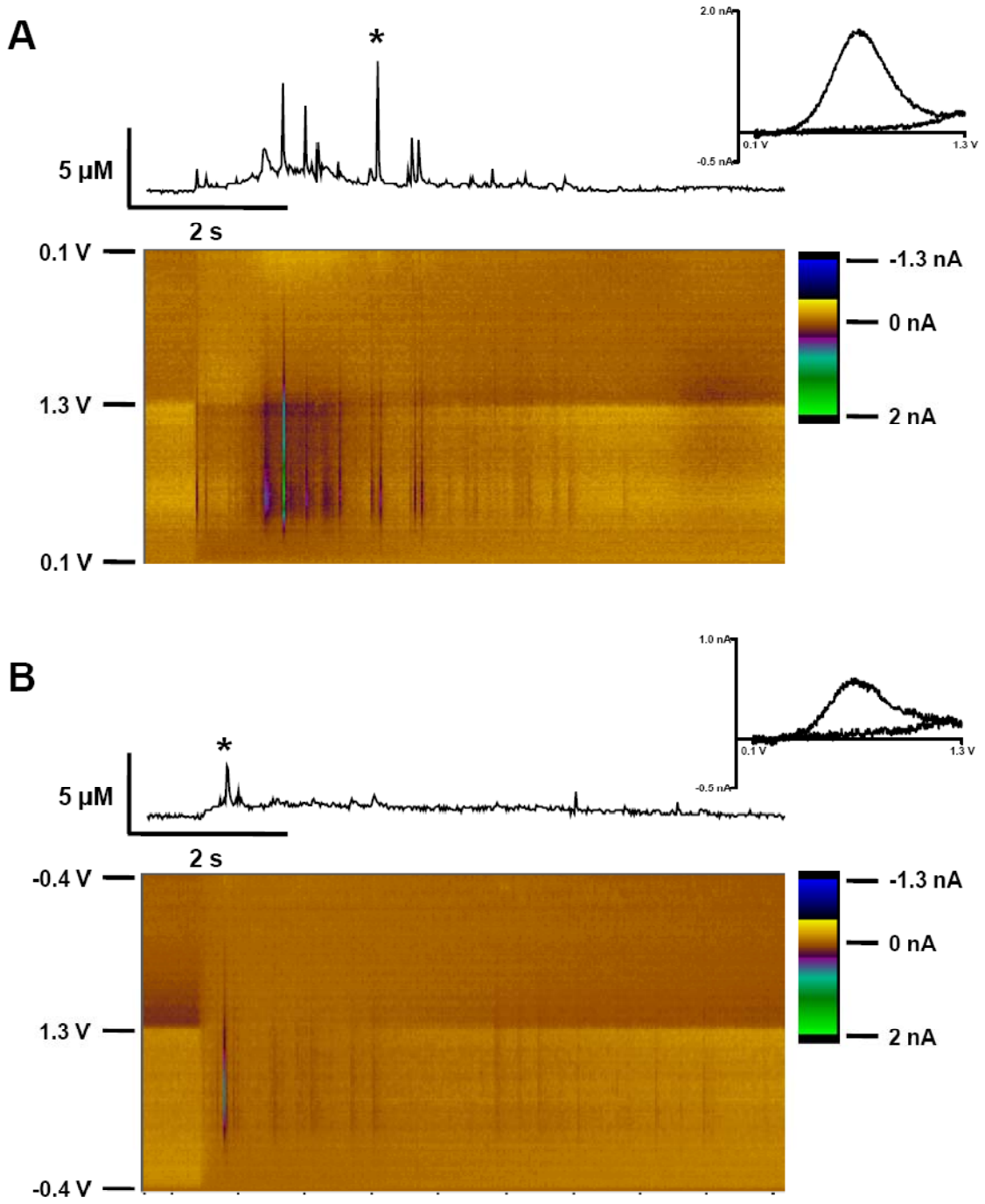

Figure 6.3. Exocytosis following tyramine treatment. FSCV was used to measure the K^+-stimulated vesicular release from a chromaffin cell prior to **(A)** and after **(B)** a 20 min incubation with 1 mM tyramine. Color plots, concentration versus time traces, and representative cyclic voltammograms (from peaks marked with an asterisk) are shown for both conditions. Concentrations extracted from peak catecholamine oxidation current.

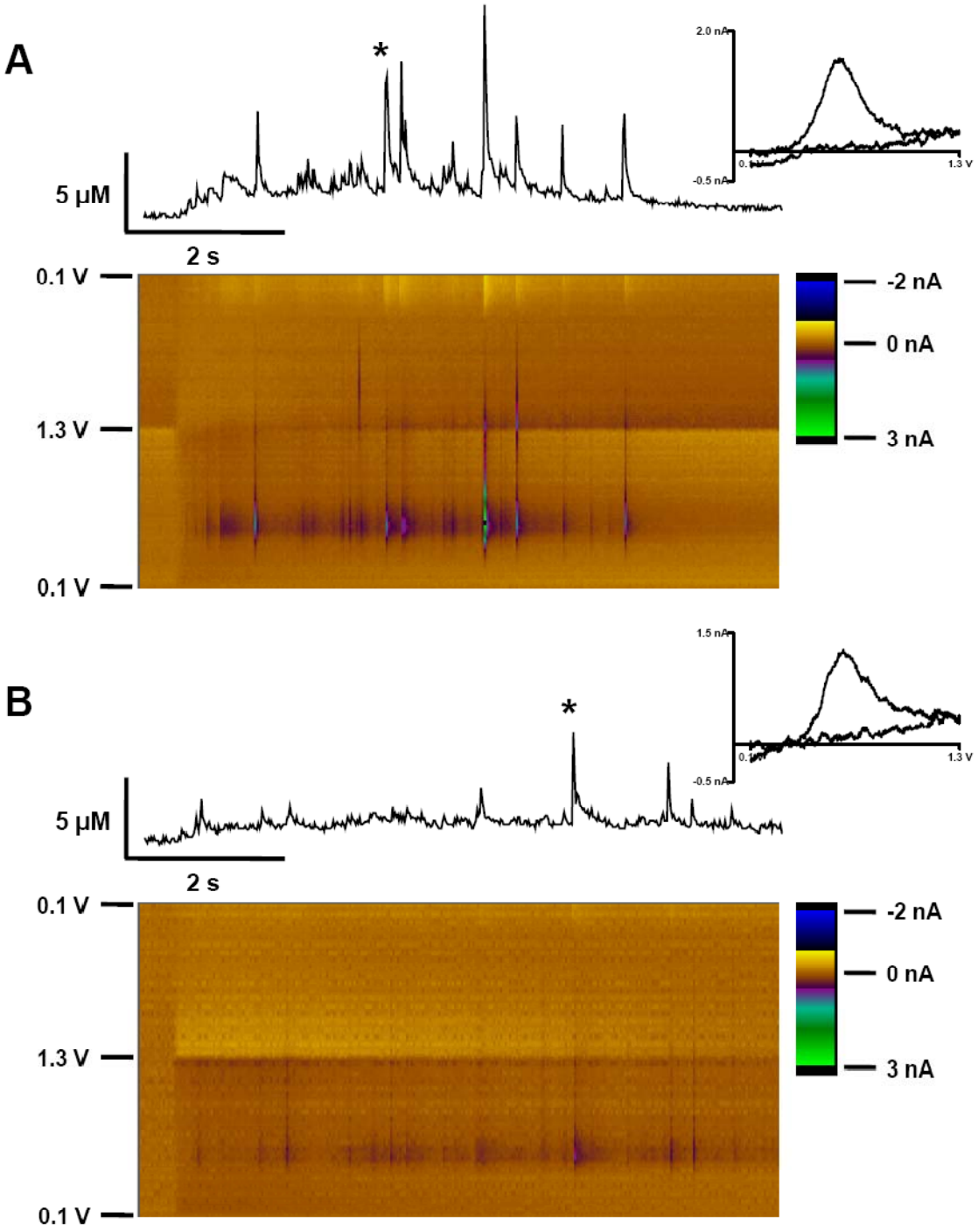

Figure 6.4. Exocytosis following octopamine treatment. FSCV was used to measure the K^+-stimulated vesicular release from a chromaffin cell prior to **(A)** and after **(B)** a 20 min incubation with 1 mM octopamine. Color plots, concentration versus time traces, and representative cyclic voltammograms (from peaks marked with an asterisk) are shown for both conditions. Concentrations extracted from peak catecholamine oxidation current.

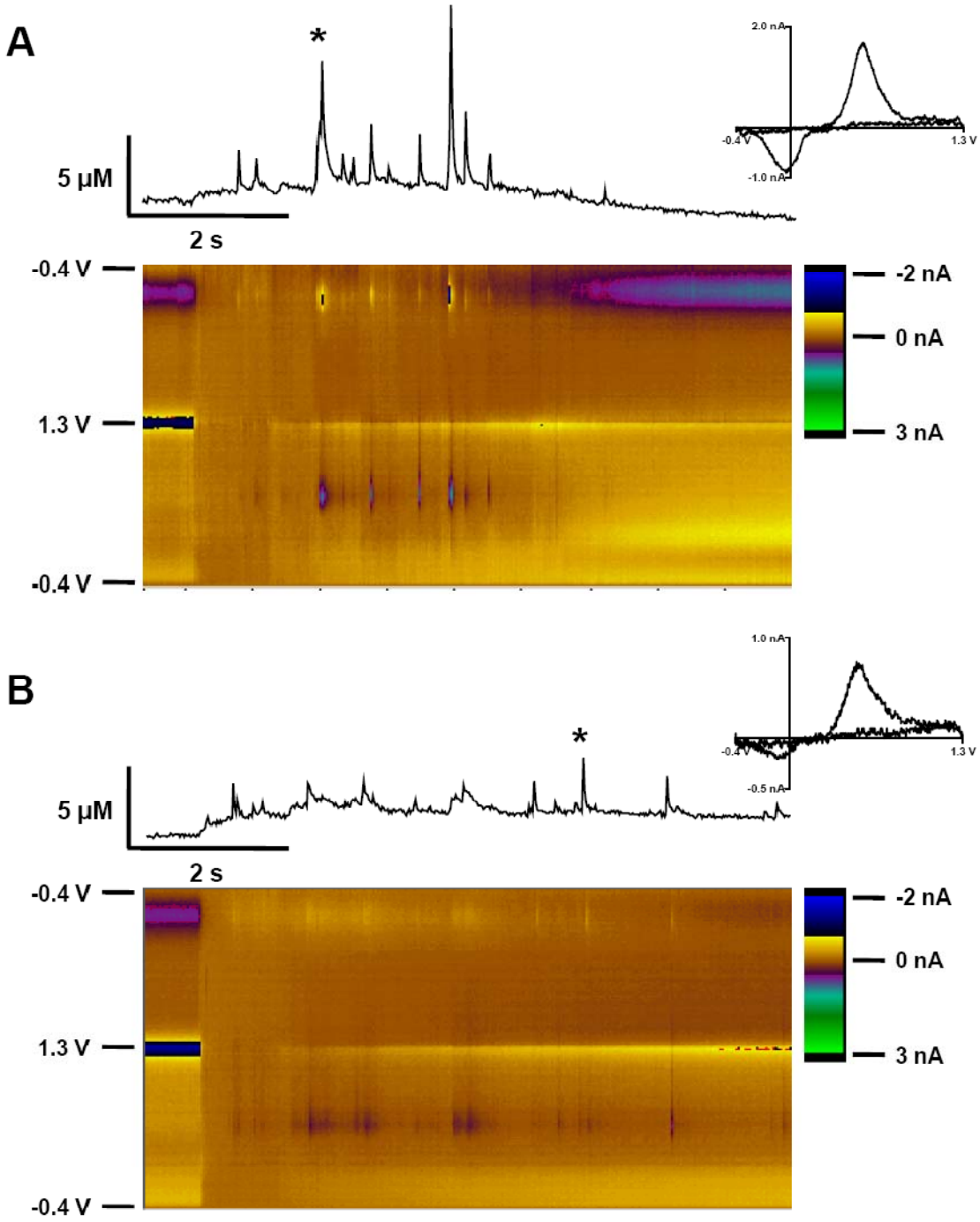

Figure 6.5. Exocytosis following synephrine treatment. FSCV was used to measure the K^+-stimulated vesicular release from a chromaffin cell prior to **(A)** and after **(B)** a 20 min incubation with 100 µM synephrine. Color plots, concentration versus time traces, and representative cyclic voltammograms (from peaks marked with an asterisk) are shown for both conditions. Concentrations extracted from peak catecholamine oxidation current.

To further investigate the fate of both the newly introduced trace amine and the displaced vesicular catecholamine, HPLC with electrochemical detection was used to probe any changes in non-vesicular stores. Total intracellular catecholamine and trace amine contents were determined from plated cells exposed to 1 mM tyramine or octopamine for 30 min at 37 ^{o}C. Surprisingly, both treatments resulted in a large enhancement of cellular catecholamine concentration (Figure 6.6). In cells incubated with tyramine (n = 2 plates), NE and E levels were 197 % and 161 %, respectively, of their values in untreated cells (n = 2 plates). Octopamine exposure (n = 2 plates) produced a comparable increase, with concentrations of NE raised to 173 % of original levels and E to 154 %. In both cases, the growth in catecholamine stores was accompanied by only modest accumulation of trace amine. Following tyramine incubation, tyramine levels were less than 6 % of the total catecholamine concentration. Octopamine was also present, but at less than 1 %. After octopamine treatment, cellular octopamine concentration was 1 % of the combined NE and E values. No other trace amines were detected.

Discussion

Incubation of isolated midbrain dopaminergic neurons, PC12 cells, and bovine chromaffin cells with L-DOPA has been shown to result in significant increases in Q (Pothos et al., 1996; Pothos et al., 1998; Colliver et al., 2000a; Pothos et al., 2002). Through application of exogenous L-DOPA, the rate-limiting step in catecholamine synthesis is bypassed and the driving force for vesicular packaging by VMAT is increased due to the resulting enhancement of cytosolic catecholamine concentration. This property of L-DOPA was even exploited in Chapter 2 to raise cellular dopamine levels at acutely dissociated midbrain neurons and facilitate the observation of exocytosis. Therefore, it was rather surprising that L-DOPA treatment of mouse chromaffin cells produced no significant change in Q as measured by amperometry (Figure 6.1). HPLC measurements of total cellular catecholamine content were also unaffected by L-DOPA treatment (Figure 6.2), confirming

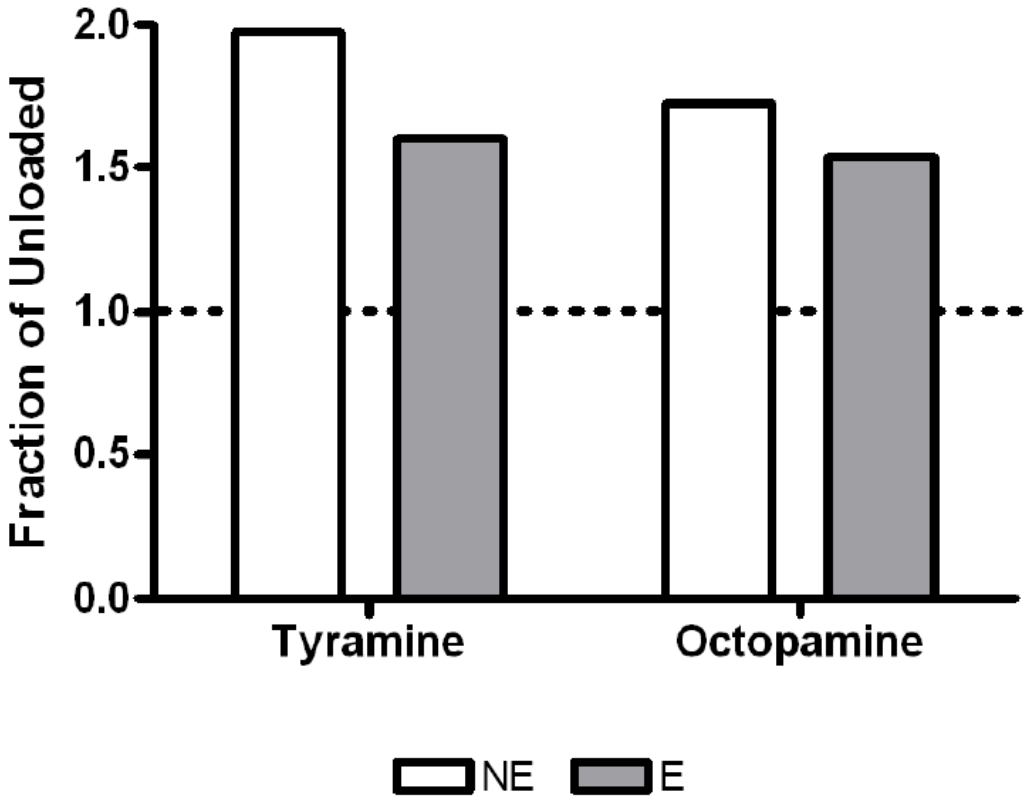

Figure 6.6. Cellular catecholamine content following trace amine treatment. HPLC with electrochemical detection was used to determine total NE and E content in untreated murine chromaffin cells and cells incubated for 30 min at 37 ^{o}C with 1 mM tyramine or octopamine. Contents measured post-incubation are shown as a fraction of the unloaded values. Data points are the averages from two 25 mm coverslips, one each from two separate preparations.

that neither the vesicular or cytosolic pools of catecholamine had been augmented. Moving further down the biosynthetic pathway, incubations with the endogenously-released catecholamines NE and E also proved ineffective at increasing Q (Figure 6.1). As a whole, the results from these loading experiments indicate that in murine chromaffin cells the vesicular pool of catecholamine is filled to a maximal capacity.

A previous report has shown L-DOPA-induced increases in Q at bovine chromaffin cells (Pothos et al., 2002), suggesting the results obtained here could be due to species-specific regulation of catecholamine synthesis and packaging. However, the vesicular events measured after L-DOPA treatment in this earlier study are slightly smaller than events observed in this laboratory at untreated bovine and mouse chromaffin cells. Thus, it's proposed that the previous work was actually measuring rescue of an artificially-induced deficit and that chromaffin cell vesicles, unlike those from catecholamine-releasing neurons or PC12 cells, are largely insensitive to L-DOPA loading in the native state. Recent experiments using intracellular patch electrochemistry to directly measure cytosolic catecholamine concentrations in chromaffin cells support this hypothesis (Mosharov et al., 2003). While resting cytosolic catecholamine concentrations were increased to roughly two-fold during a 1 h exposure to 100 μM L-DOPA, they returned to control levels within 10 min of L-DOPA withdrawal. This time course is comparable to the length of the washing and electrode placement steps used in the present study after the incubation step. Given the current results that both vesicular and cytosolic levels of catecholamine are at control levels after roughly 10 min of withdrawal, the L-DOPA-induced rise in cytosolic catecholamine must either fail to produce a corresponding increase in Q or produce a temporary increase in vesicular catecholamine levels that dissipates in unison with those in the cytosol. Research showing that loaded dopamine in PC12 cells is preferentially located to the clear halo portion of the vesicle (Sombers et al., 2005), largely absent in chromaffin cell vesicles, indicates the former as a distinct possibility.

Although chromaffin cell vesicles proved resistant to manipulations intended to increase Q, treatments expected to disrupt vesicular stores produced mostly anticipated results. At high concentrations, the trace amines are thought to mimic the actions of amphetamine and redistribute catecholamines from the vesicular compartment to the cytosol (Berry, 2004; Burchett and Hicks, 2006). Accordingly, exposure of chromaffin cells to 1 mM tyramine, 1 mM octopamine, or 100 μM synephrine noticeably reduced the number and amplitude of vesicular events measured by FSCV during K^+-stimulated exocytosis (Figure 6.3 and Table 6.1). Unlike amperometry, the area under the spikes observed by FSCV is not directly related to the total number of molecules detected. However, as the extracellular volume between the cell and the electrode is mostly confined, the peak concentration (amplitude) reached following a vesicular release event can be used as a suitable indicator of Q. Thus, similar to amphetamine treatment (Sulzer et al., 1995; Mundorf et al., 1999), incubation with high concentrations of trace amine decreases Q at chromaffin cells.

Prior to trace amine exposure, every single CV recorded during vesicular release events displayed the characteristic shape of catecholamine oxidation and reduction (Figure 6.3). Following exposure, the oxidative current at 1.0 V indicative of trace amine presence was not distinguishable in any of the CVs (Figure 6.3). The ability of FSCV to simultaneously measure trace amine-induced disruption of vesicular catecholamine stores despite no vesicular release of the trace amines themselves provides strong evidence that these molecules don't accumulate sufficiently to function as false transmitters. Although the trace amines are transported by VMAT with an affinity and velocity comparable to the catecholamines (Romanenko et al., 1998; Partilla et al., 2006), the lack of a second ring hydroxyl (Figure 5.1) renders them more lipophilic. This increased lipophilicity has been demonstrated to result in the permeation of tyramine in its unprotonated form across the chromaffin vesicle membrane (Johnson et al., 1982; Knoth et al., 1984). The current results would then suggest that high concentrations of trace amine promote depletion of vesicular

stores through competitive inhibition of catecholamine transport at VMAT. In the presence of extracellular trace amine, the transport and permeation processes most likely reach a steady state. Upon removal of extracellular trace amine, the rate of active transport is rapidly diminished and permeation of trace amine from the vesicle interior prohibits the observation of these compounds in vesicles undergoing exocytosis.

HPLC measurements of total cellular catecholamine content were used to gain greater insight into the redistribution of vesicular stores triggered by trace amine treatment. Following incubations of plated cells with tyramine and octopamine, only very low levels of the trace amines were detected. This result is consistent with both the lipid permeability discussed above and the greater metabolic turnover of trace amines relative to catecholamines (Durden et al., 1988). Importantly, the presence of measurable octopamine levels following tyramine exposure confirms that the trace amines are gaining access to the vesicle interior, as the enzyme that catalyzes this conversion, dopamine β-hydroxylase, is located on the inside of the vesicular membrane. As for the fate of the displaced catecholamines, HPLC showed substantial increases in total cellular catecholamine content (Figure 6.4). This finding is rather counterintuitive. Cytosolic regulation of catecholamine concentration is tightly controlled through rapid metabolism via monoamine oxidase (MAO) (Mosharov et al., 2003). That total cellular content is greatly enhanced indicates trace amine treatment is not only preventing the metabolism of catecholamine, but actively stimulating synthesis. Tyramine has demonstrated a higher affinity than NE and E for MAO in chromaffin cells (Youdim et al., 1986), so the lack of catecholamine degradation could be attributed to competitive inhibition by the trace amines. The increased synthesis is a novel finding, however, and less easily explained. Amphetamine has been shown to stimulate dopamine synthesis by TH (Kuczenski, 1975; Larsen et al., 2002). As high trace amine concentrations mimic several of amphetamine's effects on vesicular catecholamine stores, it is possible they might also share the ability to activate TH. Alternatively, liver microsomes

have been shown to catalyze the synthesis of catecholamines from the direct hydroxylation of the corresponding trace amines (Axelrod, 1963; Hiroi et al., 1998). If the cytochrome P450 isoforms responsible for this reaction are expressed in chromaffin cells, this pathway could also be an explanation for the measured increase in cellular catecholamine content. Future investigations will certainly be necessary to shed more light on this exciting new role for trace amine modulation of catecholamine transmission.

References

Axelrod J (1963) Enzymatic formations of adrenaline and other catechols from monophenols. Science 140:499-500.

Bath BD, Michael DJ, Trafton BJ, Joseph JD, Runnels PL, Wightman RM (2000) Subsecond adsorption and desorption of dopamine at carbon-fiber microelectrodes. Anal Chem 72:5994-6002.

Berry MD (2004) Mammalian central nervous system trace amines. Pharmacologic amphetamines, physiologic neuromodulators. J Neurochem 90:257-271.

Burchett SA, Hicks TP (2006) The mysterious trace amines: protean neuromodulators of synaptic transmission in mammalian brain. Prog Neurobiol 79:223-246.

Chaudhry FA, Edwards RH, Fonnum F (2008) Vesicular neurotransmitter transporters as targets for endogenous and exogenous toxic substances. Annu Rev Pharmacol Toxicol 48:277-301.

Colliver TL, Pyott SJ, Achalabun M, Ewing AG (2000a) VMAT-Mediated changes in quantal size and vesicular volume. J Neurosci 20:5276-5282.

Colliver TL, Hess EJ, Pothos EN, Sulzer D, Ewing AG (2000b) Quantitative and statistical analysis of the shape of amperometric spikes recorded from two populations of cells. J Neurochem 74:1086-1097.

Del Castillo J, Katz B (1954) Quantal components of the end-plate potential. J Physiol 124:560-573.

Durden DA, Nguyen TV, Boulton AA (1988) Kinetics of intraventricularly injected trace amines and their deuterated isotopomers. Neurochem Res 13:943-950.

Edwards RH (2007) The neurotransmitter cycle and quantal size. Neuron 55:835-858.

Erickson JD, Eiden LE, Hoffman BJ (1992) Expression cloning of a reserpine-sensitive vesicular monoamine transporter. Proc Natl Acad Sci U S A 89:10993-10997.

Fatt P, Katz B (1952) Spontaneous subthreshold activity at motor nerve endings. J Physiol 117:109-128.

Harata NC, Aravanis AM, Tsien RW (2006) Kiss-and-run and full-collapse fusion as modes of exo-endocytosis in neurosecretion. J Neurochem 97:1546-1570.

Hiroi T, Imaoka S, Funae Y (1998) Dopamine formation from tyramine by CYP2D6. Biochem Biophys Res Commun 249:838-843.

Hsieh S, Jorgenson JW (1996) Preparation and evaluation of slurry-packed liquid chromatography microcolumns with inner diameters from 12 to 33 microns. Anal Chem 68:1212-1217.

Johnson RG, Carty SE, Hayflick S, Scarpa A (1982) Mechanisms of accumulation of tyramine, metaraminol, and isoproterenol in isolated chromaffin granules and ghosts. Biochem Pharmacol 31:815-823.

Jones SR, Gainetdinov RR, Wightman RM, Caron MG (1998) Mechanisms of amphetamine action revealed in mice lacking the dopamine transporter. J Neurosci 18:1979-1986.

Katz B (1971) Quantal mechanism of neural transmitter release. Science 173:123-126.

Kawagoe KT, Zimmerman JB, Wightman RM (1993) Principles of voltammetry and microelectrode surface states. J Neurosci Methods 48:225-240.

Knoth J, Peabody JO, Huettl P, Njus D (1984) Kinetics of tyramine transport and permeation across chromaffin-vesicle membranes. Biochemistry 23:2011-2016.

Kolski-Andreaco A, Cai H, Currle DS, Chandy KG, Chow RH (2007) Mouse adrenal chromaffin cell isolation. J Vis Exp:129.

Kuczenski R (1975) Effects of catecholamine releasing agents on synaptosomal dopamine biosynthesis: multiple pools of dopamine or multiple forms of tyrosine hydroxylase. Neuropharmacology 14:1-10.

Larsen KE, Fon EA, Hastings TG, Edwards RH, Sulzer D (2002) Methamphetamine-induced degeneration of dopaminergic neurons involves autophagy and upregulation of dopamine synthesis. J Neurosci 22:8951-8960.

Liu Y, Peter D, Roghani A, Schuldiner S, Prive GG, Eisenberg D, Brecha N, Edwards RH (1992) A cDNA that suppresses MPP+ toxicity encodes a vesicular amine transporter. Cell 70:539-551.

Mosharov EV, Gong LW, Khanna B, Sulzer D, Lindau M (2003) Intracellular patch electrochemistry: regulation of cytosolic catecholamines in chromaffin cells. J Neurosci 23:5835-5845.

Mundorf ML, Hochstetler SE, Wightman RM (1999) Amine weak bases disrupt vesicular storage and promote exocytosis in chromaffin cells. J Neurochem 73:2397-2405.

Partilla JS, Dempsey AG, Nagpal AS, Blough BE, Baumann MH, Rothman RB (2006) Interaction of amphetamines and related compounds at the vesicular monoamine transporter. J Pharmacol Exp Ther 319:237-246.

Pellati F, Benvenuti S (2007) Chromatographic and electrophoretic methods for the analysis of phenethylamine alkaloids in Citrus aurantium. J Chromatogr A 1161:71-88.

Pothos E, Desmond M, Sulzer D (1996) L-3,4-dihydroxyphenylalanine increases the quantal size of exocytotic dopamine release in vitro. J Neurochem 66:629-636.

Pothos EN, Davila V, Sulzer D (1998) Presynaptic recording of quanta from midbrain dopamine neurons and modulation of the quantal size. J Neurosci 18:4106-4118.

Pothos EN, Mosharov E, Liu KP, Setlik W, Haburcak M, Baldini G, Gershon MD, Tamir H, Sulzer D (2002) Stimulation-dependent regulation of the pH, volume and quantal size of bovine and rodent secretory vesicles. J Physiol 542:453-476.

Romanenko VG, Gebara R, Miller KM, Njus D (1998) Determination of transport parameters of permeant substrates of the vesicular amine transporter. Anal Biochem 257:127-133.

Sombers LA, Maxson MM, Ewing AG (2005) Loaded dopamine is preferentially stored in the halo portion of PC12 cell dense core vesicles. J Neurochem 93:1122-1131.

Sulzer D, Chen TK, Lau YY, Kristensen H, Rayport S, Ewing A (1995) Amphetamine redistributes dopamine from synaptic vesicles to the cytosol and promotes reverse transport. J Neurosci 15:4102-4108.

Youdim MB, Heldman E, Pollard HB, Fleming P, McHugh E (1986) Contrasting monoamine oxidase activity and tyramine induced catecholamine release in PC12 and chromaffin cells. Neuroscience 19:1311-1318.

Appendix 1

Exploring the Origin of Post-Spike Feet

Introduction

The final steps in vesicular exocytosis are the Ca^{2+}-triggered fusion of secretory vesicles with the cell plasma membrane and the extrusion of the packaged chemical messengers into the extracellular space. Mediating this fusion are SNARE proteins on the vesicle and plasma membranes, whose interactions provide the necessary driving force for destabilization and subsequent mixing of the two phospholipid bilayers (Hanson et al., 1997; Weber et al., 1998). The initial mixing of the two membranes generates a fusion pore, a thin channel connecting the vesicle interior and the cell exterior. Expansion of the fusion pore leads to a rapid flux of transmitter into the extracellular space, resulting in the sharp current spikes generally observed during amperometric studies of exocytosis (Figures 1.5 and 1.6). Occasionally, amperometric events will also exhibit pre-spike features termed feet, resulting from a slower efflux or leak of transmitter through the fusion pore prior to expansion (Chow et al., 1992). In addition, work in this lab has noted the previously undocumented occurrence of post-spike features that closely resemble pre-spike feet (Figure A1.1) (Haynes, unpublished results). These post-spike feet are hypothesized to result from the fast endocytosis of vesicles. In a simple vesicle fusion event, the entire transmitter content is released and the vesicle membrane completely incorporates into the plasma membrane. Vesicles then recycle via the slow endocytosis pathway through formation of clathrin-coated pits (Smith et al., 2008). In contrast, fast endocytosis recycles vesicles via reclosure of the expanded fusion pore, resulting in intact vesicles that may or may not undock from the

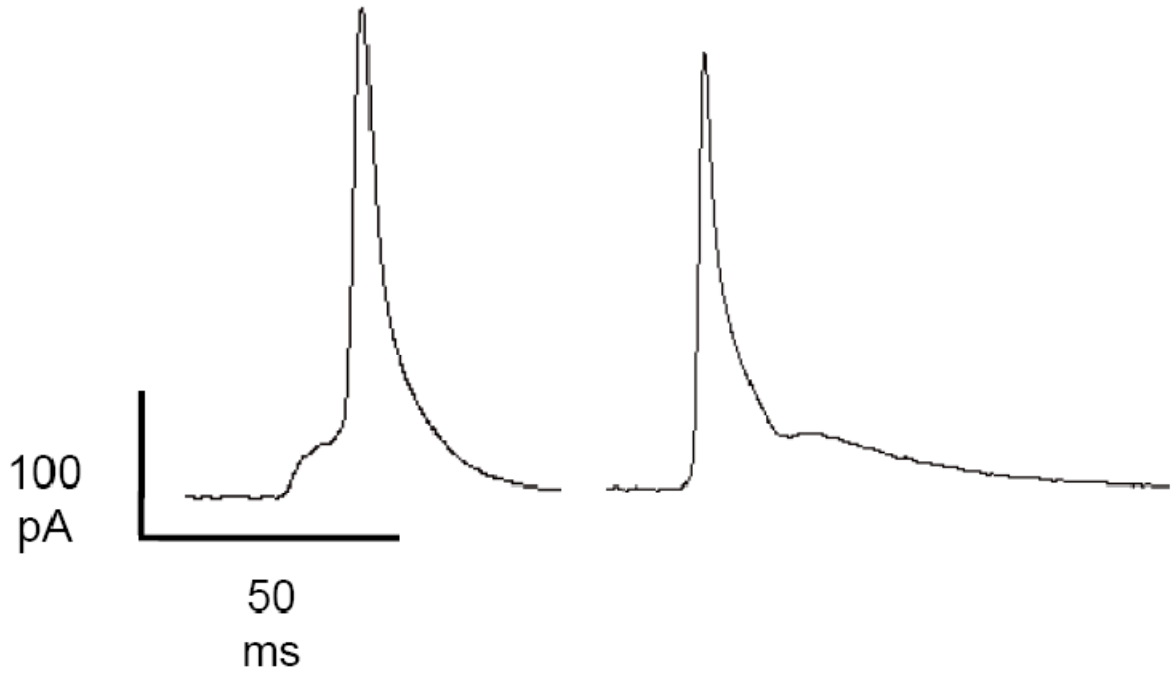

Figure A1.1. Examples of pre- and post-spike feet. Individual vesicular events recorded with amperometry at bovine chromaffin cells are shown to demonstrate the appearance of pre-spike feet (left trace) and post-spike feet (right trace). Pre-spike feet are observed as a result of the slow flux of chemical messengers through a narrow fusion pore intermediate prior to expansion. Post-spike feet are hypothesized to result from a similar intermediate formed during the fast endocytosis pathway.

plasma membrane (Harata et al., 2006). The natural assumption is that resealing the vesicle membrane would produce a second fusion pore intermediate through which the slower efflux or leak of transmitter could be detected by amperometry.

This appendix describes a single pharmacological attempt at understanding the origin of the observed post-spike feet. Amperometric recordings of exocytosis were made at isolated bovine chromaffin cells exposed to wortmannin, a furanosteroid produced by the fungus *Penicillium funiculosum*. Wortmannin is a potent inhibitor of phosphatidylinositol 3-kinase (PI3K) (Arcaro and Wymann, 1993), and has been demonstrated to selectively inhibit the slow endocytosis of reserve pool (RP) vesicles (Richards et al., 2004). This inhibition is tentatively attributed to disruption of clathrin-coat-dependent mechanisms, which are regulated by PI molecules (Cremona and De Camilli, 2001). Treatment of chromaffin cells with wortmannin produced no measurable change in RP exocytosis. The occurrence of post-spike feet was also unchanged, suggesting these features indeed result from the fast endocytosis pathway.

Materials and Methods

Preparation of Bovine Adrenal Medullary Chromaffin Cells

Bovine chromaffin cells were prepared from adrenal glands obtained at a local abattoir as previously described (Wilson and Viveros, 1981; Leszczyszyn et al., 1990). Chromaffin cells were isolated from the adrenal medulla via digestion with collagenase (Worthington Biochemical Corporation, Lakewood, NJ), followed by density gradient centrifugation in Renografin (Bracco Diagnostics, Princeton, NJ). The resulting cell suspension was plated at a density of 300,000 cells/25 mm round glass coverslip. Plates were maintained in a humidified, 5 % CO_2 atmosphere at 37 ^{o}C, and used for experiments between 3 and 7 days post-plating.

Electrodes and Electrochemistry

Disk carbon-fiber microelectrodes were prepared using T650 carbon fibers (6 µm diameter, Amoco, Greenville, SC) as previously described (Kawagoe et al., 1993). Fibers were aspirated into glass capillaries (A-M Systems, Sequim, WA), and a vertical pipette puller (Narishige, Long Island, NY) was used to seal the glass around the carbon fiber. The carbon fibers were cut at the glass seal, which was then reinforced with epoxy (15 % m-phenylenediamine in Epon 828 resin (Miller-Stephenson, Danbury, CT) heated to between 80 and 90 ^{o}C). Electrodes were kept at room temperature overnight, and then the epoxy was cured via sequential heating at 100 and 150 ^{o}C for 8 h and overnight, respectively. Prior to use, electrodes were beveled at 45 degrees on a diamond dust-embedded polishing wheel (Sutter Instruments, Novato, CA) and soaked in isopropyl alcohol for at least 20 min (Bath et al., 2000).

Amperometric recordings at single cells were made using an Axopatch 200B amplifier (Axon Instruments, Molecular Devices, Union City, CA). Electrodes were held at 0.650 V vs. a Ag/AgCl reference electrode (BASi, West Lafayette, IN), a potential sufficient to oxidize catecholamines. The output current was analog filtered at 5 kHz with a low-pass Bessel filter and acquired at 20 kHz. Post-collection, traces were further digitally filtered using a 250 Hz low-pass Bessel filter. Data collection and filtering were controlled by locally written software (Tarheel CV, Labview).

Single Cell Experiments

Glass coverslips containing plated cells were secured in a stainless steel coverslip holder and mounted on the stage of an inverted microscope (Eclipse TE300, Nikon Instruments, Melville, NY). A temperature controller (Warner Instruments, Hamden, CT) connected to the stage maintained cells at 37 ^{o}C throughout the experiments. The extracellular recording buffer contained (in mM): 145 NaCl, 3 KCl, 1.2 $MgCl_2$, 2.4 $CaCl_2$, 1.2 NaH_2PO_4, 11 glucose, and 10 HEPES, pH adjusted to 7.4 with NaOH. Exocytosis was

triggered via a single 5 s pressure ejection of 5 mM Ba^{2+} buffer from a stimulating pipette located 30 µm from the cell. Stimulating pipettes with 6 to 10 µm tip diameters were fabricated using a horizontal pipette puller (Sutter Instruments, Novato, CA) and a microforge (Narishige, Long Island, NY). Pressure ejection was controlled via a multi-channel Picospritzer (General Valve Corporation, Parker Hannifin, Fairfield, NJ). Positioning of both the electrode and stimulating pipette was controlled using piezoelectric micromanipulators (Burleigh Instruments, Exfo, Plano, TX).

Data Analysis

Amperometric spike analysis was performed using MiniAnalysis software (Synaptosoft, Decatur, GA). For inclusion, spike amplitude was required to be 5 times greater than the root-mean-squared current noise. Overlapping peaks were included in frequency and foot analysis, but excluded from individual spike analysis. Visual examination of the peaks was used to determine presence of post-spike feet. Individual amperometric spike characteristics such as quantal size (Q) and $t_{1/2}$ were averaged for an individual cell. The cumulative mean for an experimental group was then determined using the cell averages (Colliver et al., 2000). All data are presented as means ± standard errors of the mean. Statistical comparisons were performed using a Student's t-test.

Results

To investigate potential wortmannin-induced changes in post-spike foot behavior, amperometry was used to measure vesicular release at isolated bovine chromaffin cells. As wortmannin acts selectively on RP endocytosis (Richards et al., 2004), stimulated exocytosis of the RP was isolated from that of the readily releasable pool (RRP) using a 5 s application of 5 mM Ba^{2+} (Seward et al., 1996; Duncan et al., 2003). Figure A1.2 shows representative amperometric traces obtained at control cells (n =19) and cells incubated with 1 µM wortmannin for 15 min prior to recording (n =25). Wortmannin treatment produced no significant changes ($p > 0.05$, Student's t-test) in any of the baseline measures of RP

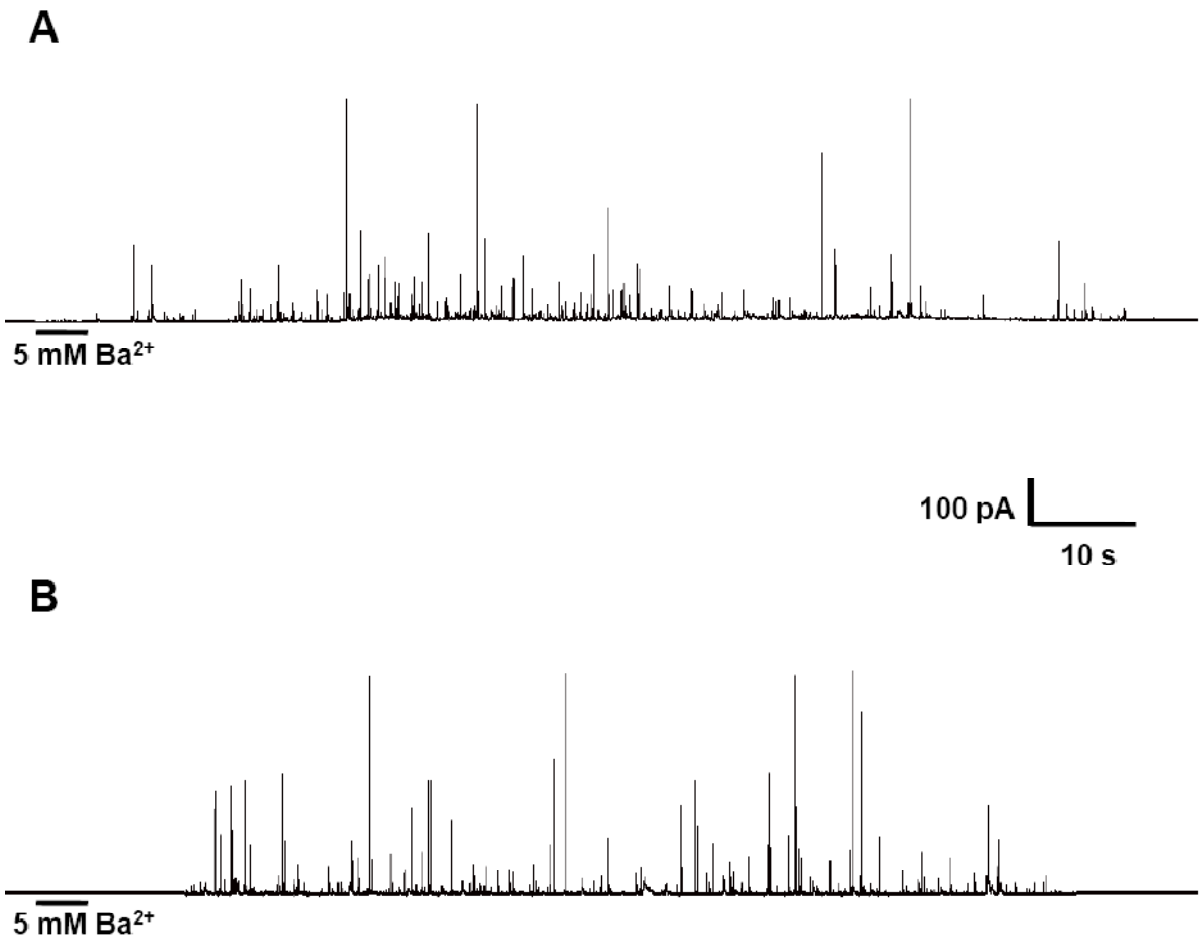

Figure A1.2. Vesicular release after wortmannin treatment. Representative amperometric traces measured in response to a 5 s stimulation with 5 mM Ba^{2+} at bovine chromaffin cells following a 15 min incubation in normal recording buffer **(A)** or 1 µM wortmannin **(B)**.

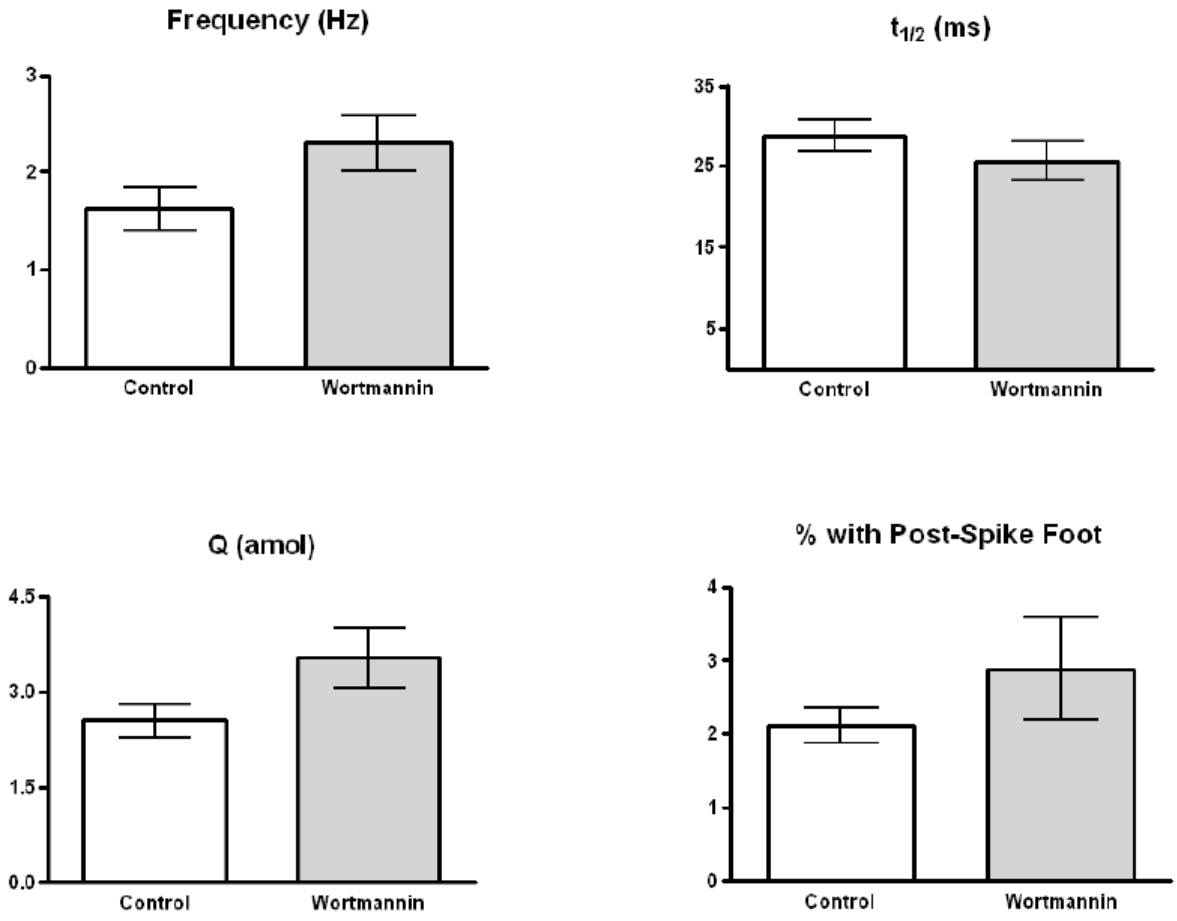

Figure A1.3. Amperometric spike characteristics following wortmannin treatment. Bar graphs show the average frequency of vesicular events and individual spike characteristics, including halfwidth ($t_{1/2}$, in ms), quantal size (Q, in amol of catecholamine), and % of events with a post-spike foot. No significant differences ($p > 0.05$, Student's t-test) were observed between control cells ($n = 19$) and cells treated with 1 µM wortmannin ($n = 25$) in any measures of exocytosis.

exocytosis (Figure A1.3). In control cells, individual vesicular events occurred at a frequency of 1.6 ± 0.2 Hz, and the average amperometric spike had a $t_{1/2}$ of 29 ± 2 ms and Q of 2.5 ± 0.3 amol of catecholamine. Similarly, events at wortmannin treated cells occurred at a frequency of 2.3 ± 0.3 Hz with an average $t_{1/2}$ of 26 ± 2 ms and Q of 3.5 ± 0.5 amol of catecholamine. Most importantly, wortmannin incubation didn't alter the prevalence of post-spike feet, with 2.1 ± 0.2 % and 2.9 ± 0.7 % of exocytotic spikes exhibiting these features in control and treated cells, respectively (Figure A1.3).

Discussion

The fungal metabolite wortmannin, an inhibitor of PI3K, has been shown to selectively halt the slow endocytosis of RP vesicles (Richards et al., 2004). Amperometric measurements at isolated chromaffin cells were conducted to determine if wortmannin treatment resulted in changes in the exocytosis of RP vesicles, specifically the occurrence of post-spike feet believed to represent fusion pore behavior solely during fast endocytosis pathways. To isolate RP exocytosis from that involving both the RRP and RP, release was stimulated using Ba^{2+} as a secretagogue (Seward et al., 1996; Duncan et al., 2003). As has been reported previously (Heldman et al., 1989; von Ruden et al., 1993), Ba^{2+}-induced vesicular release is slower and longer lasting relative to K^{+}-stimulated release (compare Figure A1.2 to Figure 4.2). A 15 min incubation with 1 µM wortmannin did not significantly alter the prevalence of post-spike feet (Figure A1.3), supporting the hypothesis that these features arise when vesicles are recycled via a fast endocytosis pathway. Inhibition of the slow endocytosis pathway produced no side effects on vesicular exocytosis, as wortmannin-treated cells showed no changes in the frequency, Q, or $t_{1/2}$ of Ba^{2+}-stimulated events (Figure A1.3). While the continued presence of post-spike feet following wortmannin incubation supports a fast endocytosis origin, it was initially surprising that no measures of exocytosis were affected. By shutting down the slow pathway, it was assumed that more vesicles would undergo fast recycling and the frequency of events and/or the prevalence of

post-spike feet would increase. That no changes were measured suggests that vesicle recycling via the slow endocytosis pathway is not a major component of Ba^{2+}-induced RP exocytosis. Future experiments with multiple stimulations could address the extent and time course to which slow endocytosis contributes to the release of RP vesicles.

References

Arcaro A, Wymann MP (1993) Wortmannin is a potent phosphatidylinositol 3-kinase inhibitor: the role of phosphatidylinositol 3,4,5-trisphosphate in neutrophil responses. Biochem J 296 (Pt 2):297-301.

Bath BD, Michael DJ, Trafton BJ, Joseph JD, Runnels PL, Wightman RM (2000) Subsecond adsorption and desorption of dopamine at carbon-fiber microelectrodes. Anal Chem 72:5994-6002.

Chow RH, von Ruden L, Neher E (1992) Delay in vesicle fusion revealed by electrochemical monitoring of single secretory events in adrenal chromaffin cells. Nature 356:60-63.

Colliver TL, Hess EJ, Pothos EN, Sulzer D, Ewing AG (2000) Quantitative and statistical analysis of the shape of amperometric spikes recorded from two populations of cells. J Neurochem 74:1086-1097.

Cremona O, De Camilli P (2001) Phosphoinositides in membrane traffic at the synapse. J Cell Sci 114:1041-1052.

Duncan RR, Greaves J, Wiegand UK, Matskevich I, Bodammer G, Apps DK, Shipston MJ, Chow RH (2003) Functional and spatial segregation of secretory vesicle pools according to vesicle age. Nature 422:176-180.

Hanson PI, Roth R, Morisaki H, Jahn R, Heuser JE (1997) Structure and conformational changes in NSF and its membrane receptor complexes visualized by quick-freeze/deep-etch electron microscopy. Cell 90:523-535.

Harata NC, Aravanis AM, Tsien RW (2006) Kiss-and-run and full-collapse fusion as modes of exo-endocytosis in neurosecretion. J Neurochem 97:1546-1570.

Heldman E, Levine M, Raveh L, Pollard HB (1989) Barium ions enter chromaffin cells via voltage-dependent calcium channels and induce secretion by a mechanism independent of calcium. J Biol Chem 264:7914-7920.

Kawagoe KT, Zimmerman JB, Wightman RM (1993) Principles of voltammetry and microelectrode surface states. J Neurosci Methods 48:225-240.

Leszczyszyn DJ, Jankowski JA, Viveros OH, Diliberto EJ, Jr., Near JA, Wightman RM (1990) Nicotinic receptor-mediated catecholamine secretion from individual chromaffin cells. Chemical evidence for exocytosis. J Biol Chem 265:14736-14737.

Richards DA, Rizzoli SO, Betz WJ (2004) Effects of wortmannin and latrunculin A on slow endocytosis at the frog neuromuscular junction. J Physiol 557:77-91.

Seward EP, Chernevskaya NI, Nowycky MC (1996) Ba2+ ions evoke two kinetically distinct patterns of exocytosis in chromaffin cells, but not in neurohypophysial nerve terminals. J Neurosci 16:1370-1379.

Smith SM, Renden R, von Gersdorff H (2008) Synaptic vesicle endocytosis: fast and slow modes of membrane retrieval. Trends Neurosci 31:559-568.

von Ruden L, Garcia AG, Lopez MG (1993) The mechanism of Ba(2+)-induced exocytosis from single chromaffin cells. FEBS Lett 336:48-52.

Weber T, Zemelman BV, McNew JA, Westermann B, Gmachl M, Parlati F, Sollner TH, Rothman JE (1998) SNAREpins: minimal machinery for membrane fusion. Cell 92:759-772.

Wilson SP, Viveros OH (1981) Primary culture of adrenal medullary chromaffin cells in a chemically defined medium. Exp Cell Res 133:159-169.

Appendix 2

Pressure Ejection, Extracellular Calcium, and Exocytosis

Introduction

The ultimate trigger for synaptic vesicle exocytosis is the influx of Ca^{2+} ions through voltage-gated calcium channels (VGCCs) (Llinas et al., 1992; Borst and Sakmann, 1996). These channels open in response to depolarization of the plasma membrane as an action potential invades the synapse. Neurotransmitter release is dependent on the appropriate timing of the Ca^{2+} influx relative to the action potential and proportional to the resulting increase in $[Ca^{2+}]_i$. This Ca^{2+}-based mechanism of stimulus-secretion coupling is conserved in most excitable cells, including chromaffin cells (Douglas and Rubin, 1961; Holz et al., 1982). The development of fluorescent Ca^{2+} indicators (Grynkiewicz et al., 1985) provided researchers the necessary tools to monitor this coupling in real time (Finnegan and Wightman, 1995). In these experiments, Ca^{2+} influx is generally triggered via pressure ejection of depolarizing agents. Ideally, these agents are dissolved in the extracellular recording buffer to ensure the secretagogue effect is distinct from any other changes in the local cell environment. For experiments where such controls aren't possible, it is necessary to understand the extracellular Ca^{2+} ion concentration dynamics that result from mixing of the stimulus volume with the stationary recording buffer.

To examine the interplay between extracellular Ca^{2+} levels, pressure ejection-mediated alterations in the cellular environment, and exocytosis-triggering Ca^{2+} influx, the fluorescent dye fura-2 was used to record changes in $[Ca^{2+}]_i$ at bovine chromaffin cells following pressure ejection of a high $[K^+]$ secretagogue. To isolate the role of Ca^{2+} ion

dynamics, the only variable in these experiments was the presence or absence of Ca^{2+} in the recording buffer and the stim. The presence of Ca^{2+} in the stim solution was sufficient to support K^+-induced Ca^{2+} influx, suggesting a significant contribution of the stim to the local extracellular ion concentrations sensed by cells during pressure ejection. However, the significantly diminished amplitude of this Ca^{2+} transient combined with the normal Ca^{2+} responses observed with Ca^{2+}-free stims indicate that dilution of secretagogue ions by the extracellular buffer occurs on a timescale relevant to VGCC activation and exocytosis.

Materials and Methods

Preparation of Bovine Adrenal Medullary Chromaffin Cells

Bovine chromaffin cells were prepared from adrenal glands obtained at a local abattoir as previously described (Wilson and Viveros, 1981; Leszczyszyn et al., 1990). Chromaffin cells were isolated from the adrenal medulla via digestion with collagenase (Worthington Biochemical Corporation, Lakewood, NJ), followed by density gradient centrifugation in Renografin (Bracco Diagnostics, Princeton, NJ). The resulting cell suspension was plated at a density of 300,000 cells/25 mm round glass coverslip. Plates were maintained in a humidified, 5 % CO_2 atmosphere at 37 ^oC, and used for experiments between 3 and 7 days post-plating.

Fluorescent Measurements of Intracellular Ca^{2+}

Intracellular Ca^{2+} dynamics were monitored using the ratiometric dye fura-2 (Invitrogen, Carlsbad, CA). Plated cells were incubated for 20 min at 25 ^oC in extracellular recording buffer with 1 µg/mL esterified fura dye and 0.1 % (w/v) BSA, washed twice with buffer without dye, and then incubated for 20 min at 25 ^oC in buffer without dye for deesterification. Ca^{2+} bound and unbound dye were excited at 340 and 380 nm, respectively, using a computer-controlled high speed wavelength switcher (Sutter Instruments, Novato, CA). Emission was monitored at 510 nm using a CCD camera and acquisition software (Empix Imaging, Mississauga, ON, Canada).

Single Cell Experiments

Glass coverslips containing plated cells were secured in a stainless steel coverslip holder and mounted on the stage of an inverted microscope (Eclipse TE300, Nikon Instruments, Melville, NY). A temperature controller (Warner Instruments, Hamden, CT) connected to the stage maintained cells at 37 ^{o}C throughout the experiments. The extracellular recording buffer contained (in mM): 145 NaCl, 3 KCl, 1.2 $MgCl_2$, 2.4 $CaCl_2$, 1.2 NaH_2PO_4, 11 glucose, and 10 HEPES, pH adjusted to 7.4 with NaOH. Ca^{2+} influx was triggered via a single 3 s pressure ejection of 60 mM K^+ buffer from a stimulating pipette located 30 µm from the cell. Stimulating pipettes with 6 to 10 µm tip diameters were fabricated using a horizontal pipette puller (Sutter Instruments, Novato, CA) and a microforge (Narishige, Long Island, NY). Pressure ejection was controlled via a multi-channel Picospritzer (General Valve Corporation, Parker Hannifin, Fairfield, NJ). Positioning of both the electrode and stimulating pipette was controlled using piezoelectric micromanipulators (Burleigh Instruments, Exfo, Plano, TX).

Results

The ratiometric dye fura-2 was used to measure changes in $[Ca^{2+}]_i$ at isolated bovine chromaffin cells following depolarization of the plasma membrane with a 3 s pressure ejection of 60 mM K^+. Three experimental conditions were tested. Serving as the control, Ca^{2+} influx was recorded in cells (n =19) where both the extracellular buffer and the stim solution contained physiological Ca^{2+} levels (2.4 mM). Additionally, responses were monitored when Ca^{2+} was completely removed from the extracellular buffer (n = 14 cells), the stim solution (n = 5 cells), or both (n = 5 cells). As expected, depolarization of cells in the absence of both stim and buffer Ca^{2+} resulted in no increase in $[Ca^{2+}]_i$ as measured by Fura-2 (data not shown). Representative rises in $[Ca^{2+}]_i$ for the other three conditions are shown in Figure A2.1. Several key properties of the intracellular Ca^{2+} transients are summarized in Figure A2.2. Under control conditions, the K^+-triggered influx raised $[Ca^{2+}]_i$

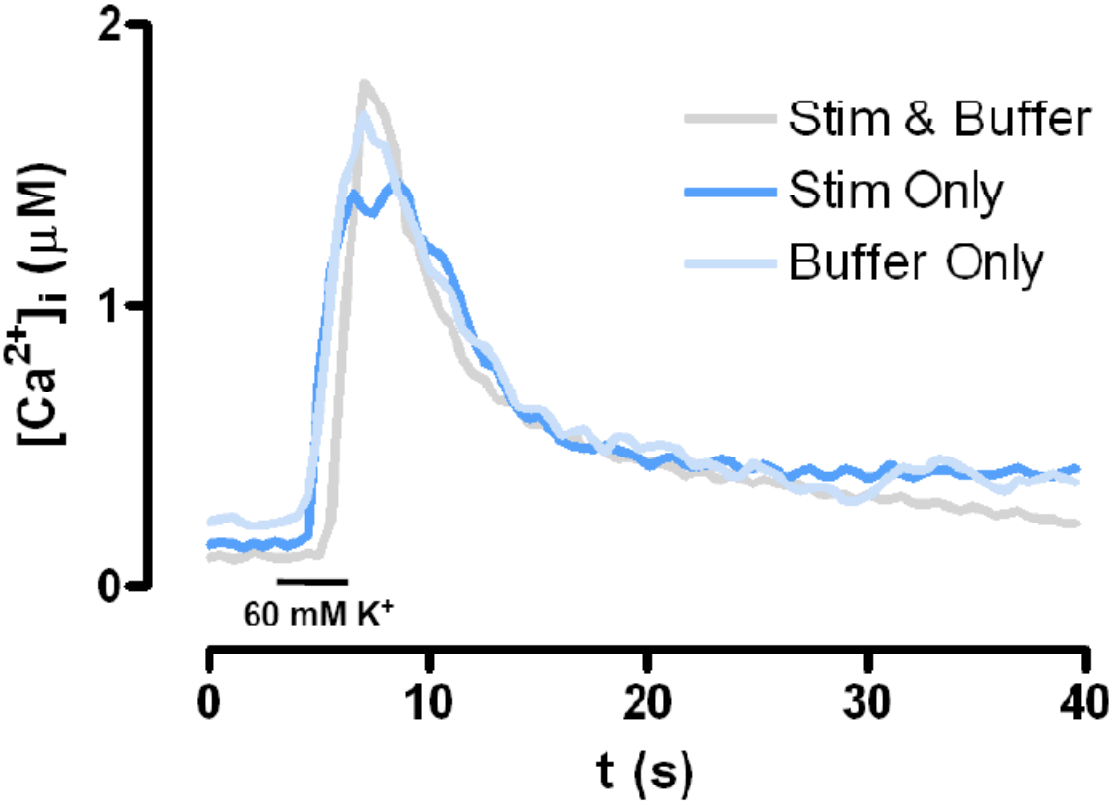

Figure A2.1. Effect of extracellular Ca^{2+} on intracellular Ca^{2+} responses. Fura-2 was used to monitor increases in $[Ca^{2+}]_i$ at bovine chromaffin cells after 3 s pressure ejection of 60 mM K^+. Representative traces from three different extracellular Ca^{2+} conditions are shown: Ca^{2+} in both the buffer and stim solution, in the stim solution only, or in the buffer only.

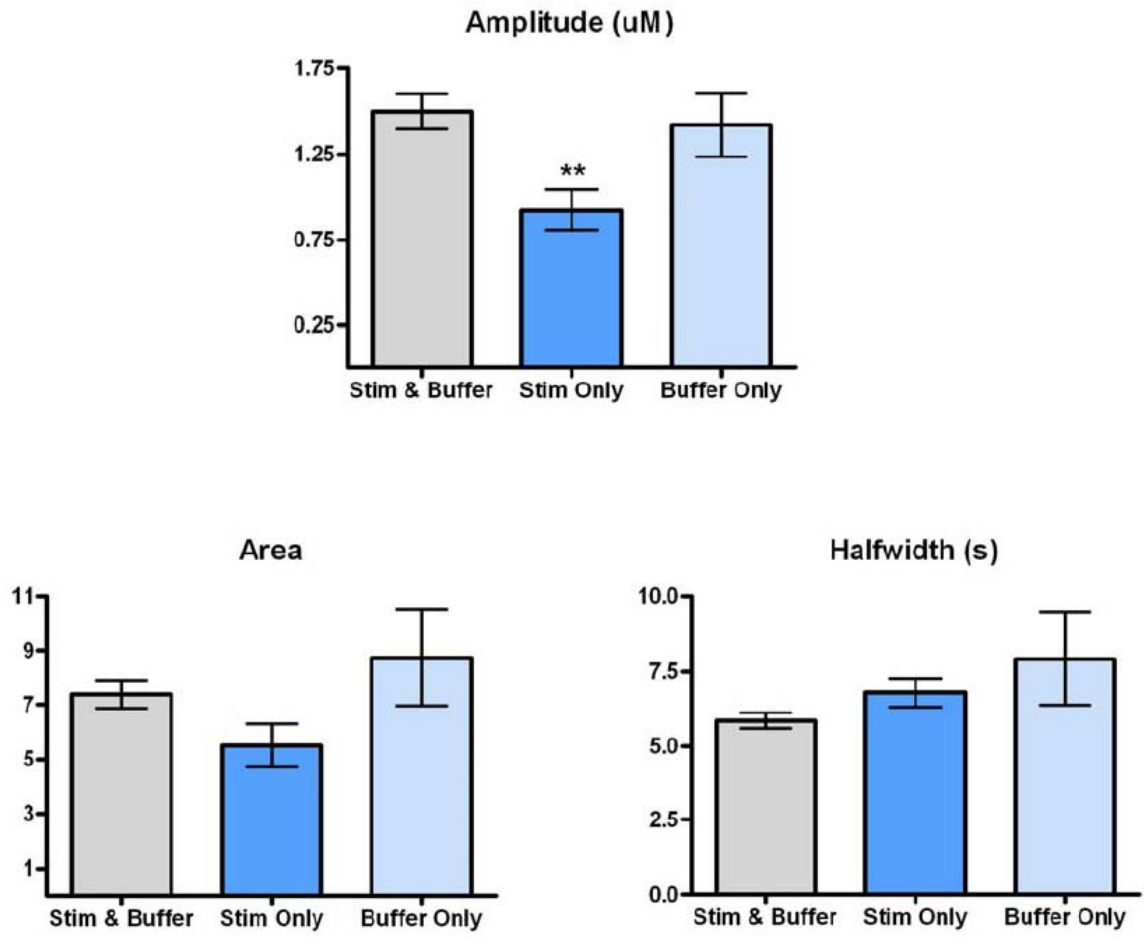

Figure A2.2. Intracellular Ca^{2+} dynamics depend on buffer Ca^{2+}. Graphs show the average amplitude (in µM), area (in arbitrary units), and halfwidth ($t_{1/2}$, in s) of the increase in $[Ca^{2+}]_i$ at isolated bovine chromaffin cells following a 3 s stimulation with 60 mM K^+. Experiments were performed with Ca^{2+} present in both the buffer and stim solutions (n = 19 cells), stim only (n = 14 cells), or buffer only (n = 5 cells). No significant difference ($p > 0.5$ for all measures, one-way ANOVA) was observed upon removal of Ca^{2+} from the stim solution. Removal of Ca^{2+} from the extracellular buffer resulted in a significant decrease ($p < 0.01$) in the amplitude of the $[Ca^{2+}]_i$ signal, but did not affect ($p > 0.05$) the overall size or time course.

by an average of 1.50 ± 0.10 μM. Removal of Ca^{2+} from the extracellular buffer significantly depressed ($p < 0.01$, one-way ANOVA) this amplitude to 0.92 ± 0.12 μM, while no significant difference ($p > 0.05$) was observed upon removal of Ca^{2+} from the stim solution (1.42 ± 0.19 μM). However, the total area and $t_{1/2}$ of the intracellular Ca^{2+} responses were unchanged ($p > 0.05$) relative to control values at cells were extracellular Ca^{2+} was present only in the buffer or stim solution.

Discussion

The influx of extracellular Ca^{2+} ions through VGCCs on the plasma membrane is necessary for generation of the rapid increases in $[Ca^{2+}]_i$ that trigger exocytosis. Demonstrating this, depolarization of chromaffin cells with 60 mM K^+ produced no rise in $[Ca^{2+}]_i$, as measured by fura-2, when Ca^{2+} was removed from both the extracellular recording buffer and the stim solution. Removal of Ca^{2+} from only one of these solutions produced more subtle effects (Figures A2.1 and A2.2). The intracellular Ca^{2+} transients observed when Ca^{2+} was present only in the extracellular buffer were statistically indistinguishable from those in control conditions, suggesting that the small stim volume minimally impacts the local cell environment. However, with the exception of a decrease in amplitude, the responses at cells where Ca^{2+} was present only in the stim solution were also unchanged from control conditions. These results would indicate that the effective extracellular $[Ca^{2+}]$ at a cell during pressure ejection is largely due to the $[Ca^{2+}]$ in the stim solution, not the recording buffer. Both data can be explained by a model of pressure ejection in which the effects of rapid mixing of the two solutions are equal or greater to volume displacement. Thus, the Ca^{2+}-containing stim is rapidly diluted by the Ca^{2+}-free buffer, resulting in a lower effective extracellular $[Ca^{2+}]$ at the cell, a smaller driving force for Ca^{2+} influx, and smaller rise in $[Ca^{2+}]_i$. Similarly, the absence of Ca^{2+} from the stim is overwhelmed by the larger volume of Ca^{2+}-containing buffer, resulting in no change in the effective extracellular $[Ca^{2+}]$ sensed by the cell. This initial mixing must occur on a timescale

comparable to the depolarization-induced opening of VGCCs, in the ms regime. Future experiments in which the [Ca^{2+}] in the recording buffer and stim, duration of pressure ejection, and distance of the stimulating pipette from the cell are varied would provide valuable insight into the kinetics of extracellular ion equilibration occurring at the local cell environment. Additionally, simultaneous detection of $[Ca^{2+}]_i$ with fluorescent dyes and exocytosis with amperometry could be used to demonstrate how changes in the intracellular Ca^{2+} transient impact vesicular release.

References

Borst JG, Sakmann B (1996) Calcium influx and transmitter release in a fast CNS synapse. Nature 383:431-434.

Douglas WW, Rubin RP (1961) The role of calcium in the secretory response of the adrenal medulla to acetylcholine. J Physiol 159:40-57.

Finnegan JM, Wightman RM (1995) Correlation of real-time catecholamine release and cytosolic Ca2+ at single bovine chromaffin cells. J Biol Chem 270:5353-5359.

Grynkiewicz G, Poenie M, Tsien RY (1985) A new generation of Ca2+ indicators with greatly improved fluorescence properties. J Biol Chem 260:3440-3450.

Holz RW, Senter RA, Frye RA (1982) Relationship between Ca2+ uptake and catecholamine secretion in primary dissociated cultures of adrenal medulla. J Neurochem 39:635-646.

Leszczyszyn DJ, Jankowski JA, Viveros OH, Diliberto EJ, Jr., Near JA, Wightman RM (1990) Nicotinic receptor-mediated catecholamine secretion from individual chromaffin cells. Chemical evidence for exocytosis. J Biol Chem 265:14736-14737.

Llinas R, Sugimori M, Silver RB (1992) Microdomains of high calcium concentration in a presynaptic terminal. Science 256:677-679.

Wilson SP, Viveros OH (1981) Primary culture of adrenal medullary chromaffin cells in a chemically defined medium. Exp Cell Res 133:159-169.